1.0

4.5
5.0
5.6

2.8

2.5

1.1

3.2

3.6

4.0

2.2

2.0

1.8

1.25

1.4

1.6

MICROCOPY RESOLUTION TEST CHART
NATIONAL BUREAU OF STANDARDS-1963-A

(5)

AD A137532

DTIC FILE COPY

DTIC

FEB6 84

THE WEST SPITSBERGEN CURRENT:
TRANSPORT, FORCING, AND VARIABILITY

by

Dennis Joe Hanzlick

A dissertation submitted in partial fulfillment
of the requirements for the degree of
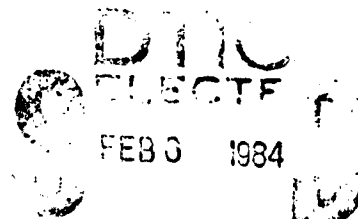
Doctor of Philosophy

University of Washington

1983

Approved by _____
(Chairperson of Supervisory Committee)

Program Authorized
to Offer Degree _____

Date _____1 December 1983_____

FEB 3 1984

A

Doctoral Dissertation

In presenting this dissertation in partial fulfillment of the requirements for the Doctoral degree at the University of Washington, I agree that the Library shall make its copies freely available for inspection. I further agree that extensive copying of this dissertation is allowable only for scholarly purposes, consistent with "fair use" as prescribed in the U.S. Copyright Law. Requests for copying or reproduction of this dissertation may be referred to University Microfilms, 300 North Zeeb Road, Ann Arbor, Michigan 48106, to whom the author has granted "the right to reproduce and sell (a) copies of the manuscript in microform and/or (b) printed copies of the manuscript made from microform."

Signature_____

Date_____

University of Washington

Abstract

THE WEST SPITSBERGEN CURRENT:
TRANSPORT, FORCING, AND VARIABILITY

by <u>Dennis</u> <u>Joe</u> <u>Hanzlick</u>

Chairman of Supervisory Committee: Knut Aagaard
Research Professor
School of Oceanography

The West Spitsbergen Current provides the major oceanic influx of heat and mass into the Arctic Ocean. Recent measurements show that the flow has significant lateral structure and exhibits large variability over a broad range of time scales. Wind forcing appears to be particularly important.

During 1976-77, the mean volume transport was 5.6 Sv northward and ranged from 1.4 Sv southward to 11.9 Sv northward. The largest transports occurred in late fall and winter, and the minimum was in March. The corresponding mean heat transport was 46 TW (one tera-watt (TW) = 10^{12}W), with a range of 8 TW southward to 122 TW northward and a seasonal pattern similar to that of the volume transport. The alongshore and cross-isobath turbulent heat fluxes were respectively 1 and 2 orders of magnitude smaller than the alongshore advective mean flux. Three-year long current records showed consistent seasonal fluctuations but little interannual variability between 1976 and 79. However, typical velocities were only about one-half as large as those measured in 1971-72, indicating that significant interannual changes can occur.

Current records indicate lateral structure over the upper slope west of Spitsbergen with cross-isobath length scales of 10-20 km.

The regional wind stress curl can account for the northward volume transport of the West Spitsbergen Current, and the curl and flow are related at the annual time scale. The oceanic response can be in the Sverdrup mode only if forcing is at time scales much longer than a month, and this response will lag the forcing by about six months.

Numerical model results indicate that, while barotropic instability is not an important factor in the variability of the flow, baroclinic instability may contribute to the variability at time and length scales of 3-4.5 days and 30-50 km.

The dispersion characteristics of the second mode coastal trapped wave which could be supported by the stratification and topography west of Spitsbergen include corresponding wavelength and period ranges of 260-1000 km and 4-14 days. The associated velocity structure is essentially barotropic and contains a node over the slope. These features are consistent with observations. Both the first and third trapped wave modes are not important in explaining variability in the range of a few days to a few weeks.

Meandering of the banded flow may contribute to the short period variability, and it is also likely that the northeastward passage of cyclones across the region, in conjunction with bottom topography and the deep extent of atmospheric forcing, contributes to the variability of the flow at time scales corresponding to the frequency of their passage.

TABLE OF CONTENTS

LIST OF FIGURES

v

LIST OF TABLES

ACKNOWLEDGEMENTS

I take pleasure in acknowledging the support and guidance, patience and friendship of Knut Aagaard throughout this work, as well as his confidence in me which sometimes exceeded my own. I thank L.K. Coachman and D.F. Winter for their critical reading of this manuscript.

Steve Harding was instrumental in assembling the current meter moorings, and Clark Darnell was largely responsible for their deployment and recovery. Dick Tripp performed the initial translation of the data tapes into a form suitable for analysis. I thank George Dworski for his advice on techniques of time series analysis.

I thank Herb, the custodian, whose late night humor was a refreshing tonic. I extend particular appreciation to RAC for providing moral support and many timely gastronomic gifts during the latter stages of this work, and to Eileen for her expertise and time in the assembly of this manuscript and for returning me safely from the summits of many cascade peaks.

I am grateful and indebted to those special people whose love and support helped me weather some of the rare darker hours, and whose laughter and good spirits brightened my own even more during the many up-times. They are precious to me.

1. Introduction

The West Spitsbergen Current (hereafter referred to as WSC) is commonly considered to be the northern extension of the Norwegian Atlantic Current, and it forms one of the branches of the circulation pattern of the Greenland-Norwegian sea system. It flows northward along the continental margin west of Spitsbergen, entering the Arctic basin on the east side of the Greenland-Spitsbergen passage (Fram Strait). Previous work (cf. Aagaard and Greisman, 1975) has shown that it provides the major component in the mass and heat balances of the Polar Basin.

Beginning in summer 1976, moored current and temperature recorders have been deployed in the WSC at 79°N, and the data records from 1976-79 and 1980-81 provide the basis for this work. The data have been used to estimate the volume and heat transports by the current and to define the structure and variability of the flow. In addition to the presentation of basic results, there is a discussion of the dynamics of the current with emphasis on explaining the length and time scales of the observed variability and on ascertaining the nature of the forces driving the flow.

1.1 Description of the Greenland-Norwegian sea region

1.1.1 Bathymetry

Figure 1 shows the geographic setting and place names for the Greenland-Norwegian sea region. Deep basins separated by submarine ridges are the dominant features of the bottom topography of the region (Fig. 2). Mohn Rise, a section of the mid-Atlantic ridge, separates the Greenland Sea from the Norwegian Sea to the southeast. The sill depth of Mohn Rise is about 2500 m. The Greenland Sea itself is divided by the Greenland Fracture Zone into a northern basin ranging to 3100 m deep and a southern basin averaging about 3600 m deep. Glaciated continental shelves form the lateral boundaries of the region. Off Greenland, the shelf break generally lies at 200-400 m, while on the eastern side of the basin the shelf break is typically shallower, 100-300 m. The slope region, subtended approximately by the 2500 m and 300 m isobaths, narrows from a width of about 350 km off northern Norway
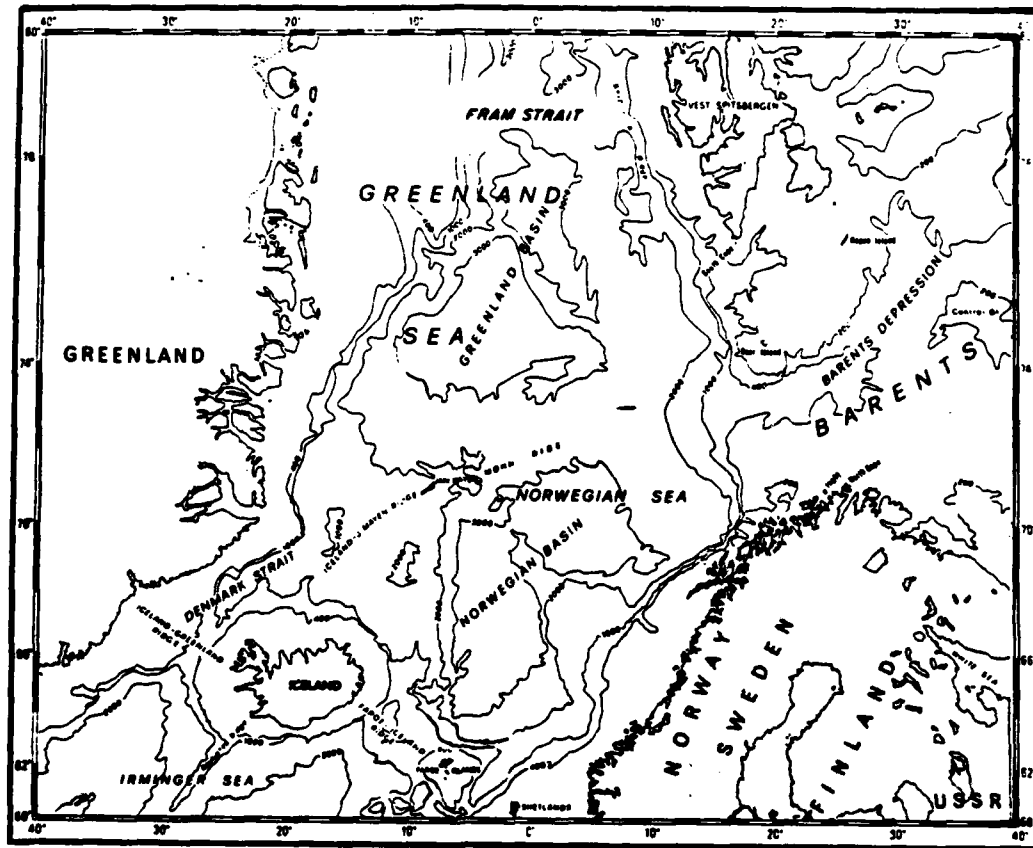
Figure 1.   Geographic setting and place names for the Greenland-Nor-
wegian sea region. (adapted from Trangeled, 1974)

3
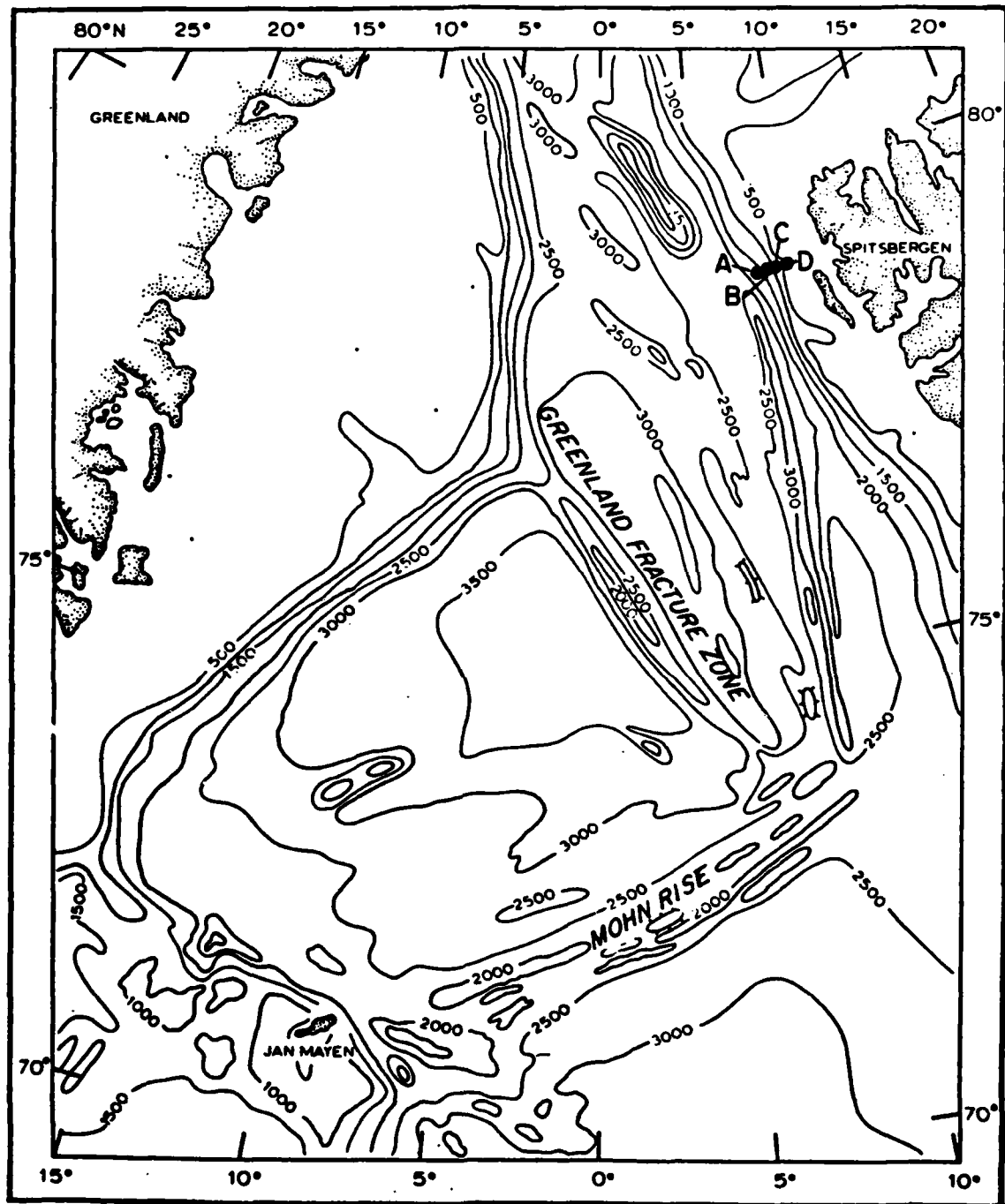
Figure 2.   Bottom topography of the Greenland-Norwegian sea region.
            Depths are in meters.   (from Johnson and Vogt, 1973)

down to 50-60 km west of Spitsbergen. This represents a seven-fold increase in the average bottom slope.

Figure 3 shows the depth profile west of Spitsbergen at 79°N, and the mooring locations where the current records which form the basis of this investigation were obtained. The shallow shelf extends from the Spitsbergen coast westward to about $8^{\circ}45'$E where the depth increases sharply from about 200 m to nearly 1100 m at 8°E, a very steep slope of about 6×10^{-2}. Between 8°E and $6^{\circ}45'$E the depth increases only slightly to about 1300 m, and the bottom slope is a magnitude less than that of the segment nearer shore. West of $6^{\circ}45'$E, the bottom slope increases again, to about 2×10^{-2}, as the seabed descends to a depth of roughly 3000 m at the foot of the continental slope. For the most part, the isobaths west of Spitsbergen run north-south. In the mooring area at 79°N they are oriented along 352° true.

1.1.2 Hydrographic features

The primary focus of this study is on the WSC, and therefore I only note the salient features of the entire Greenland-Norwegian sea region as they bear on the character of the WSC. In the references can be found much more detail of the hydrography and circulation of the larger area.

While the WSC is a major component of the Greenland Sea circulation, it has long been recognized that its ultimate source is much farther south. Consequently, the water properties of the WSC differ from those of the rest of the Greenland sea region.

Several earlier references offer excellent descriptions of the hydrography of the Greenland and Norwegian seas as well as of the Barents Sea. Among them is the classic work of Helland-Hansen and Nansen (1909). Using observations dating from about 1900, they produced the first comprehensive treatise on the oceanographic regime of the area. Much later, Kiilerich (1945) synthesized data collected between 1891 and 1933 into a cohesive discussion of the hydrographic features and circulation. Lee (1963) reviewed the hydrography of the Norwegian, Greenland and Barents seas, summarizing the work up to that time. His discussion centered on the water masses and currents, and included fluctuations in the hydrographic regime and variations in volume transport. Trangeled (1974) provided an exhaustive bibliography
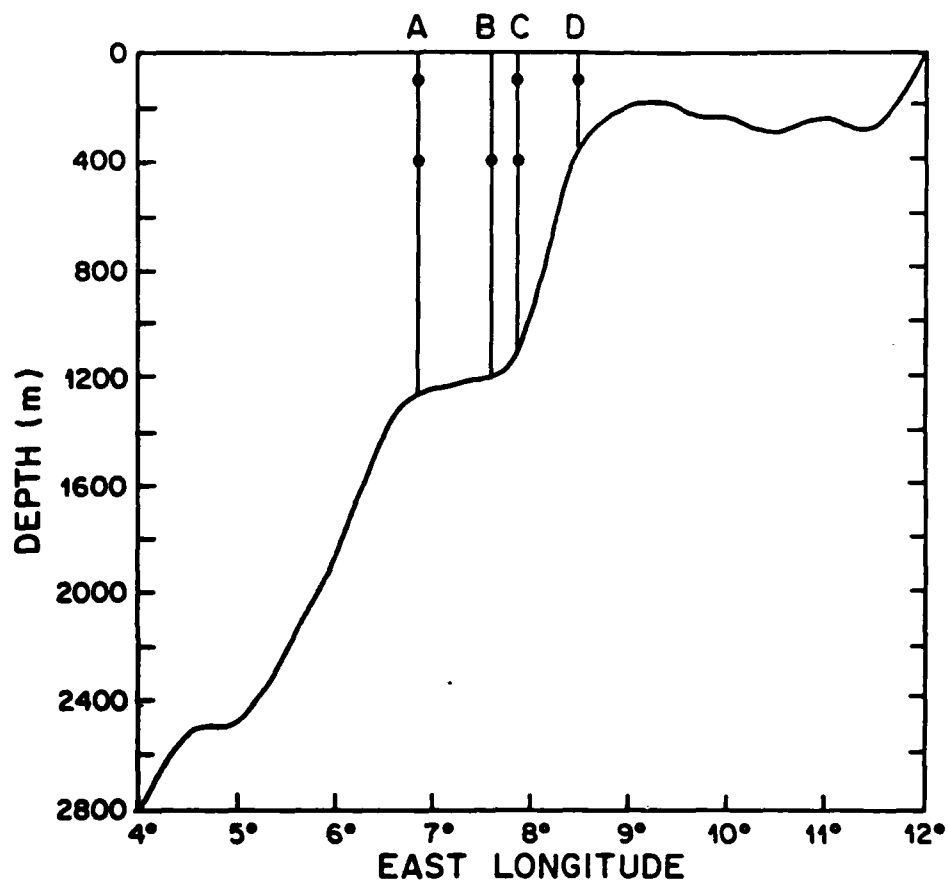
Figure 3. Bottom profile and mooring locations west of Spitsbergen along 79°N. The letters A, B, C, and D identify the respective mooring locations.

and a brief summary of the 1870-1970 literature on the oceanography of the Norwegian, Greenland, and Barents seas as well as the waters around Iceland. While their primary emphasis was on the North Polar Basin, Coachman and Aagaard (1974) also reviewed the oceanography of the Greenland Sea. Their discussion covered the major water masses, features of the circulation, and both wind and thermohaline forcing of the motions. Of recent works dealing with the hydrography of the Greenland Sea, probably the most comprehensive is that of Carmack (1972), upon which the following summary draws heavily. Additionally, Dietrich's (1969) atlas, containing hydrographic sections obtained in the Greenland and Norwegian seas during IGY investigations in 1958, provides a fine visual complement to these other sources. In another context, Swift (1980) also presented a recent overview of the hydrography of the Greenland and Norwegian seas.

Carmack recognized three basic water masses in the Greenland Sea: Alantic water, Polar water, and Deep water. He assumed all Greenland Sea water masses either to be mixtures of these or to be results of local modifications due to surface processes. He identified the deep water as typically having temperatures less than 0C and salinities of 34.85-34.95. This deep water mass, delineated by the 0C isotherm, forms a huge domed feature centered on the prime meridian at 75°N in the Greenland Sea. The WSC, both where it flows northward and where a portion of it curves westward near 77°-80°N, depresses the 0C surface along the eastern and northern perimeters of the Greenland Sea, forming the eastern and northern boundaries of the deep water.

Together, the Atlantic water (T > 0C, S > 34.90) and polar water (S < 34.60) constitute the upper source waters of the Greenland Sea. The upper waters may in turn be categorized as belonging to one of four regions according to the respective current systems. These are 1) the East Greenland Current area, 2) the Greenland gyre area, 3) the Norwegian Current area, and 4) the WSC area, which is the primary concern in this paper.

The East Greenland Current flows southward mainly over the continental margin off the east coast of Greenland. It embodies two water masses: 1) polar water, whose cold temperature (<0C) and relative freshness (30.0-34.0) reflect its polar origin, and 2) Atlantic water which exhibits high temperature and salinity with maxima at the core of

>2.0C and> 35.0, respectively. The layer of Polar water extends downward from the surface to about 150 m. The Atlantic layer occurs between 150-800 m, the result of subsurface contributions of water from both the WSC and the Polar Basin.

The upper water of the Greenland gyre forms a thin layer (50-200 m), and according to Kiilerich (1945) is composed of a mixture of Polar water and Atlantic water. Carmack and Aagaard (1973) characterized the upper water of the gyre by its salinity, between 34.60 and 34.90. Just prior to winter, the overall density of the upper water near the center of the gyre is high, while the vertical stability is fairly low. Carmack and Aagaard viewed the increase in density and the subsequent sinking of this water due to winter cooling as an important part of the deep water formation process. Carmack (1972) pointed out that near the northern and southern edges of the gyre, T-S correlations show a consistent salinity maximum, providing evidence of the zonal movement of Atlantic water.

The West Spitsbergen Current has its immediate origins in the Norwegian Atlantic Current which flows northward into the Norwegian Sea basin. Extending to about 800 m, it is characterized by a monotonic decrease of both temperature and salinity with depth. Polar water is absent as a component of the upper water in this region. Because water temperatures remain warm, 4-5C even in winter, the eastern Greenland-Norwegian sea region is ice free year round. This warm, saline water forms the major component of surface waters in the Norwegian Sea. While the Norwegian Atlantic Current is commonly considered to be an extension of the North Atlantic Current, Reid (1979) has proposed that outflow from the Mediterranean may add a major subsurface contribution.

1.1.3 General circulation

The general pattern of water movement in the Greenland-Norwegian sea basin has been known for hundreds of years. Early in this century, Helland-Hansen and Nansen (1909) charted the basic circulation using modern hydrographic methods. While there have been some modifications and refinements in their scheme since then, there has not been any drastic change in the picture. Figure 4 shows the prominent features of the circulation in the area. The southward flowing East Greenland Current and the northward flowing WSC form the western and eastern
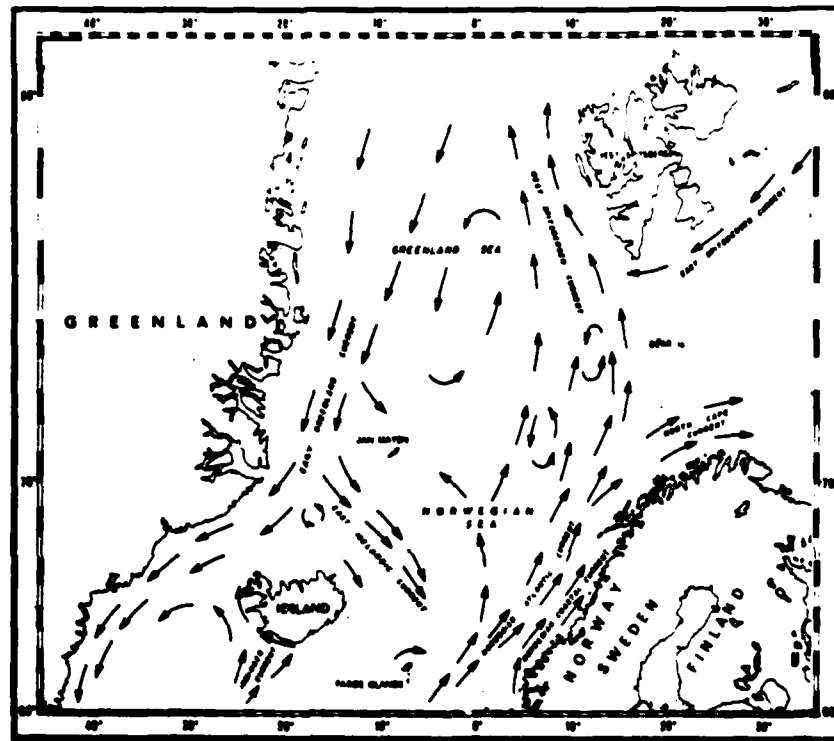
Figure 4. Prominent circulatory features in the Greenland-Norwegian sea region (from Trangeled, 1974).

boundaries of the cyclonic Greenland gyre. Zonal flows close the gyral circulation on the northern and southern edges. Earlier conceptualizations indicated a major cyclonic gyre in the Norwegian Sea, while more recent work (Fuglister, 1954; Alekseev and Istoshin, 1960; Metcalf, 1960; Aagaard, 1970) has shown that the northward flow in the southern and eastern portions of the Norwegian Sea is much broader than depicted earlier. This implies that the Norwegian Atlantic current extends farther west than thought, and that the gyral feature is smaller and displaced farther to the west.

1.1.4 Forcing of the circulation

There have been several attempts to determine the mechanisms responsible for the general circulation. Krauss (1955) argued that the variability of the winds in the area precluded the possibility of their producing the observed circulation. Instead, he proposed a thermohaline forcing mechanism which relied upon coastal freshwater runoff. This implies, for instance, that the Norwegian Atlantic Current is a secondary phenomenon primarily driven by the coastal current. Some support for the idea may be found in variations of the coastal currents around Iceland, which Stefansson (1962) felt were likely maintained by spring and summer freshwater runoff. Coachman and Aagaard (1974) pointed out, however, that rainfall of about 100 m per year ("...high, even for western Norway") would be needed to drive even a modest circulation of the type envisioned by Krauss. Worthington (1970), considering the Norwegian Sea as a mediterranean basin, suggested that replacing the deep, dense outflow to the south from the Norwegian Sea necessitated the inflow of surface waters from the North Atlantic. Thermohaline effects probably do contribute to the circulation, but it may be difficult to ascertain their exact role.

There is also evidence that wind-forcing does play a major role in driving the circulation, contrary to Krauss' (1955) argument. Aagaard's (1970) calculated annual mean circulation driven by wind stress curl was qualitatively similar to the observed circulation. He found that Sverdrup dynamics could account for transports of the magnitudes seen in the Greenland and Norwegian seas; specifically, his calculations yielded a southward return transport of 35 Sv in the East Greenland Current, in agreement with the transport inferred from direct

current measurements. Also, his calculated wind-driven transports of Atlantic water into the Polar Basin through the Greenland-Spitsbergen passage agreed well with transports calculated from dynamic sections. While he termed these agreements fortuitous, his interpretation was that the calculated annual mean wind-driven transports were of realistic magnitudes. He also noted that the wind-driven circulation is largely internal to the Greenland and Norwegian seas.

Semtner (1976) studied the long-term circulation in the Arctic Ocean and Greenland Sea using a three-dimensional, atmospherically forced numerical model. He used the same wind field over the Greenland Sea that Aagaard (1970) used for the mean annual case. His simulation produced a northward flowing Norwegian Current, an intense southward flowing East Greenland Current, a southward return flow of Atlantic water beneath the surface East Greenland flow, and a large cyclonic gyre over the Greenland and Norwegian basins. All these features qualitatively resemble observed features of the circulation in the Greenland and Norwegian seas (Fig. 4).

In connection with observed variability in the WSC, Greisman and Aagaard (1979) proposed that wind stress curl acting over the Greenland-Norwegian sea region drives a northward Sverdrup flow which is ultimately concentrated by topographic effects, and is identifiable as the WSC. Thus, they contended that the WSC and its fluctuations are not driven locally, but by wind forcing over the Greenland-Norwegian sea.

1.2 Description of the West Spitsbergen Current

1.2.1 Hydrographic features

The most obvious characteristics of the WSC are its relatively high temperature and salinity, reflecting its origin far to the south. Water from the North Atlantic enters the southeastern Norwegian Sea through the Faroe-Shetland channel, flowing northward along the continental margin as the Norwegian Atlantic Current. Mosby (1970) assigned typical temperature and salinity values of about 9C and 35.3. to the Atlantic water core in the southeastern Norwegian Sea. Farther north, near the southern tip of Spitsbergen, a contribution from the East Spitsbergen Current slightly freshens the upper layer of the flow and strengthens its shallow (~50 m) halocline. Continuing northward, the

flow loses both heat and salt. Even so, summer temperatures in the upper layers reach 6C and rarely fall below OC in the winter.

Several of the salient features are apparent in Fig. 5, which shows contours of temperature and salinity in vertical sections along 79°N in late summer 1968 and 1969. Notably, in 1969 a core region of high salinity (S >35.2) and high temperature (T> 4C) lay just seaward of the shelf break at about 200 m depth at 7°30'E. Within the halocline in the top 100 m, the salinity increased from 32 to 35, while the temperature increased from about 2C to 4C. The cooler, fresher water near the surface was a contribution of Polar water from the East Spitsbergen Current. In 1968, the center of the salinity core (S> 35.1) lay at about the same position as in 1969. However, in 1968 the halocline region was only about half as thick, and the salinity step was only about 1. Clearly, a marked influence of the East Spitsbergen Current present in 1969 was absent in 1968 at the same location and time of year. Figure 6 (from Greisman, 1976; based on hydrographic data obtained between 1954-72) shows a T-S envelope for the WSC, demonstrating the high temperature and salinity.

Vertical profiles of temperature, salinity and sigma-t obtained in early September, 1977 (Fig. 7) show the marked variation in properties in the upper 50 m. The homogeneity in the upper 25 m gives way to a sharp gradient region between 25 m and 35 m in which the temperature decreases about 1.5C and the salinity increases about 0.2. Below 50 m, the water is nearly homohaline, while the temperature decreases almost linearly. A sharp pycnocline lies at 30 m, and the increase in density in the top 50 m is roughly 1.5 times greater than between 50 and 1000 m. Below 50 m, the density increases by about 0.25 sigma-t units almost linearly down to 1000 m, and the static stability, E, is low, with values in the range 2-3 x 10^{-6} m^{-1}. The extreme changes in vertical structure in the WSC are therefore confined for the most part to the upper 100 m.

1.2.2 Previous estimates of volume and heat transports

Greisman (1976), summarized the results of earlier investigations of the WSC. Of necessity my own review contains some of the same information.
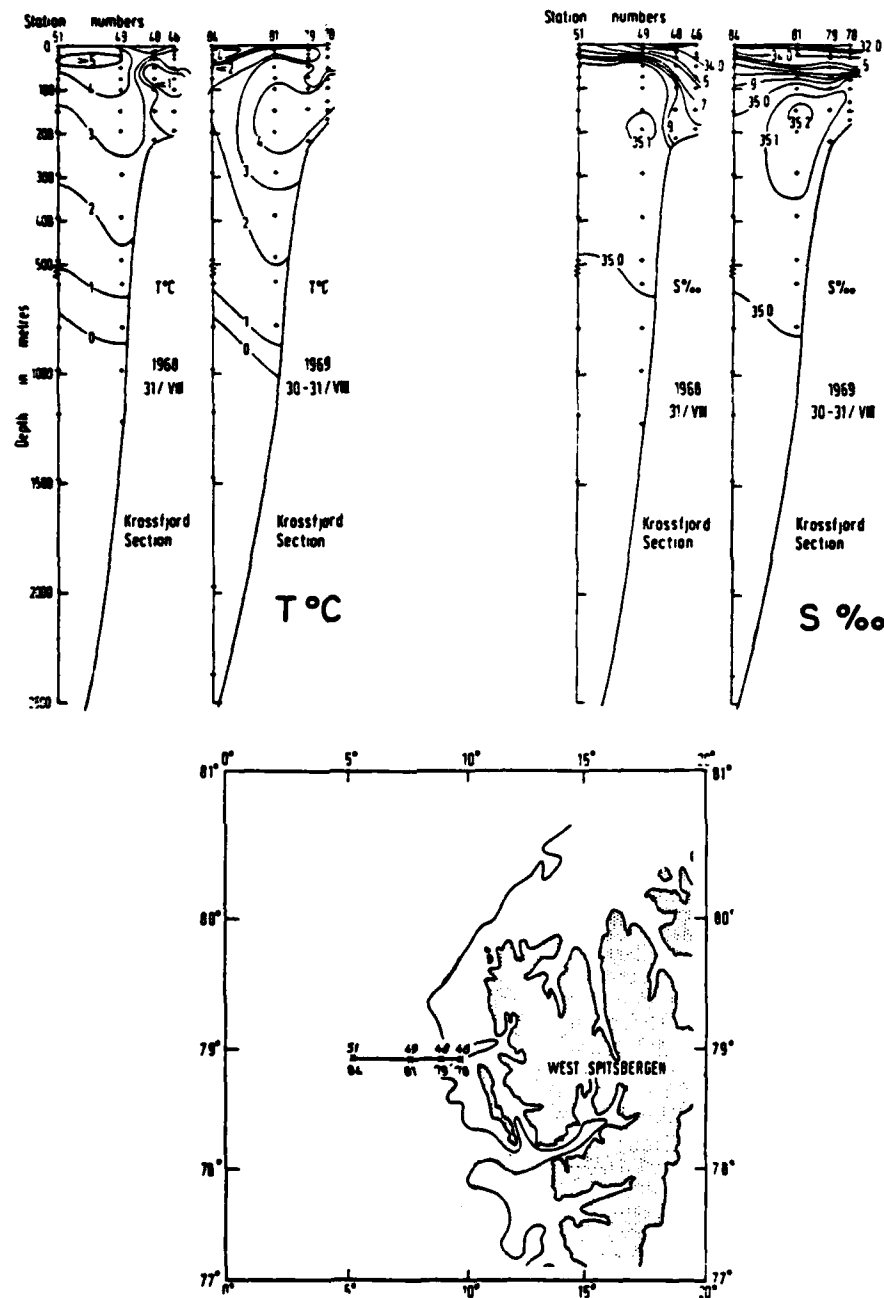
Figure 5. Contours of temperature and salinity west of Spitsbergen along 79°N. Data were obtained in late August of both 1968 and 1969. (from Dickson and Doddington, 1970).
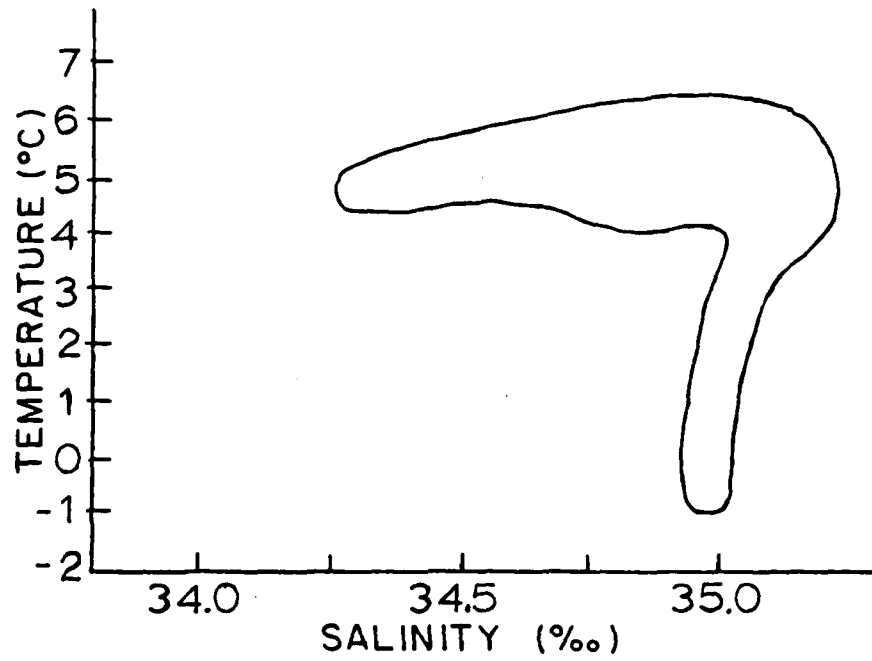
Figure 6.   Temperature-salinity envelope for historical data obtained
in the West Spitsbergen current. (from Greisman, 1976).
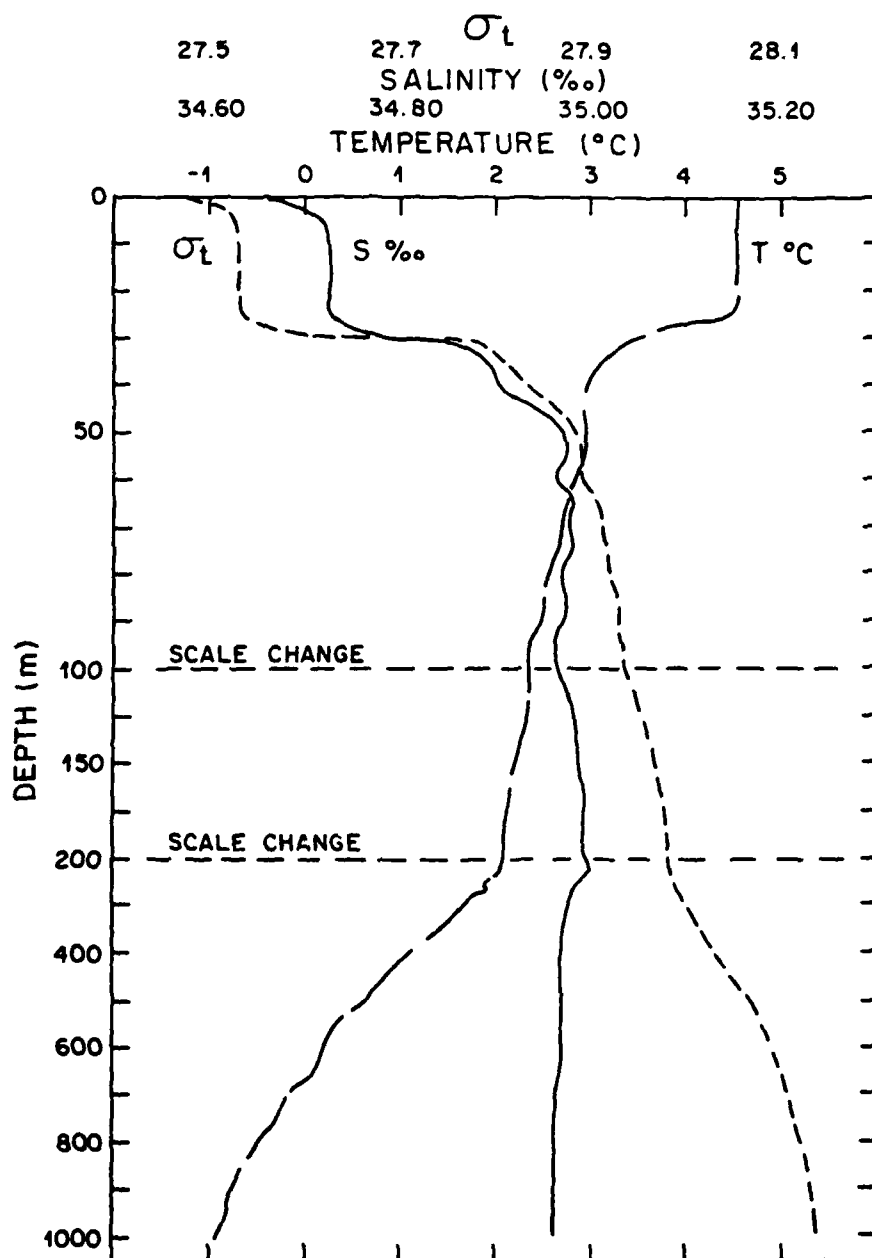
Figure 7. Vertical profiles of temperature, salinity, and sigma-t obtained September 4, 1977 at 78°57'N 7°38'E. Johan Hjort sta. 950.

In a study of the volume transport of the WSC, Hill and Lee (1957) and Lee (1961a) utilized hydrographic observations beginning in 1949. The data were from a section extending west of Bear Island about 80 km across the eastern branch of the current. Referenced to a level of 750 db, their calculated transport above 400 m depth varied between 3.2 Sv to the north and 0.2 Sv to the south. These values are very likely low because: 1) contributions below 400 m were neglected, 2) their survey did not extend westward across the entire stream, and 3) their calculations did not include the barotropic contribution. They determined a semi-annual cycle with maxima in January-February and July and minima in April and October. They also found a correlation between the transport above 400 m and the strength of the southerly wind component during the preceding 10 days.

Kislyakov (1960) published transport values across 74°30'N varying between 6.7 Sv and 0.6 Sv to the north, based on a reference level of 1000 db from data obtained between 1954-59. He also established a correlation between the volume transport above 200 m and the longshore (north-south) atmospheric pressure gradient. Both Kislyakov and Hill and Lee found a residual northward transport when their respective forcing mechanisms were zero.

Using 13 years of hydrographic measurements, Timofeyev (1962) reported a maximum transport across 78°N of about 3 Sv in December-January and a minimum of about 2 Sv in May, relative to 1000 decibars. Mandel (1976) estimated a mean volume transport of Atlantic water in the depth interval 0-500 m of 4.3 Sv. with a maximum of 5.8 Sv in November and a minimum of 2.5 Sv in April. He estimated this to represent about 75% of the transport to a reference depth of 1000 m. His calculations were based on a linear relation between the water level at Barentsburg (~78°N, 12.5°E) and the volume flow of the WSC.

Greisman (1976) was the first to estimate transports using long-term direct current records obtained west of Spitsbergen. From current meter data obtained in 1971-72 on two moorings west of Spitsbergen at 79°N, he estimated a mean northward transport of about 7 Sv. His method involved drawing isotachs of northward velocity in the cross-section during 11 weeks when all current meters were operating, computing the regression relation between the integrated transport and the velocity at one of the current meters over the slope west of Spitsbergen for the

same period, and then using that regression relation along with the entire single current record to estimate a monthly time series of transport during 1971-72. He identified a maximum of 10.7 Sv northward in September and a minimum of about 3 Sv in February. Using hydrographic data from two cruises in 1971 and 1972, he estimated the baroclinic component of the transport at about 3.5 Sv, i.e., one-half the total. One reason for the disparity between Greisman's transport figures and the others above is that the direct current measurements allowed an estimate of the total transport, while the reliance upon dynamic calculations limited earlier investigators to the baroclinic portion only.

Greisman (1976) also used temperature records concurrent with the velocity records to estimate the amount of heat advected into the Arctic basin by the WSC. He calculated a yearly average of about 67 TW, a summer value of 100 TW, and a winter value of 50 TW (one tera-watt (TW) = 10^{12}W). Mandel (1978) calculated a mean heat transport of 28 TW in the 0-500 m depth interval along 78°N between 2°E and the coast of Spitsbergen over the period 1949-74. He identified a seasonal pattern with a maximum in late July and a minimum in April.

Aagaard and Greisman (1975) reviewed previous budgets and formulated new mass and heat budgets for the Arctic Ocean. They showed that the WSC plays a major part in the heat budget, transporting about two-thirds of the oceanic heat flux into the Arctic. It is likely then, that large variations in this flow at very long time scales (months to years) as suggested by earlier investigators may be reflected in changes in the oceanic regime in the Arctic Basin.

1.2.3. Temporal variability

The previous discussions of the WSC have been largely in terms of mean values of mass and heat transports, but there is ample evidence of significant low-frequency variability about the mean values. Figures 8, 9, 10 and Table 1 all demonstrate the probable existence of such variability.

Figure 8, taken from Lee (1961b), shows 2-3 month time scale fluctuations of volume transport as derived from hydrographic data across the West Bear Island section over the interval 1949-1959. Figure 9, from Mandel (1979) shows the year-to-year fluctuations of volume and
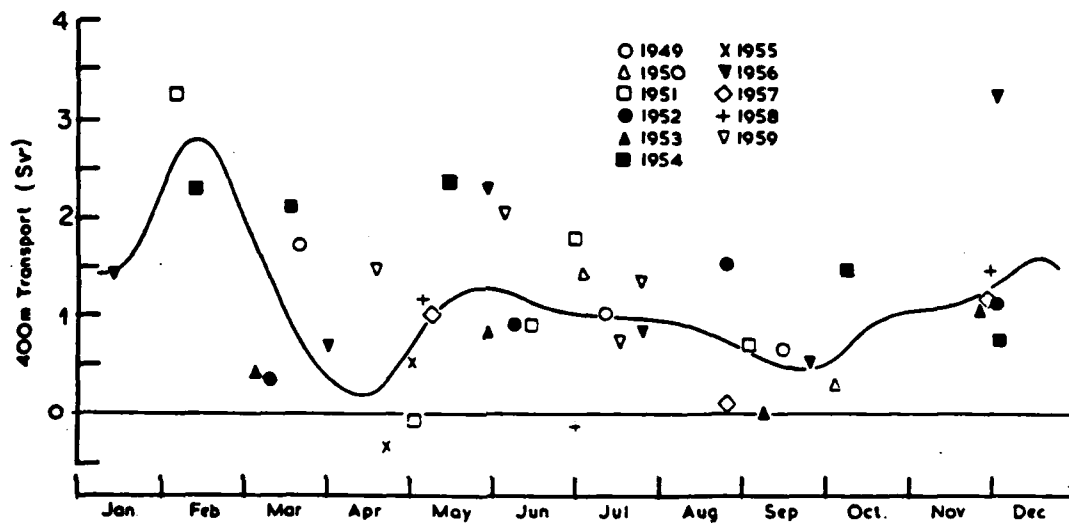
Figure 8.   Volume transport estimates (Sv) for the West Spitsbergen
            Current across the Bear Island section (74°30'N) in the 0-
            400 m layer. The curve represents means over all years.
            Positive sign indicates northward transport. One Sv = 10^6
            $m^3 s^{-1}$. (from Lee, 1961b).
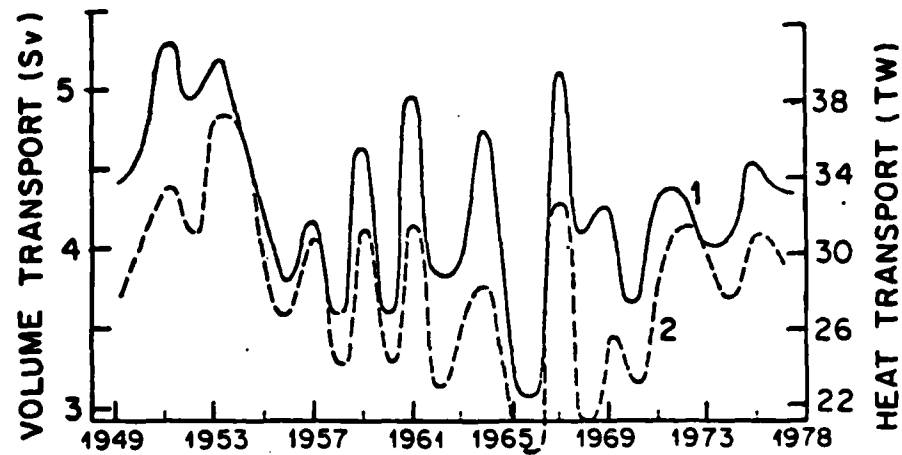
Figure 9.   Volume (Sv, solid line 1) and heat (TW, dashed line 2)
transports of the West Spitsbergen Current northward across
the Barentsberg section at 78°N.   One Sv = 10^6 m^{3}s^{-1}; one
TW = 10^{12}W.   (from Mandel, 1979).
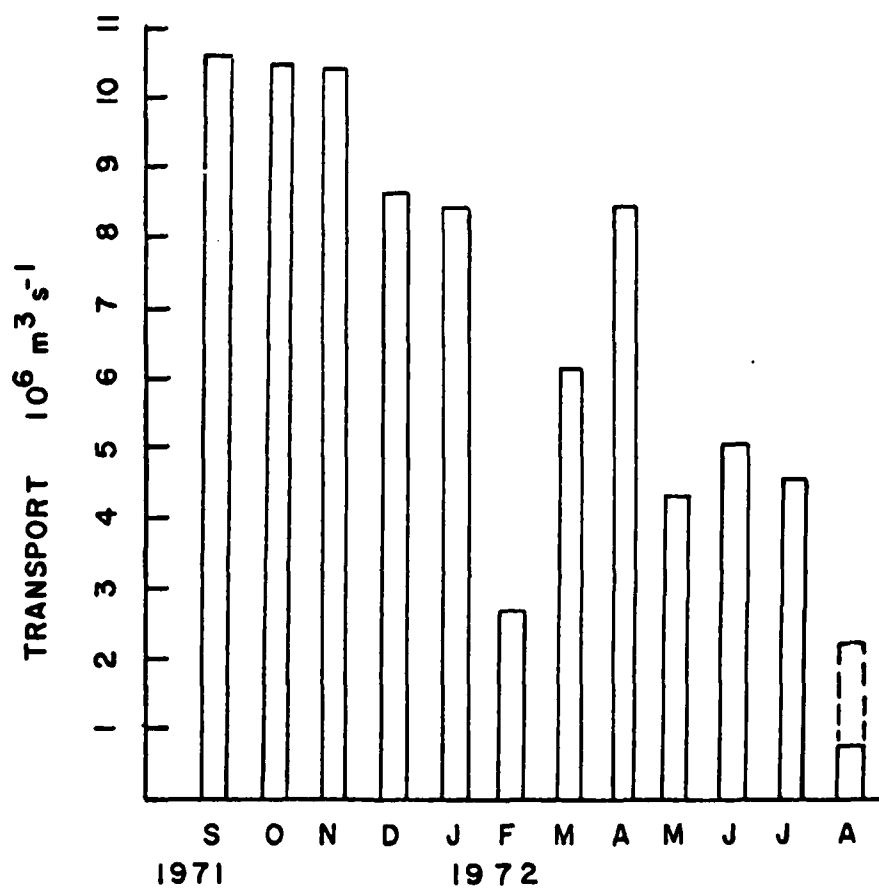
Figure 10. Northward volume transport (Sv) of the West Spitsbergen Current in 1971-72 computed from direct current measurements in conjunction with velocity contours determined from hydrographic data. One Sv= 10^6 m^{3}s^{-1}. (from Greisman, 1976)

Table 1. Annual mean volume and heat transports, and transport
temperature of Atlantic water entering the Arctic basin
across the Barentsburg-ice edge section west of Spits-
bergen along $78^\circ N$, (from Timofeyev, 1962).
One Sv = 10^6 m^3s^{-1}; one TW = 10^{12}W.

Year	Sv	TW	$^\circ$C
1933	2.7	18.7	1.6
1934	2.9	29.4	2.4
1935	2.9	20.7	1.7
1936	3.8	32.1	2.0
1939	3.9	32.1	2.0
1952	2.7	26.3	2.3
1953	3.1	25.4	2.0
1954	3.9	26.8	1.7
1956	3.9	31.0	1.9
1957	2.6	18.7	1.7
1958	3.2	24.6	1.8
1959	2.6	20.0	1.8
1960	2.4	18.2	1.7

heat transports northward across the Barentsburg section at 78°N from 1949-77. These results were obtained from a linear relationship formulated between the monthly-averaged temperature and water level at Barentsburg and the temperature and geostrophic transport of the WSC. Table 1 lists the volume and heat transports for various years between 1933 and 1960 determined by Timofeyev (1962) from hydrographic data obtained along 78°N from Spitsbergen westward to the ice edge. The largest year-to-year variations are on the order of 50%. The monthly transport estimates in Fig. 10, from Greisman (1976), were derived from direct current measurements, and exhibit monthly to seasonal fluctuations. In contrast to the long-term variability noted above, Hill and Lee (1957) provided evidence of variability with a time scale on the order of a few days. They reported on four workings of a section west of Bear Island within 48 hours which gave transport values from about 0.1 Sv southward to 1 Sv northward. Neglecting detailed comparisons, it is clear from the above that the volume flow may be variable over time scales from days to years.

Using hydrographic data taken in late summer of successive years during 1965-1969, Dickson and Doddington (1968, 1970) detected a trend of increasing temperature and salinity in the flow west of Spitsbergen at 79°N. However, they also pointed out the presence of short-term variability. For example, in 1969 the high-salinity core (>35.1) in the section at 79°40'N was larger than that at 79°N, and the temperatures associated with the core were higher than at 79°N. They therefore questioned the validity of regarding the hydrographic changes between successive annual surveys as true interannual changes, because of aliasing by the short-term variability of the flow.

The temperature of the WSC also appears to fluctuate in time, which in turn influences heat transport estimates. Solonitsina (1976, 1978) has described low-frequency temperature fluctuations in the WSC, both seasonal and interannual. Table 1 includes temperatures used by Timofeyev (1962) to calculate heat transports of the WSC at 78°N for various years between 1933 and 1960. These temperature values represent essentially the depth-averaged temperatures over the upper 1000 m. The greatest apparent interannual change, 0.80C, occurred between 1933 and 1934, but other years also showed large variability.

1.2.4 Spatial variability

Many investigators have presented evidence of spatial variability in the flow on the eastern side of the Greenland and Norwegian seas. Helland-Hansen and Nansen (1909) recognized a pattern of waviness in the isolines of their vertical sections in the Norwegian Atlantic Current. They termed the undulations "puzzling waves", and postulated that they were due either to large lateral variations of the currents or to internal waves, favoring the former. Later observations (Helland-Hansen, 1934) seemed to support the idea that the waviness corresponded with lateral variations in the flow. Lee (1959) concluded that the waviness was probably due to vortices about 10 km in diameter and that the system of vortices changed only slowly. Saelen (1963) believed that the waviness was due to eddies, both stationary and moving, and Dickson (1972) suggested that the Norwegian Atlantic Current was made up of a number of streams fairly constant in position, producing a pattern of wavy isolines with a scale of 40-80 km which approximately followed bottom contours.

Earlier, Alekseev and Istoshin (1956) had published a chart of surface currents using primarily data obtained from post-World War II Soviet hydrographic work. Although they gave no estimates of the lateral scale, the lower limit would correspond to their station spacing, which was typically 20-40 km. Their chart portrayed the Norwegian Atlantic Current as splitting into eastern, western and central branches which reunite farther north to form the WSC. Furthermore, they asserted the existence of elongated eddies between the various streams and branches, and they concluded that a close link existed between the patterns of flow and the bottom topography. Kislyakov (1960), looking at hydrographic observations at intervals of 24 km between 7°-16°E across $74^\circ30'$N, identified four different northward flowing streams. According to his findings, the number of streams remained constant, but their positions varied laterally 16 to 24 km to either side of a mean position. Interestingly, he also found that velocity fluctuations among the streams tended to be out of phase. Further evidence of the banded structure comes from a chart of geopotential topography by Eggvin (1961) which clearly shows three streams of the WSC with a typical scale of 50 km west of Bear Island. Rudels and Andersson (1982) presented a velocity section across Fram Strait at

79°N which was derived from hydrographic data and referenced by direct current measurements. A region of reversed velocity in the WSC suggested the scale of the lateral structure in the flow to be about 15 km. In addition, a separate data set containing data obtained at intervals of about 10 km shows core-like features in temperature contours in a section along 80°N. These features indicate lateral structure in the flow, as does the 20/400 db dynamic height anomaly which exhibits three obvious maxima between 2°-11°E (Fig. 11).

With respect to the WSC and the Norwegian Atlantic Current, the implication of these investigations is that the entire system is composed of a filamentous structure of northward flowing streams separated by elongated eddies. The length scales associated with the lateral structure appear to range from kilometers to tens of kilometers.
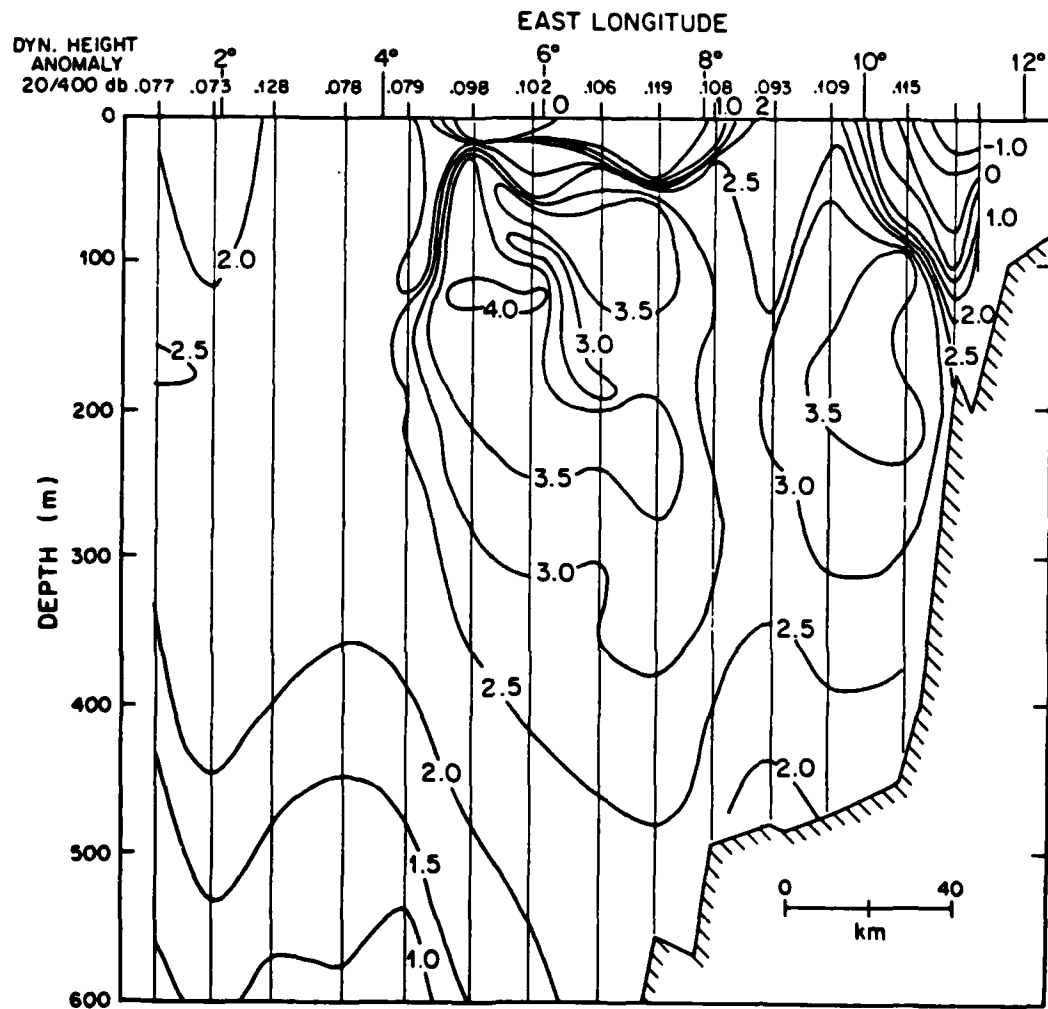
Figure 11. Temperature contours and dynamic height anomaly (dyn. m, 20/400 db) west of Spitsbergen along 80°N obtained November 26-27, 1977. <u>Polarsirkel</u> cruise. (prepared by S. Hillman).

2. Experimental design, data sources

2.1 Mooring details

During successive years beginning in July 1976, direct current measurements were made at various locations in the WSC. Figure 3 shows the positions of the four moorings deployed the first year. The following year, after recovery of the previous year's moorings, new moorings were deployed at locations B and C and, after that, only at location C. The taut-line moorings (using Kevlar line) carried two current meters each, suspending the upper instrument at a depth of about 100 m and the lower at about 400 m. Sampling intervals were 40 minutes for the first year and 60 minutes for the following years. Table 2 gives the basic deployment details for all the current meters used in this study.

In order to minimize the effect of the recirculating flow on estimates of volume transport, i.e., to restrict the estimates to that which actually passes into the Arctic basin, the mooring section was located along 79°N, which is north of the region where the recirculating flow curves westward. The varying lateral spacing of the moorings was designed to allow the estimation of several different length scales across the flow, while the 300 m vertical separation of current meters permitted some investigation of the vertical structure in the upper part of the water column.

Each mooring used an AMF model 242 release, Aanderaa RCM-4 current meters, and subsurface steel sphere flotation. The internally recording current meters used a modified Savonius rotor magnetically coupled through the pressure case to count revolutions over the sampling interval, providing an average speed for the interval. A thermistor and magnetic compass gave instantaneous temperature and direction values at the end of each sampling interval. A large vane oriented the current meter with the flow.

The current meter rotors were calibrated by towing at known speeds in a tow tank operated by the U.S. Army Corps of Engineers at Bonneville, Washington. Thermistors were calibrated at the NOIC facility in Bellevue, Washington, and magnetic compasses were calibrated at Sand Point Naval Air Station in Seattle, Washington. The calibration procedures were the same as detailed by Greisman (1976).

The Aanderaa data tapes were read, edited and converted to 7-track computer-compatible tape at the Department of Oceanography Computer Services facility. An initial machine scan produced a listing of the data and flagged the speed values considered unreasonable. The data listing was used to establish start and end times for the record manually and to correct obviously erroneous speed values by linearly interpolating between the nearest acceptable data points. Subsequent analysis of the edited data was done on the computers at the University of Washington Academic Computer Center.

2.2 Measurement errors

Aanderaa RCM-4 current meters have been used widely, and their performance is well documented. After calibration, errors in speed indications may range up to 2-3 cm s^{-1}, and compass errors are probably in the vicinity of 5°. Thermistors are accurate to within $\pm$ 0.1C and appear stable over time. Among the current meters, the maximum speeds recorded ranged to 75 cm s^{-1}, while the means were about 5-15 cm s^{-1}, so that errors were approximately an order of magnitude greater than the expected instrument error. With the upper current meters at 100 m depth and with subsurface flotation, contamination due to surface effects or to pumping by vertical mooring motions is within the error limits of the data.

2.3 Hydrographic data sources

Table 3 lists ship cruises which provided hydrographic data used in this investigation. Hydrographic coverage in the mooring area is sparse, especially in winter. Some stations were taken in conjunction with mooring deployment and recovery, providing hydrographic data concurrent with direct measurements. In general, suitable geographic position and confidence in the accuracy of the data were the two primary considerations in selecting the hydrographic stations, although the most serious problem was probably wide lateral spacing.

2.4 Designation convention for current records

A simple convention is adopted for identifying the year, mooring location, and depth of the various current records mentioned in the subsequent discussions. The format used is My-ddd; where M is the

Table 2. Details of current meter moorings deployed near 79°N in the West Spitsbergen Current.

Current Record	Water Depth (m)	Latitude (°N)	Longitude (°E)	Depth (m)	Start	Stop
A1-98	1248	78°58.8'	006°54.1'	98	07/16/76	09/02/77
A1-398				398	07/16/76	09/04/77
B1-398	1198	78°57.0'	007°38.0'	398	07/15/76	09/04/77
C1-92	1142	78°57.8'	007°53.6'	92	07/15/76	09/01/77
C1-392				392	07/15/76	08/31/77
D1-93	343	78°59.2'	008°32.1'	93	07/15/76	08/17/77
B2-110	1210	78°57.2'	007°35.6'	110	09/05/77	08/19/78
B2-410				410	09/05/77	06/20/78
C2-100	1150	78°58.3'	007°50.6'	100	09/05/77	08/19/78
C2-400				400	09/05/77	08/19/78
C3-100	1150	78°58.8'	007°50.0'	100	08/20/78	06/23/79
C3-400				400	08/20/78	06/07/79
C5-84	1124	78°47.7'	007°33.8'	84	09/09/80	07/29/81
C5-384				384	09/09/80	04/20/81
C5-984				984	09/09/80	06/08/81

mooring location, either A, B, C or D; y is the year number with $y = 1$ for 1976-77, $y = 2$ for 1977-78, etc.; and ddd is the depth in meters at which the current record was obtained. Thus A1-98 refers to the current record obtained at mooring location A during 1976-77 at a depth of 98 m, and C3-400 refers to mooring location C, 1978-79, and depth of 400 m. The designation CB refers to bridged current records from location C.

Table 3. Cruises which provided hydrographic data used in this study.

Ship	Year	Month	NODC ID
Armauer Hansen	1926	8	580259
Atka	1954	1	310445
G.O. Sars	1956	10	580999
Ernest Holt	1957	5, 7	740709
G.O. Sars	1958	4, 5, 6	580013
Johan Hjort	1958	9	580957
Atka	1962	7, 8	310965
Edisto	1964	9	310296
G.O. Sars	1965	5	580064
Arvakur	1971	9	
Meteor	1972	7	060157
G.O. Sars	1976	7	
Johan Hjort	1977	9	
Polarsirkel	1977	11	

3. Volume transport of the West Spitsbergen Current

3.1 Data preparation and transport calculation method

The current records from moorings A, B, C and D were used to calculate the volume transport of the WSC during the 1976-77 deployment interval. Tides and higher frequency signals were first removed by applying a filter with a cutoff of 40 hours. Filtering was accomplished by Fourier transforming, zeroing the coefficients which corresponded to those frequencies beyond the desired cutoff, cosine-tapering the truncated end, and then transforming back to the time domain to construct the filtered data series. The resulting time series were then sub-sampled at 24-hour intervals. To arrive at a suitable averaging interval for the data, the autocorrelation function was calculated for each of the north-south velocity records. After Davis (1976) and Bryden and Pillsbury (1977), the time scale of independence (TSI) for the respective records is:

$$TSI = \sum_{\tau=-m\Delta t}^{\tau=+m\Delta t} C^2(\tau)\, \Delta t \ ,$$

where $m\Delta t$ is the greatest lag τ for which the autocorrelation $C(\tau)$ differs from zero at the 95% confidence level. The TSI is the time interval beyond which successive velocity measurements may be considered to be statistically independent of each other. The TSI for the downstream velocity components varied from about 8 days to 19 days and averaged 13.7 days. The final data series used to estimate volume transports were then obtained by averaging the 24-hour data over 14-day intervals.

Figure 12 shows the cross-section used for calculating the transport of the flow. The spatial limits for the flow were chosen according to criteria outlined below, and within the zero isotach the current meters were assigned sub-areas to which their respective measurements applied. The deeper current records at moorings B and C were highly correlated (see Table 4), and so those velocities were averaged before making the transport calculations.

The western limit of the current was taken to be $3^\circ 30'E$ after considering hydrographic data and the direct current measurements from 1971-72. The hydrographic data showed a sharp decrease of the tempera-
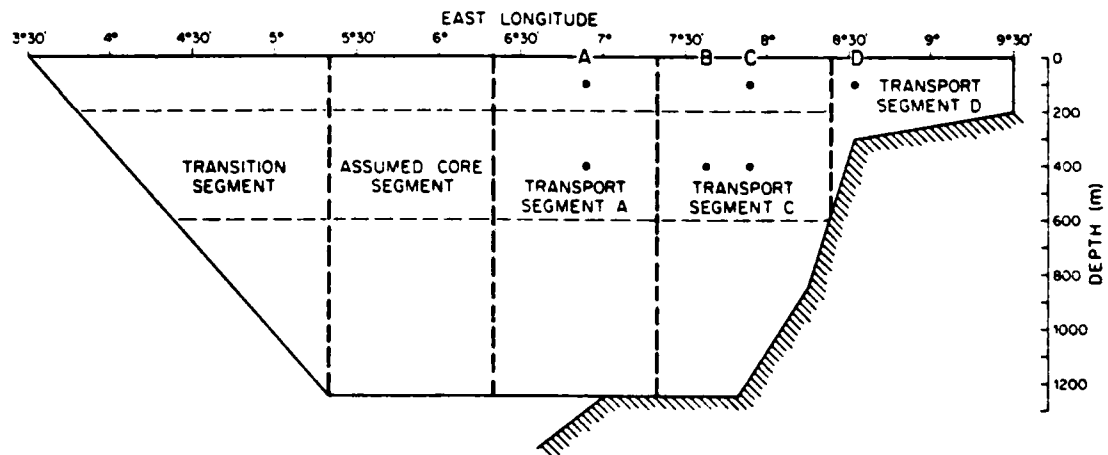
Figure 12. Cross section used in this study for calculating volume and heat transports of the West Spitsbergen Current. Segment designations correspond with mooring location designations. Flow was considered barotropic below 600 m.

Table 4. Cross-correlation coefficients for records of alongshore velocities at four mooring sites in the West Spitsbergen Current during 1976-77. R_u and R_l respectively represent the cross-correlation at zero lag between upper and lower pairs of current meters on the various moorings.

Site	B	C	D
A	-------	$R_u = -.42$	$R_u = +.16$
	$R_l = -.41$	$R_l = -.52$	-------
B		-------	-------
		$R_l = +.71$	-------
C			$*R_u = -.03**$
			-------

*Maximum value was +.30 with D leading C by 37 days.

**This value not significantly different from zero at the 95% confidence level.

ture at 30 m depth between 3^0-4^0E. This temperature transition is one indication of the frontal boundary between the WSC and the East Greenland Current, and the location is approximately the same as that determined by Greisman (1976) by linear interpolation between sets of current meter data taken both near the southward flowing East Greenland Current and near the highest velocity core of the WSC.

The eastern limit was set at $9^0$30'E, well shoreward of the shelf break. Transports east of $9^0$30'E calculated from geostrophic velocities referenced to 250 db were about 0.3 Sv, so that excluding this region probably introduces an error of less than about 10-15%, even if a barotropic component of equal magnitude is included.

Figure 13 shows contours of dynamic height referenced to 600 db. The dynamic height values were obtained by averaging the available data from various cruises near 79^0N by one-degree bins between 2^0-4^0E and by half-degree bins between 4^0-9^0E. The number of stations averaged ranged from 2 to 11, with the densest coverage between 6^0-9^0E. Mooring locations A and C appear to lie in separate velocity cores (Fig. 13), and the dynamic field indicates the presence of a third velocity core between 5^0-6^0E. With the contour plot of dynamic heights as a guide, the transport section was partitioned into five segments. Three of these corresponded to the three mooring locations A, C and D, the fourth encompassed the third core between 5^0-6^0E, and the fifth included the westernmost fringe across which the velocity was assumed to linearly approach zero at $3^0$30'E. The vertical boundary between mooring A and C segments was assumed to be the midpoint between them, and that between mooring C and D segments was assumed near the shelf break. Preliminary transport calculations for only mooring A and C segments yielded values of about 1 to 2 Sv in each. The transport of the indicated core between 5^0-6^0E was assumed to be comparable. Specifically, the segment for that core was assumed to be the same size as mooring segment A, and the mooring A current records were taken to be representative of the velocities in the assumed segment. Essentially, mooring segment A was doubled in area to include the westernmost core at 5^0-6^0E indicated by the hydrographic data.

Baroclinic contributions to the transport were considered negligible below 600 m. This depth was determined by averaging and contouring the available hydrographic data by one-half degree intervals between
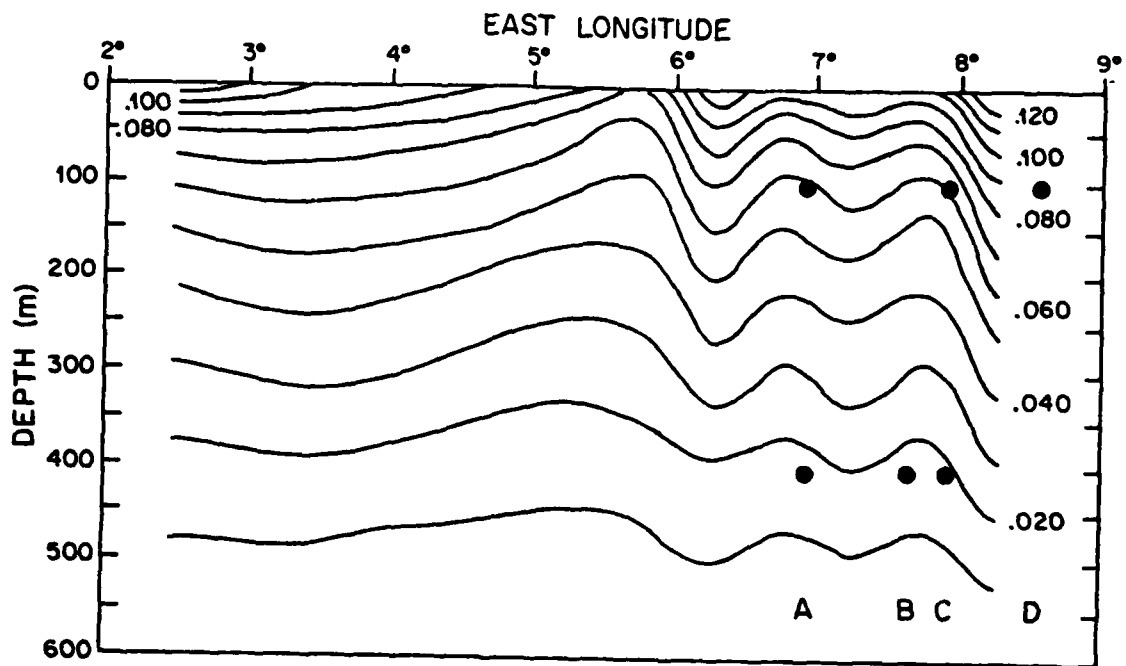
Figure 13. Contours of dynamic height anomaly (dyn. m, 0/600 db) west of Spitsbergen along 79°N. Values were obtained by averaging available hydrographic data by one-degree bins between 2°-4°E and by half-degree bins between 4°-9°E.

5^0-9^0E, calculating average dynamic depths, and then selecting the geometric depth at which the vertical gradient of dynamic depth became nearly uniform across the flow. The 600 db reference level corresponds with that determined by Palfrey (1967) and Greisman (1976). Calculations using more recent hydrographic data from various stations across the current indicated that the contribution of geostrophic transport from the 600-1000 m depth interval could amount to 10-25% of that above 600 m; this was judged sufficiently small that baroclinicity below 600 m was neglected. The velocity between 600 m and the lower boundary of the section was assumed to be entirely barotropic and was assigned a constant fraction of the velocity measured at 400 m depth. This fraction, 0.86, was determined by assuming a linear velocity profile, performing a linear regression between the upper and lower northward current speeds at moorings A and C, and using the resulting slope to extrapolate the velocity to 600 m.

From $9^0$30'E, the zero isotach coincides with the sea bottom westward to about 7^0E where the bottom slope increases by a factor of three. From about 7^0E the zero isotach extends horizontally at a depth of about 1250 m westward to $5^0$20'E, which marks the eastern edge of the assumed transition zone. From this point the zero isotach angles upward to the west and intersects the surface at $3^0$30'E. This shape resembles that used by Greisman (1976, p. 38), although it was arrived at differently. It also incorporates an assumption that speeds in the WSC diminish across the transition region toward the East Greenland Current, essentially providing a conservative transport estimate. Placing the zero isotach at 1250 m depth admittedly contradicts the assumption that below 600 m the flow is entirely barotropic. Including the area in the section between 1250 m depth and the bottom between $3^0$30' and 7^0E and basing the velocity on the mooring A current measurements would at most add slightly more than 1 Sv to the total transport. Direct current measurements do show a mean northward velocity component of 3.9 cm s^{-1} during 1980-81 at 984 m depth at mooring location C, but there are no direct current data available for the deep region west of about 7^0E. Omitting this western deep region by placing the zero isotach at 1250 m thus reflects the choice to seek a conservative estimate of the total transport.

3.2 Lateral structure of the flow

Rather than simply being spatially uniform, or even uniformly varying, the north-south (v-component) velocity field in the mooring section west of Spitsbergen shows significant variation across the stream. Note the waviness in the geostrophic field (Fig. 13), with its implied geostrophic velocity structure between 5°-9°E. Since one degree of longitude at 79°N corresponds to about 21 km, the dynamic height contours indicate a fairly small spatial scale of about 20 km for the variability. Figure 11 shows similar evidence of lateral structure at 80°N.

The weekly mean velocities for 1976-77 plotted as stick diagrams (Fig. 14) illustrate the spatial and temporal variability. One immediate observation is that the speeds varied markedly among the moorings, more so laterally than vertically. Sudden reversals occurred at moorings B and C around January 1, 1977 which are not common to the records from A and D. Over the last three months of the deployment, speeds at mooring C increased by a factor of three. No such strong trend appeared at any of the other moorings, even B which was only 5.5 km away. In addition, the speeds at C1-392 actually exceeded those at C1-92 at C over those final 3 months. As well, the directional variability differed markedly among the moorings; the current was most nearly unidirectional at mooring D and least so at mooring A. This is likely due to several factors: 1) the strong influence of topography at mooring D constrained the flow there to follow bottom contours; 2) the greater distance of mooring A than mooring C from the very steep portion of the slope region, which allowed for less of a channeling influence at mooring A; and 3) the location of mooring A near a sharp discontinuity in bottom slope made for increased sensitivity to small perturbations which increased the incidence of fluctuations in direction as the flow adjusted to conserve potential vorticity.

The results of cross-correlation calculations (Table 4) show the cross-stream structure to be rather complicated. Records of C1-92V and D1-93V are essentially uncorrelated at zero lag, so that the 14 km separation between the two is greater than the local correlation length scale (refer to Fig. 3 for mooring locations). In contrast, the analogous correlation between A1-98V--D1-93V, separated by 35 km, is 0.16,
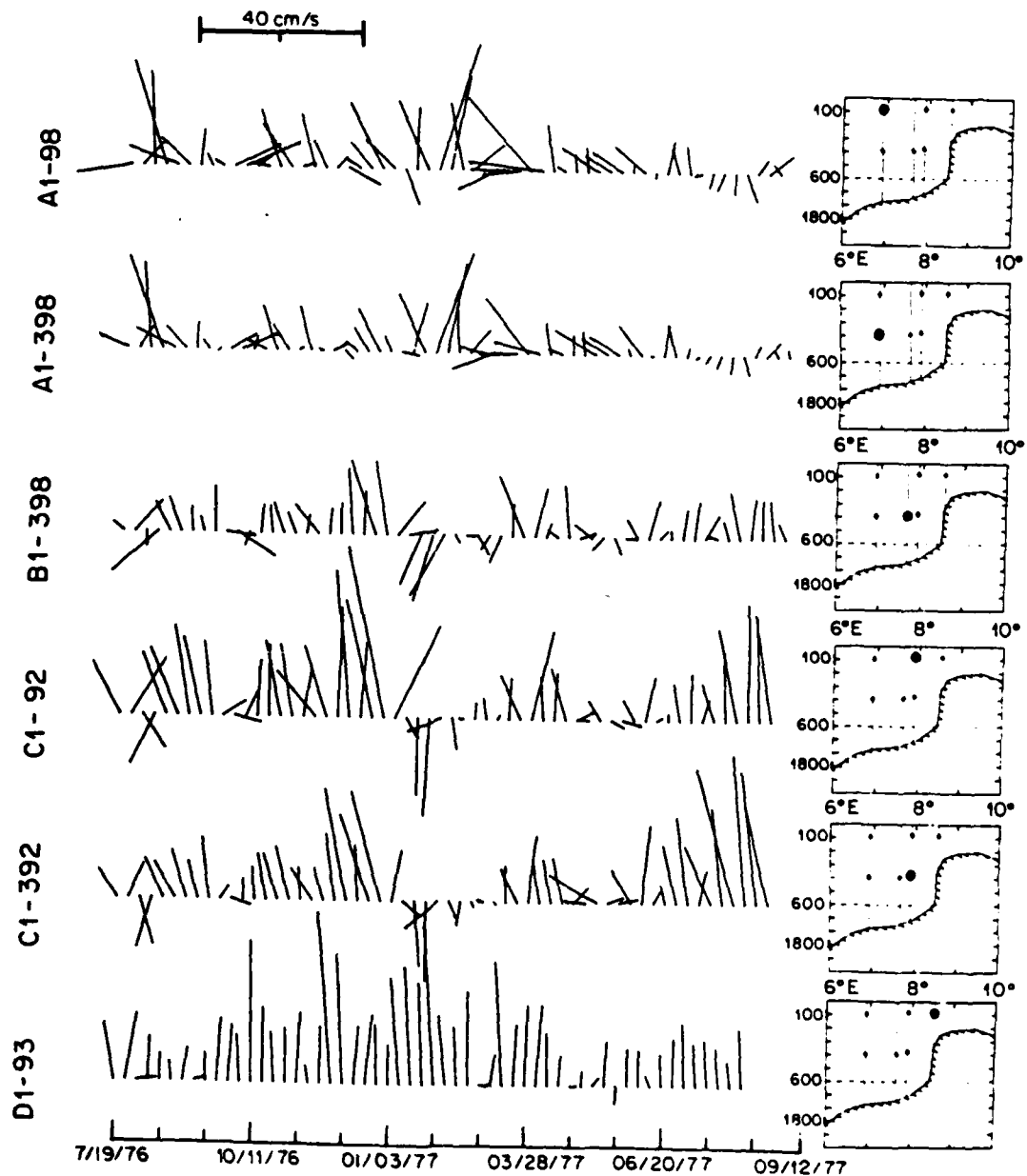
Figure 14.   Stick diagrams of weekly mean velocity for all current records obtained in 1976-77. Current meter locations are shown at the right.

significantly different from zero at the 95% confidence level. Interestingly, the cross-correlations between Al-398V--B1-398V, and between Al-98V--C1-92V and Al-398V--C1-392V are consistently and significantly negative. This means that periods when the velocity at mooring C exceeded the local northward mean at C corresponded with periods when the velocity at A was less than the northward mean at A, and vice versa. One effect of this complicated cross-stream structure is to increase the error in estimates of the volume transport.

3.3 Estimation of rms error

Fandry and Pillsbury (1979) presented an objective method of estimating the barotropic transport across an oceanographic section, and they applied it to the transport of the Antarctic Circumpolar Current through Drake Passage. With this method, the values for the rms error in the objective estimate of the transport depended upon the number of current meters at a given level, on the correlation length scale of the flow, and on the noise. Specifically, using a spatial correlation function everywhere positive, they found that for current meter spacing less than or equal to the correlation length and for measurement noise variance less than 10%, the rms error in the transport estimate is less that 20%. For current meter separations larger than the correlation length or for a spatial correlation function which crosses zero, the error can be 2 to 3 times greater.

Applying this method rigorously to the WSC is not possible for several reasons: 1) the spatial correlation function is complicated and does cross zero, 2) the current meter moorings are not equidistantly spaced, so that the velocities cannot simply be linearly averaged, and 3) the current meter mooring separation is not always less than the correlation length scale. Nevertheless, the Fandry and Pillsbury method provides at least a guide line for estimating the probable error in the transport. Their Fig. 2a (p. 451) shows that for a spatial correlation function which crosses zero and for data spacing somewhat greater than the correlation length scale, the rms error in calculated transports is in the neighborhood of 0.8, i.e., about 80% of the transport value. Thus, the probable errors in the transport estimates of the WSC are roughly as large as the estimates themselves.

3.4 Volume transport based on all current records, 1976-77

The solid curve of Fig. 15 is a plot of the volume transport of the WSC computed from direct current records obtained during 1976-77. Calculations were based on the cross section portrayed in Fig. 12.

3.4.1 Mean and range

During 1976-77, the transports averaged by two-week periods over the deployment interval ranged from 1.4 Sv southward to 11.9 Sv northward. The average was 5.6 Sv northward and of this, approximately 1.9 Sv was below 600 m depth. Assuming that the barotropic flow per unit area of transport cross section above and below 600 m was about the same, then the ratio of cross-sectional areas above and below 600 m gives a barotropic component above 600 m of 2.7 Sv, and together with the contribution from deeper than 600 m, the total barotropic transport for the entire section is 4.6 Sv. The difference between the total transport and the barotropic transport is then 1.0 Sv and corresponds to the baroclinic contribution. This is only one-half the baroclinic transport value of 2 Sv between $3^{o}30'-8^{o}30'E$ referenced to 600 db calculated from hydrographic data obtained during a single cruise in November, 1977. However, it does agree more closely with a value of 0.7 Sv calculated from the bin-averaged hydrographic data.

Timofeyev (1963) calculated an absolute value of about 3.0 Sv for the volume transport of the WSC. This figure is less than the total transport of 5.6 Sv estimated from the present current meter data, but roughly three times the estimated value of 1.0 Sv for the baroclinic contribution during 1976-77. Timofeyev's hydrographic data were sparsely distributed among months and years, so that in 9 of the 13 years, transport estimates were drawn from only a single section. Mandel (1976) estimated a mean volume transport of the WSC in the 0-1000 m layer to be 5.7 Sv. His computational method involved formulating a relationship between the water level at Barentsburg and the geostrophic velocity across $78^{o}N$ as determined from hydrographic data and referenced to 1000 meters. He then used monthly mean water level data to estimate the inflow of water into the Arctic basin over the interval 1949-73. Greisman (1976) calculated a total mean annual value of 7 Sv. This is the only other estimate based on direct, long-term current measurements.
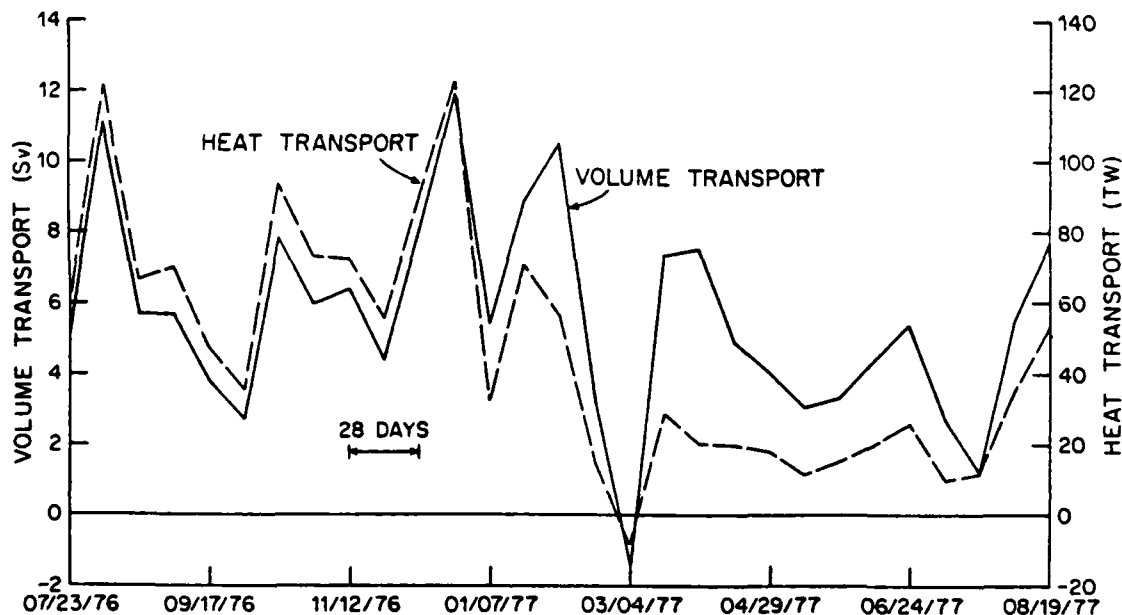
Figure 15. Estimates of volume (Sv) and heat (TW) transports of the West Spitsbergen Current in 1976-77. Estimates are based on two-week averages of direct measurements of alongshore velocity and temperature obtained west of Spitsbergen along 79°N. Positive value means northward transport. One Sv = 10^6 m^3s^{-1}; one TW = 10^{12}W.

Various other investigators: Lee (1961b), Kislyakov (1960), Mosby (1938), and cited in Mosby (1962); Laktionov (1959), Zaitsev (1960), Zaitsev, et al. (1961), Treshnikov (1960), have estimated the mean volume transport of the WSC using hydrographic data. Their estimates ranged from about 1 to more than 4 Sv, but they were based on data from various latitudes and seasons, on sections of different lateral extent across the flow, and on differing reference levels, so that a comparison does not seem possible.

After investigating the reference levels used in the WSC by previous investigators, Palfrey (1967) reached the conclusion that either 600 db or 1000 db could be used (Timofeyev chose the 1000 db reference level). However, as shown in Table 5, the mean velocity shears in the upper part of the water column calculated from direct current measurements show that the degree of baroclinicity does vary markedly. Over the same depth range, the vertical shear ranged from 0.003 to 0.0163 cm s^{-1} per m between 1976 and 1981. Specifically, the vertical shear during 1976-77 was about one-half that observed in any other year, and the values of 0.84 and 0.86 for the ratios of mean velocities (A1-98V/A1-398V and C1-92V/C1-392V, respectively) were noticeably higher than for other years. This is consistent with only a small baroclinic contribution to the transport during 1976-77.

However, note that in 1980-81, the only period which included a deep moored current meter near 1000 m, the mean vertical velocity shear between 84 m and 384 m was greatest, but there was also significant shear between 384 m and 984 m (0.007 cm s^{-1} per m) as well as a mean velocity of 3.9 cm s^{-1} at 984 m. In that year, neither the assumption of no baroclinicity below 600 m nor the assumption of a zero-velocity reference level at 1000 db would have been correct. The direct current evidence shows that major differences between various estimates of the baroclinic transport because of temporal variability in the baroclinic contribution are to be expected.

A comparison of other measured velocities also supports the possibility that the natural variability of the WSC admits large disparities in mean transport estimates. At nearly the same mooring location as C (79°N, ~8°E), the average velocities at the upper and lower current meters in autumn 1971-72 shown by Greisman (1976) were roughly four times those during autumn 1976-77. The year-long mean velocity at

Table 5. Mean vertical velocity shear, ratios of lower (V_1) to upper (V_u) velocities, and ratios of velocity differences to upper velocities for moorings with vertically separated current meters. Positive shear indicates a higher northward V_u than V_1.

Year	Mooring	Shear cm s^{-1} per m	V_1/V_u	$(V_u-V_1)/V_u$
1976-77	A1	.003	0.84	0.16
1976-77	C1	.005	0.86	0.14
1977-78	B2	.009	0.65	0.35
1977-78	C2	.011	0.72	0.28
1978-79	C3	.012	0.71	0.29
1976-79	CB	.008	0.77	0.23
1980-81	C5	.016	0.62	0.38

the upper current meter was about twice as great in 1971-72 than in 1976-77, so that Greisman's larger transport in 1971-72, about 7 Sv, is reasonable for that time (Forcing by wind stress curl is discussed in Section 5, and one result is that the magnitude of the wind stress curl in 1971-72 was nearly twice that in 1976-79, so that there is a dynamic basis for the difference in mean velocity during these respective periods). On the other hand, only one of the 1971-72 moorings, with two current meters, was near the core of the WSC, and thus the data coverage was much sparser than in 1976-77. Furthermore, the deeper of the current meters ceased operating about 75 days after it was deployed in early September, so that Greisman essentially relied upon a single year-long current record to estimate the annual transport. This is important because of another point of comparison: for a 75-day interval beginning September 9 during each of 1971 and 1976, the ratios of mean upper to lower northward velocities were 0.60 and 0.66, respectively (Table 6). The analogous ratio of year-long means during 1976-77 was 0.86. At least during 1976-77, therefore, the vertical shear in fall was different from that for the year as a whole. (Note, however, that the two sets of ratios are more nearly equal in 1977 and 1978.) This raises the question of whether or not the transport based on the fall currentpattern in 1971-72 was truly representative of the entire year. Indeed, geostrophic transports across $79^{o}N$ referenced to 500 db between about $5^{o}30'-8^{o}30'E$ calculated from data obtained on cruises in September and November, 1977 were 0.02 and 1.2 Sv, respectively, indicating significant fluctuations on a time scale of only a few months. Finally, application of the objective error limits (see earlier) shows that the expected error for Greisman's transport estimate is greater than the estimate itself. Nevertheless, based on current record comparison, it seems likely that the transport in 1971-72 actually was greater than in 1976-77.

3.5 Volume transport using bridged current records, 1976-79

Only at mooring location C were current meters maintained for all three years 1976-79, and therefore the three-year bridged current records from mooring location C were used to estimate volume transport for the entire period. The gaps of about 4 days between the first and second years' data and of 9 hours between the second and third years'

Table 6 Mean northward velocity (cm s^{-1}) and vertical velocity dif-
         ference at mooring location C for 75 days beginning 9 Sep-
         tember in respective years. V_u and V_1 correspond to upper
         and lower current meters, typically at 100 and 400 m depth.

	1971*	1976	1977	1978
V_u	28.6	7.0	18.9	16.6
V_1	17.3	4.6	12.6	10.6
$V_u - V_1$	11.3	2.4	6.3	6.0
$V_1/V_{u(75\ da)}$	0.60	0.66	0.67	0.64
$V_1/V_{u(1\ yr)}$		0.86 (1976-77)	0.72 (1977-78)	0.71 (1978-79)

*Greisman (1976)

data were bridged by inserting the appropriate linear trend in the gap, graphically copying the ends of each data series halfway across the gap, and then picking off data values at the proper sampling interval. Thus, the data which filled the gaps most closely resembled the measured data nearest in time on either side of the gaps.

A regression relation between the total transport and segment C transport during 1976-77 was used to estimate transport for all three years 1976-79. The regression relation was calculated after deleting transport values during two intervals, one in August 1976 and the other in late January, early February 1977 (Fig. 14), when transports of segments A and C were in significant opposition. It was decided that the segment C transport was not a good index of the total transport during these two anomalous periods. No other such extreme reversals occurred at C in subsequent years. Omitting the anomalous values, the correlation coefficient between total transport and segment C transport during 1976-77 was 0.69, and the regression relation was:

total transport (Sv) = 1.09 x segment C transport (Sv) + 2.56.

Bi-weekly values of total transport for 1976-79 were calculated from this relation, and the results are plotted in Fig. 16. For comparison, the graph includes the first year's transport estimates which were calculated using all six current records.

3.5.1 Comparison with 1976-77 transport estimates

The mean total transport of 5.3 Sv during 1976-77 based only on the transport of segment C is nearly the same as the corresponding value of 5.6 Sv calculated by using all segments. Over their common span, the two transport curves (Fig. 16) show moderate similarity both in magnitude and timing of fluctuations. The largest discrepancy occurs during late July and August 1977 when the total transport calculated from segment C exceeded that derived from all six current records by about 5 Sv. The stick diagrams in Fig. 14 show that the velocity increased markedly during this period at mooring location C, clearly biasing upward any transport estimate based only on segment C. Although it appears that the regression relation does yield approximate estimates of the total mean transport and fluctuations, the preceding
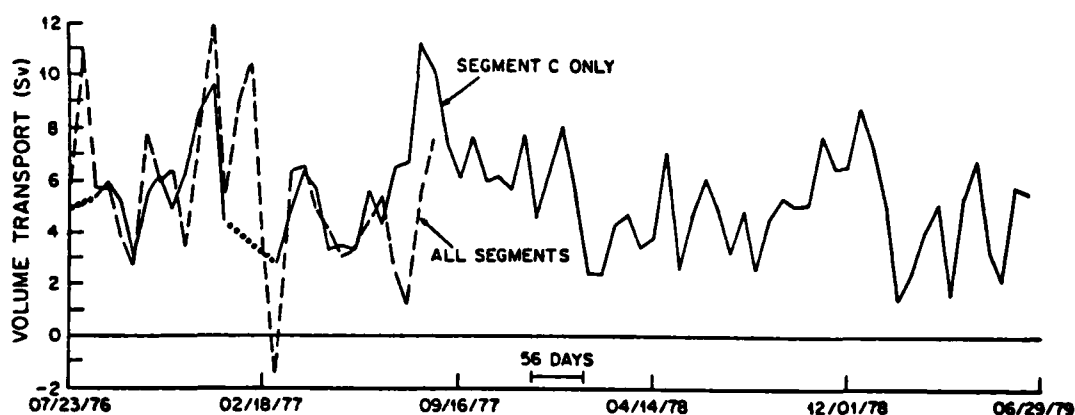
Figure 16.   Estimates of volume transport (Sv) of the West Spitsbergen Current in 1976-79. Estimates are based on two-week averages of bridged records of alongshore current measured at mooring location C (78°58'N 7°54'E) west of Spitsbergen. Estimates based on 6 current records at four mooring locations in 1976-77 are included for comparison. Dotted segments indicate periods when the current records at mooring C were not representative of the entire flow. Positive value means northward transport. One Sv = 10^6 m^3s^{-1}.

comparison demonstrates the importance of proper spatial coverage when measuring flow having variable lateral structure.

3.5.2 Seasonal and interannual variability

In general, the plot of the calculated volume transport during 1976-77 (Fig. 15) shows a maximum in late fall and winter and then a decrease through spring. This pattern agrees qualitatively with findings by Timofeyev (1962) based on hydrographic data from 13 different years obtained from a section along 78°N from Barentsburg westward to the ice edge. Note however, that there is also a large peak in August 1976 and a minimum in March 1977. Mandel (1976) presented a seasonal pattern, based on several years of data, of a maximum in November (7.7 Sv) and a minimum in April (3.3 Sv). Greisman's (1976) calculations showed a maximum in September with nearly the same value in October and November 1971, then a sharp decrease to a low value in February, and high values in May and April (Fig. 10). The minimum in August 1972 contrasts with the large value in August 1976. The basic seasonal pattern interpreted from all these data appears to be of larger transports occurring in fall and winter and smaller transports in spring. This is a pattern which corresponds to that of the strength of atmospheric circulation in the region; the relationships between atmospheric forcing and the flow are treated in Section 5.

Timofeyev's (1962) analyses provided evidence for year-to-year variations in transport. Using hydrographic sections along 78°N, the mean transport in 1956 was 3.9 Sv, while in 1960 it was only 2.4 Sv. Likewise, Kislyakov (1960) reported mean transports in several years ranging from 3.2 Sv in 1954 to 4.9 Sv in 1957 (excluding a suspiciously low value of 0.8 Sv in 1955). Mandel (1979) showed variations on about a three year cycle which appeared to be superimposed on a much longer cycle of at least 30 years (Fig. 9).

In an attempt to provide a consistent basis for the following discussion of the long-term transports and patterns of fluctuation, only the transport values computed by using the regression relation are used. For the entire three-year interval, the transport averaged 5.3 Sv, only slightly less than the first year's average of 5.6 Sv.

The mean transports for the first 52 weeks, the second 52 weeks, and the remaining 46 weeks were respectively, 5.3, 5.7, and 5.0 Sv.

Thus, during 1976-79, there appeared to be little interannual change in the mean transport. There appeared to be a weak seasonal variation with maximum values in November-December and minimum values in May, which corresponds generally with Timofeyev's (1962) results. Comparing the three year-long segments shows that the cycle was not smooth. During the second year the transport completed a cycle upon which short-term variations with time scales of 6 to 8 weeks and magnitudes to ± 3 Sv were superimposed. In contrast, in late fall and winter of the first and third year, the transport fluctuated sharply over somewhat longer time scales and with greater magnitudes than during the second.

Some caution should be used regarding the transport values calculated only from the flow at mooring location C. Recall that during the first year's deployment, the current records from mooring C were negatively correlated with those of mooring A. This means that the flows at locations A and C tended to compensate each other. If this is generally true, inclusion of mooring location A current data in the transport calculating scheme for all three years would have diminished the magnitudes of the transport peaks and smoothed out the transport curve. Obviously no such tempering can occur using only mooring C data, and the results may reflect only the temporal charcteristics of this particular current core rather than those of the total flow. Thus, inferences about the total transport determined only from the single location rest heavily upon the assumption that to some degree, the magnitude and variability of the core flow at mooring C reflect those of the total transport.

In light of the possible biasing of seasonal and interannual variability caused by basing inferences on data from only one mooring location, it bears repeating that the transport measurements based on all four locations during 1976-77 did show a distinct seasonal pattern which agreed with the results of previous investigators.

4. Heat Transport of the West Spitsbergen Current

4.1 Data preparation and transport calculation method

The temperature records were used in conjunction with the current records to estimate the heat flux accomplished by the WSC during the 1976-77 deployment. As with the northward volume transport, the mean heat flux was calculated for each segment of the entire section, and these values were then summed to yield the total heat transport.

A representative temperature profile was arrived at by referring to hydrographic data obtained west of Spitsbergen near 79°N. The water column was considered in two parts, above and below 600 m, as was done with the velocity. The temperature in the upper part was sampled by instruments typically located at 100 m and 400 m. The former was assumed to represent the temperature between the surface and 200 m, and the latter between 200 m and 600 m. This is sufficient in the vertically averaged sense, as is apparent from the discussion of error estimation in 4.2.

The temperature below 600 m was inferred from the temperature measured at 400 m. Figure 17 shows two temperature profiles obtained by averaging data from different seasons over several years. One profile derives from temperature data between 7°-8°E, and the other from data between about 5°-8°E. While the profiles differ consistently by about 0.3C, they are remarkably linear and have nearly identical slopes. In each case the temperature at 600 m is about 0.9C colder than that at 400 m, i.e.,

$$T_{600} = T_{400} - 0.9C.$$

From 600 m, the temperature was taken to decrease linearly to -1C at the depth of the zero isotach used in the volume transport calculations. Inspection of several temperature profiles shows this is not true in every case. Some temperature profiles reached -1C shallower than the zero isotach, and some were not linear, being either concave upward or downward. However, the assemblage of profiles below 600 m is very nearly as described by the simple model.

To calculate the mean heat transport for 1976-77, the successive 14-day averaged temperatures were used to derive the vertical tempera-
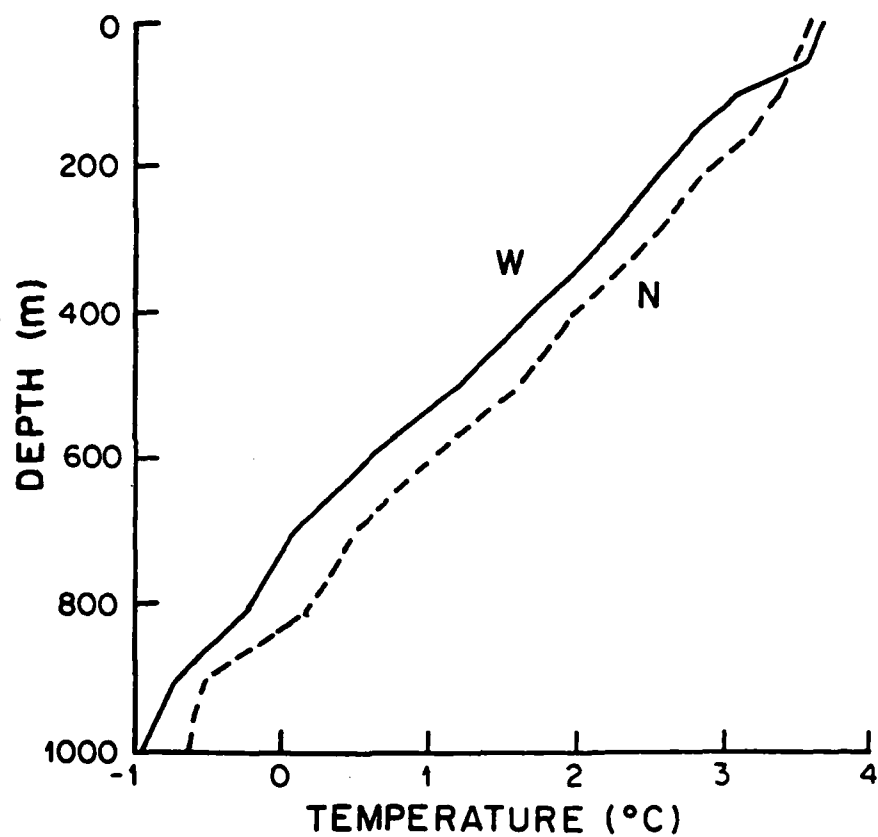
Figure 17. Average temperature profiles in the West Spitsbergen Current near 79°N. Profile W was obtained by averaging all available temperature data between 5°-8°E; N by averaging between 7°-8°E.

ture structure. These temperature profiles were then multiplied by the corresponding volume transports segment-by-segment to yield a time series of 29 bi-weekly heat transport values. A reference temperature of -0.1C was used, as in Aagaard and Greisman (1975). The product of density and specific heat was assumed to be unity in CGS units.

4.2 Error estimation

Errors in the heat transport estimates arise both from errors in the volume transport estimates and from errors due to the simplified vertical temperature distribution. The first of these was discussed previously, and it was found that errors in the volume transport estimates may be as large as the estimates themselves. The errors introduced by the simplified temperature representation depend on the complexity of the actual temperature profile. Comparisons were made between the transport temperatures derived from two original temperature profiles and those derived from the simplified representations of the same two profiles. Data were from hydrographic stations taken at very nearly the same geographic location, but with one in early September 1977 and the other in November 1977. These stations were selected as worst-case examples since they showed extremely high gradients. Figure 18 shows these profiles and their representation for heat transport calculations. For profile A, the difference in transport temperatures between the two is only about 5%, and for profile B it is about 9%. These discrepancies are comparable to those which would be expected from uncertainties of 0.1C in the readings of the thermistors measuring a temperature of about 2C. The conclusion is therefore that errors in the volume transport estimates are principally responsible for errors in the heat transport estimates, and that errors in the temperature representation contribute less than 10%. Errors in the heat transport estimates may thus approach the estimates themselves.

4.3 Heat transport by mean flow, 1976-77

Figure 15 (p. 40) shows a plot of heat transport by mean flow of the WSC averaged over two-week intervals during 1976-77.

4.3.1 Mean, range of variation

The mean heat transport during 1976-77 was 46 TW northward, with a
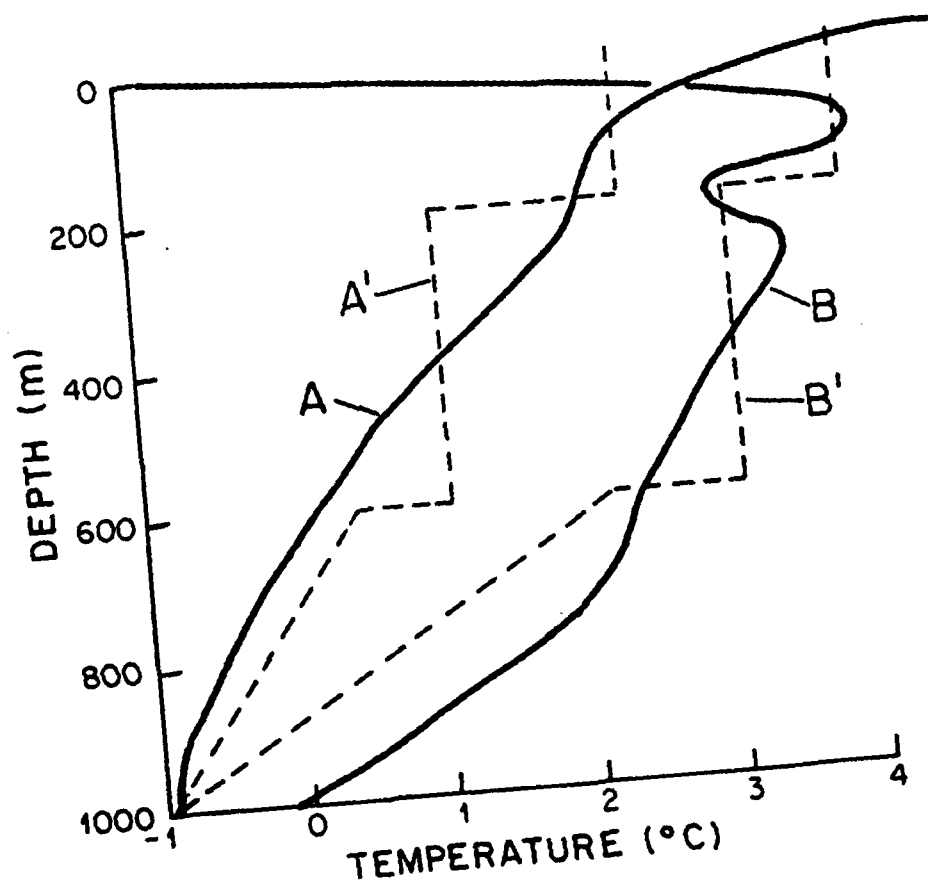
Figure 18.   Actual (A,B) and simplified (A',B') temperature profiles used to investigate the possible transport errors associated with characterizing the vertical temperature distribution by a simplified profile based on temperatures measured at depths of about 100 and 400 m.   Profile A is based on CTD data, _Johan Hjort_, sta. 950, 78°57'N 07°38'E, 09/04/77; profile B on CTD data, _Polarsirkel_, sta. 8, 79°00'N 08°34'E, 11/20/77.

maximum of 122 TW northward and a minimum of 8 TW southward (one tera-watt (TW) = 10^{12}W). Table 7 lists earlier estimates of mean heat transport for the WSC. These estimates were derived by various methods such as direct measurement, budget calculations, and geostrophic calcu-lations in conjunction with temperature data, and they were generally based on a reference temperature of OC. The range is a wide one, from about 18 TW to 130 TW northward. The maximum, which was the residual needed to balance a heat budget, is nearly twice the next largest value and three to four times as large as the rest. If it is excluded as dubiously large, the average of the remaining six estimates is 34 TW, with which the 1976-77 estimate of 46 TW compares favorably.

4.3.2 Seasonal fluctuations

The variable nature of the heat transport during 1976-77 is evi-dent in Fig. 15. It ranges from 122 TW northward in late December 1976 to 8 TW southward in early March 1977. The figure suggests that the variability during the first half of the deployment, July 1976 - Feb-ruary 1977, is greater than that during the second half, and in fact the variance during the first half is 2.4 times that during the second half. Furthermore, the heat flux was generally higher in late summer, fall and winter than in spring and early summer. Figure 19 shows the bi-weekly heat transports by spatial segments over the 1976-77 deploy-ment, and it is apparent that the same trends of greater variability and generally greater heat transport over the first half hold for the individual segments as well. In addition, on two occasions, large fluctuations in the segment A and C mean heat transports opposed each other. Generally the heat transport of segment C was greater than that of either segment A or D. Since the areas assigned to A and C were approximately the same, this was due to higher velocity and temperature at mooring C. The same is not true for the heat transport of segment D. Here the velocity was actually higher, but the total cross section assigned to segment D was smaller than that assigned to either A or C. This biasing is aptly demonstrated by comparing the mean heat trans-ports per unit area for segments A, C, and D which were respectively 26, 39, and 100 in arbitrary units. Thus if the total flow had been represented by the velocity and temperature measured at mooring D, the heat transport estimates would have been larger by about a factor of

Table 7. Previous estimates of the mean heat transport of the West Spitsbergen Current. One TW = 10^{12}W.

Source	Heat Transport (TW)
Zaitsev, et al. (1961)	127.9
Mosby (1962)	17.6
Timofeyev (1963)	30.5
Vowinckel and Orvig (1970)	22.6
Aagaard and Greisman (1975)	68.1
Mandel (1978)	28.0
Rudels and Andersson (1982)	38.0
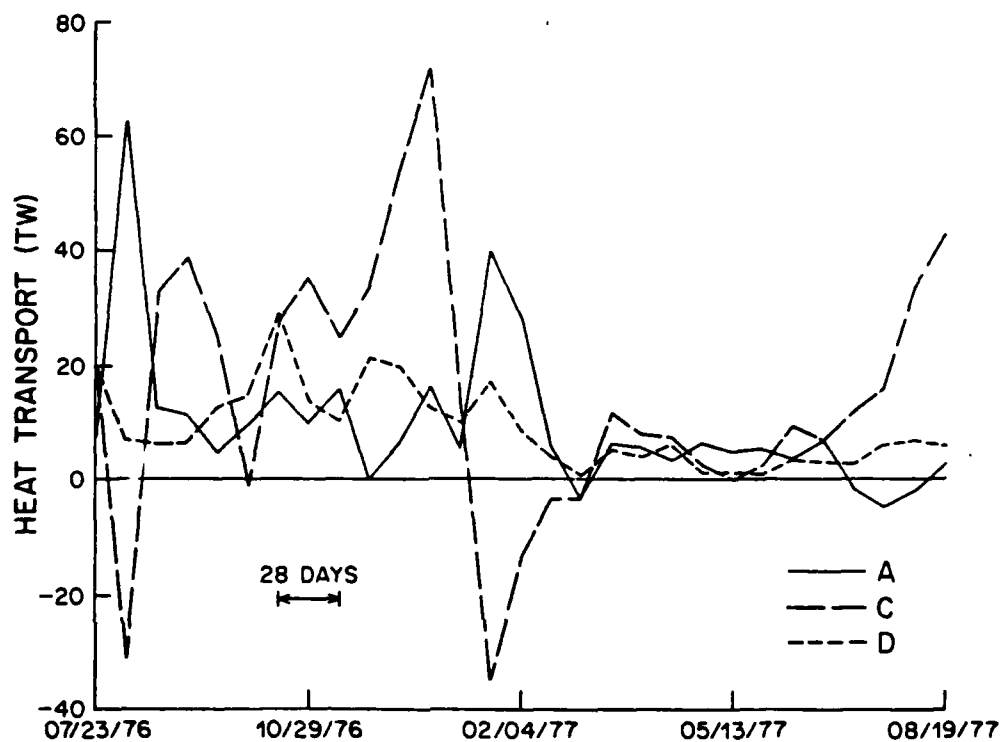
Figure 19.   Bi-weekly mean heat transport (TW) of individual transport
cross-sectional segments corresponding to mooring loca-
tions A, C, and D in the West Spitsbergen Current during
1976-77. Positive value means northward transport.   One TW
= 10^{12}W.

three, again illustrating the importance of adequate determination of the lateral current structure.

Virtually all investigations of the volume and heat transports of the WSC reveal seasonal fluctuations, generally with similar timing and characteristics. Hill and Lee (1957) interpreted hydrographic data obtained during 1949-56 west of Bear Island along 74°25'N to show that the volume (and presumably also heat) transport of the WSC executed a seasonal cycle with maxima in January and July and minima in April and October. However, the scatter of the data points used by Hill and Lee (Fig. 3, p. 109) leaves so much latitude in fitting a curve that their interpretation is questionable. Timofeyev (1963) showed a pattern for the mean heat transport which had a minimum of about 12 TW in April, a maximum of about 48 TW in October (both northward), and an annual mean of 31 TW over the time span 1933-60. However, as Lee (1963) pointed out, all but three of his eighteen hydrographic sections fell in the period May-September so that seasonal fluctuations were not really detectable. For the 0-500 m layer and relative to 0C, Mandel (1978) determined a seasonal pattern with a minimum heat transport of 13 TW in late April sharply increasing to a maximum of 46 TW in late July. The mean was 28 TW northward. His method involved linearly correlating the water level and temperature at Barentsburg with the geostrophic velocity and temperature of the WSC at 78°N, and then using historical water level and temperature observations at Barentsburg to calculate mean monthly and mean yearly volume and heat transport estimates dating back to 1949. Statistically, his correlation was significant at a confidence level of 95%, but it is difficult to assess the actual degree to which the flow velocity and temperature are represented by conditions at Barentsburg, which lies in an inlet on the west side of Spitsbergen. Furthermore, Pattullo, et al. (1955) showed that at high latitudes, seasonal steric effects may account for nearly 50% of the observed change in recorded sea level over a yearly cycle. Whether or not Mandel took this into account is not mentioned. However, it seems that even if the accuracy of the absolute magnitudes determined by Mandel may be uncertain, the seasonal pattern may still be representative. Greisman (1976) calculated a heat transport of 99 TW for July-November and about 50 TW for December-June, a pattern consistent with that reported by Timofeyev (1963) and Mandel (1978).

In general, the seasonal pattern of heat transport of the WSC appears to be greater transport in fall and winter than in spring and summer, similar to the volume transport.

Figure 15 shows shorter-term fluctuations imposed upon the seasonal pattern of heat transport for 1976-77. Especially between July 1976 - March 1977, the heat transport executed several sharp fluctuations with peak values separated by about 10 weeks and with changes of 100% and greater in times as short as two weeks. Neither of the seasonal heat transport patterns determined by Timofeyev and Mandel showed such short-term fluctuations, but this is likely due to averaging over several years.

Visually comparing the 1976-77 volume and heat transport plots in Fig. 15 shows that they are unmistakably correlated, so it appears that at least on time scales of a few months or so, fluctuations in the heat transport were largely due to fluctuations in the volume transport. The absence of major changes in the temperature records simultaneous with the major changes in the heat transport support this conclusion.

The temperature records themselves do show a strong annual signal however, especially at about 100 m (Fig. 20). Maxima of 5-6C generally occurred in August-September, and minima of 0 to -1C in February-March. At about 400 m, the magnitude of the seasonal fluctuation is much smaller (Fig. 20), the temperature ranging from slightly greater than 3C to slightly less than 1C. As well, the maxima and minima are not nearly as sharp as those at 100 m, and so the seasonal signal is much less distinct at 400 m.

4.3.3 Transport (integrated) temperature

One way of considering the seasonal temperature fluctuations of the flow is to calculate the transport temperature (integrated temperature) by dividing the total heat transport by the corresponding volume transport. The results for 1976-77 are plotted in Fig. 21. The average transport temperature for the entire interval was about 2.0C. Because of the broad summer maximum spanning the first 26 weeks, followed by a fairly sharp transition to a broad winter minimum spanning about 26 weeks, the temperature appeared to show a decreasing trend. Also plotted in Fig. 21 is the transport temperature for segment C for the same interval, which had a mean of about 1.9C for the entire interval
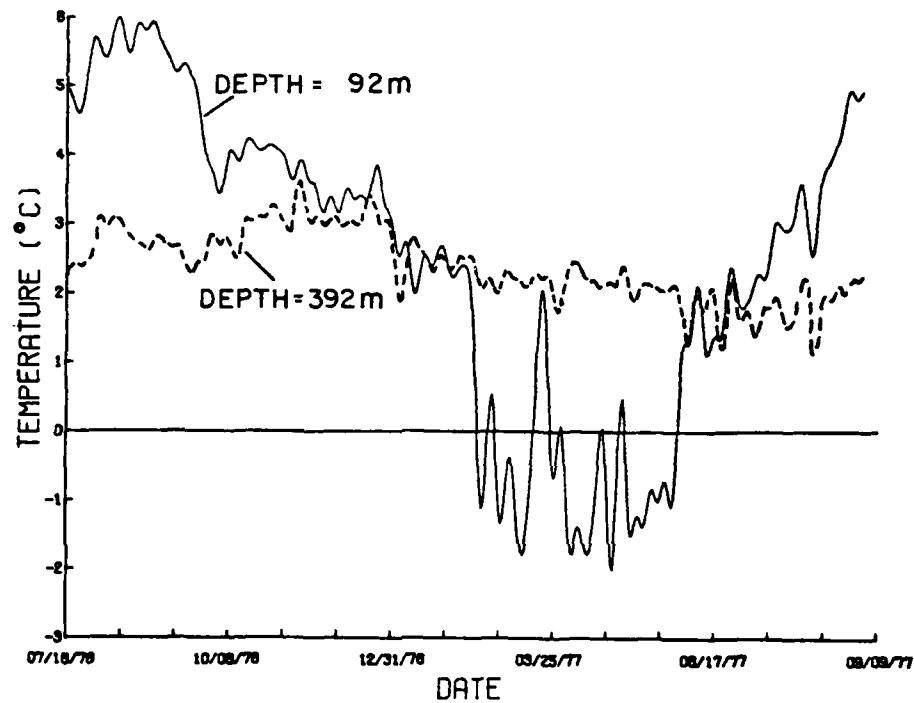
Figure 20.   Temperature records from depths of 92 and 392 m at mooring
location C (78°58'N 07°54'E) during 1976-77.   Fluctuations
with periods less than 168 hours have been removed by
filtering.
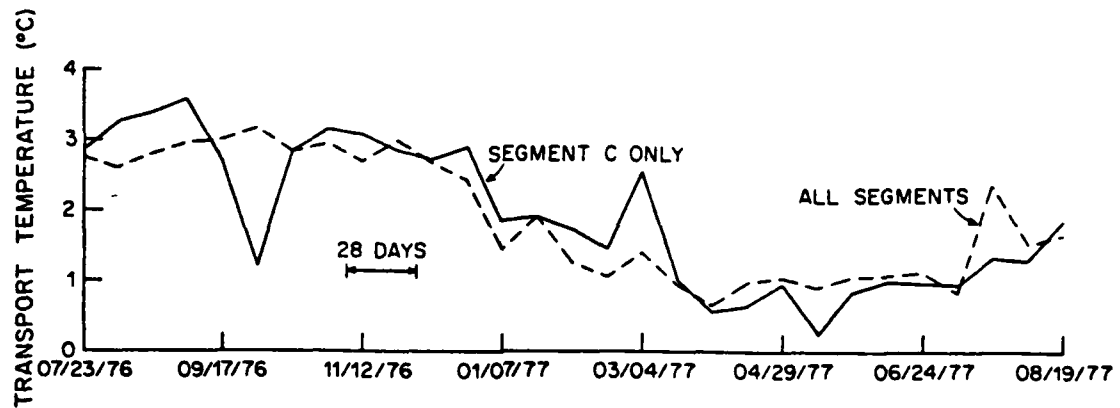
Figure 21. Transport (integrated) temperature of the West Spitsbergen Current (all cross-sectional segments), and of cross sectional segment C only, during 1976-77. Transport temperature was calculated by dividing bi-weekly estimates of heat transport by the corresponding estimates of volume transport.

and showed the same basic pattern as the transport temperature for the entire flow section. If it is assumed that the transport temperatures for the flow section and for segment C are similar in other years also, then segment C can be used to estimate the temperature history of the entire flow over 1976-79. The results are plotted in Fig. 22, and it appears that the decreasing trend in 1976-77 actually was a part of a trend of slightly decreasing temperature over the three year interval. Three broad maxima occurred in autumn of successive years, and the minima occurred in March-April. The correspondence of the transport temperature for 1976-77 and the average transport temperature of the flow through segment C over the entire interval 1976-79 suggests little long-term temperature change in the WSC during this three-year period. Because both the heat transport and the transport temperature depend on the volume transport, it is not possible to isolate the role which water temperature changes play in determining long-term variations in heat transport of the WSC. Mandel (1979) claimed that there was a 2-3 year cycle in volume and heat transports between 1949-76 (cf. Fig. 9). However, the data series used in this present study are not sufficiently long to examine this question.

4.4 Heat transport by turbulent processes

4.4.1 Alongshore transport, seasonal fluctuations

The heat flux effected by mean advective processes may be complemented by heat flux due to turbulent processes, that is, by the correlated fluctuations of velocity and temperature about their respective means.

For 1976-77, the turbulent heat transport was estimated by calculating the products of daily averaged velocity and temperature fluctuations, then averaging these daily products in groups of 14 days, and finally multiplying the 14-day averaged values by the appropriate subarea of the transport cross section. The results are shown in Fig. 23.

The average northward turbulent heat transport over the entire 1976-77 interval was 3 TW, less than a tenth of that due to mean advection. The maximum turbulent heat transport of about 16 TW northward occurred both in late December 1976 and in early March 1977, and
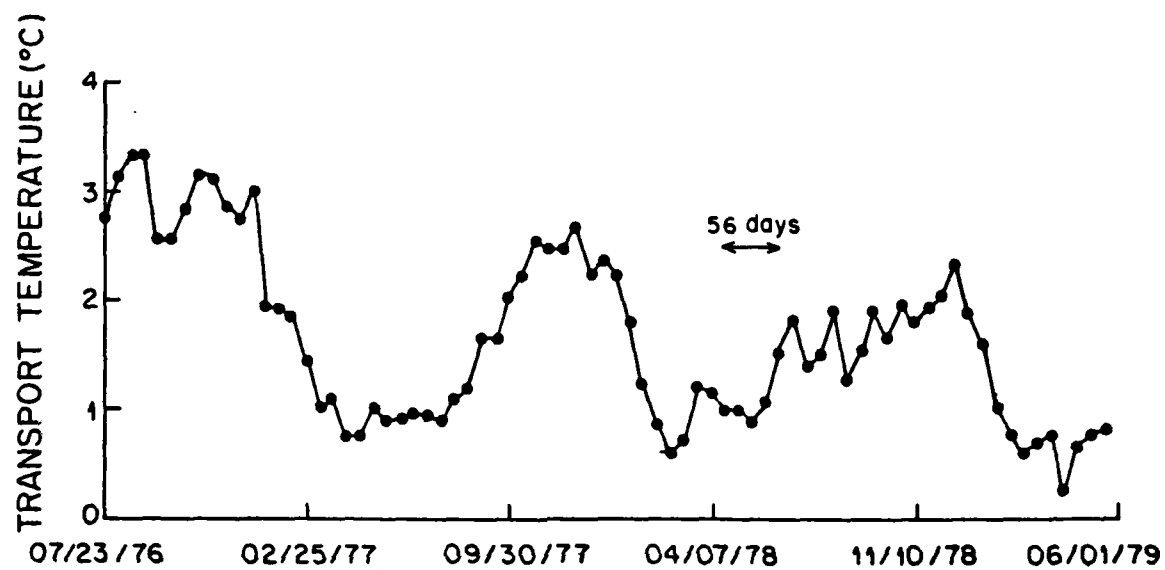
Figure 22. Transport (integrated) temperature of cross-sectional
segment C during 1976-79. Transport temperature was cal-
culated by dividing bi-weekly estimates of heat transport
by the corresponding estimates of volume transport.
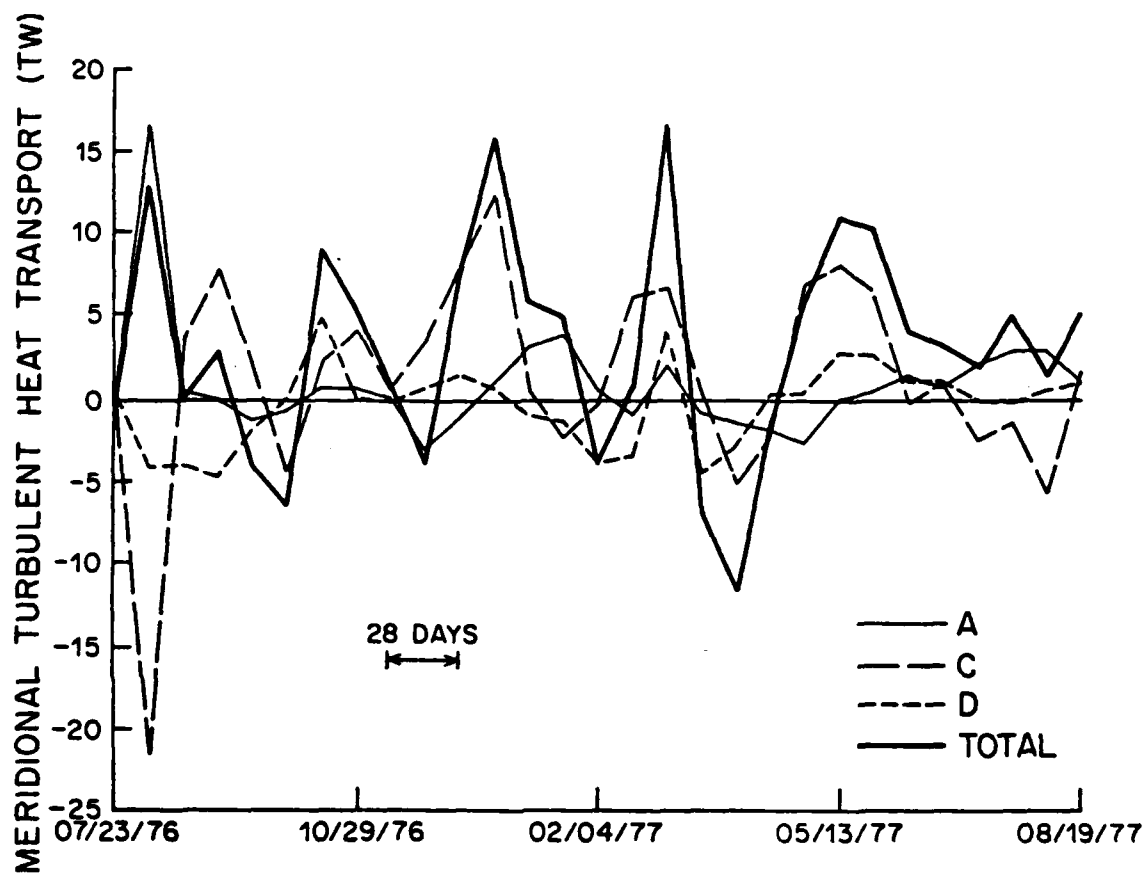
Figure 23. Bi-weekly total and segment-by-segment meridional turbu-
lent heat transport (TW) of the West Spitsbergen Current
during 1976-77. Values represent the averaged product of
fluctuations of temperature and alongshore velocity mul-
tiplied by the appropriate area of the transport cross
section. Positive value means northward transport. One
TW = 10^{12}W.

the minimum of -12 TW (southward) occurred a month later in early April. Particularly during the first half of the deployment, the mean and turbulent heat transports showed very similar patterns of variations. Agreement between the two was much poorer after the early part of January, about midway through the deployment interval, which is roughly when the temperatures at the moorings first approached or fell below their respective record-length means. This also corresponded to an interval when the velocity records showed higher variability. For example, in early March 1977 the maximum in the turbulent heat transport coincided with the minimium in the mean advective heat transport. During the interval April 27-May 11, 1977, in each of the transport section segments but especially at mooring C, negative velocity and temperature fluctuations combined to produce a large northward turbulent heat flux. At the same time the mean flow showed very little change. The minimum turbulent transport during the interval March 25-April 7, 1977 resulted from the combination of positive velocity fluctuations and negative temperature fluctuations.

The sign of the velocity fluctuations was particularly important in determining the direction of the turbulent heat transport during the 1976-77 deployment. Between late February and early April 1977, the velocities at the various moorings changed rapidly from negative to positive values in phase with each other to produce the maximum northward and maximum southward turbulent heat flux values.

Only during late July and early August, 1976 were the turbulent heat transport contributions from the different moorings in significant opposition. The transport for segment C was about 22 TW southward while that for segment A was 17 TW northward. For both segments, the temperatures were 2.5-3.5C above their respective means. However, the velocity in segment A underwent a sharp positive change to 30 cm s^{-1} greater than its mean, and at the same time the velocity in segment C showed a negative change to about 25 cm s^{-1} less than its mean. Very similar sharp velocity fluctuations in January 1977 produced no such striking opposition in turbulent heat flux because the temperatures in segments A and C stood very nearly at their mean values and varied little at that time.

The year-long plot of alongshore turbulent heat transport (Fig. 23) displays five peaks which occurred at an interval of about 70 days.

Whether or not this signal is real is difficult to determine. The only other evidence of such a long-period signal during 1976-77 is a variation with a period of about 60 days which shows up in the alongshore velocity at mooring D. Except for the first two months of the deployment, it appears the variation of the total turbulent heat flux in the alongshore direction was dominated by segment C. This follows from the fact that mooring C had higher variance than moorings A and B, and variance comparable to that at mooring D.

4.4.2 Cross-isobath flux

The cross-isobath turbulent heat flux was -0.17 W cm^{-2} (offshore) averaged over all six current records during 1976-77. In comparison, the alongshore turbulent heat flux was 1.20 W cm^{-2} northward. The standard deviations for the flux values for each current record were roughly ten times the mean values for both the cross-isobath and alongshore fluxes. The largest offshore heat flux, -1.98 W cm^{-2}, occurred at mooring C. Other large values were +1.01 and +0.75 W cm^{-2} respectively at moorings A and D (positive values indicate onshore, eastward turbulent heat flux). One possible explanation is that the average local horizontal temperature gradient had opposite signs at A and C, and this is possible if A and C were on opposite sides of a velocity extremum. In this case, assuming in general that geostrophy obtains, the isotherms would slope oppositely on either side of the velocity extreme. The current records and hydrographic data imply that the WSC does possess lateral structure, so that such a situation may obtain. The location over the shelf break and closer access to the coastal flow over the shallow shelf preclude a similar speculation for mooring D.

The mean advective alongshore heat flux is roughly an order of magnitude greater than the alongshore turbulent heat flux and about two orders of magnitude greater than the cross-isobath turbulent heat flux. Thus, the turbulent fluxes appear to have little significance for the WSC as far as heat transport is concerned.

5. Forcing of the West Spitsbergen Current

The earlier sections have been devoted to describing the WSC and quantifying the volume and heat transports. In this section attention is focused on dynamic aspects related to forcing and long-term fluctuations of the flow.

5.1 Wind forcing of the mean flow

The Icelandic low is the major atmospheric circulation feature of the Greenland-Norwegian sea region (Vowinckel and Orvig, 1970). In particular, contours of annual mean air pressure (Fig. 24) show a huge elongated low pressure trough which extends northeastward from Iceland, passing north of Norway and along the northern periphery of the Soviet Union. The feature is even more pronounced in January (Fig. 25), but fades by July (Fig. 26) so that rather weak pressure gradients prevail. Thus, the winter circulation is much more intense than the summer circulation. The winter pattern usually persists until March, when both the Siberian high and the Icelandic low begin to weaken dramatically, leading into the transition to the summer pattern. By October, the Siberian high and the Icelandic low have re-formed and approach their wintertime strengths.

The April and October air pressure distributions (not shown) more closely resemble the January than the July distribution so that the Icelandic low is a significant factor for roughly 8-9 months of the year. Consequently, the annual mean winds reflect the influence of the low, and are directed toward the southwest over the central Greenland-Norwegian sea area.

As one means of addressing atmospheric forcing of the WSC, daily surface pressure data were taken from National Weather Service (NWS) pressure maps for the northern hemisphere. These were used to investigate the relationship between velocity measurements in the WSC between 1976-79 and the atmospheric pressure distribution over the Greenland and Norwegian seas. Surface locations for a 5-point pressure grid were chosen at 75°N 15°W, 75°N 0°E, 75°N 15°E, 80°N 0°E, and 70°N 0°E. The pressure records extended from July 1, 1976 to June 30, 1979 and constituted a time series 1095 days long. They were used variously to calculate time series of simple pressure differences, wind stress, and
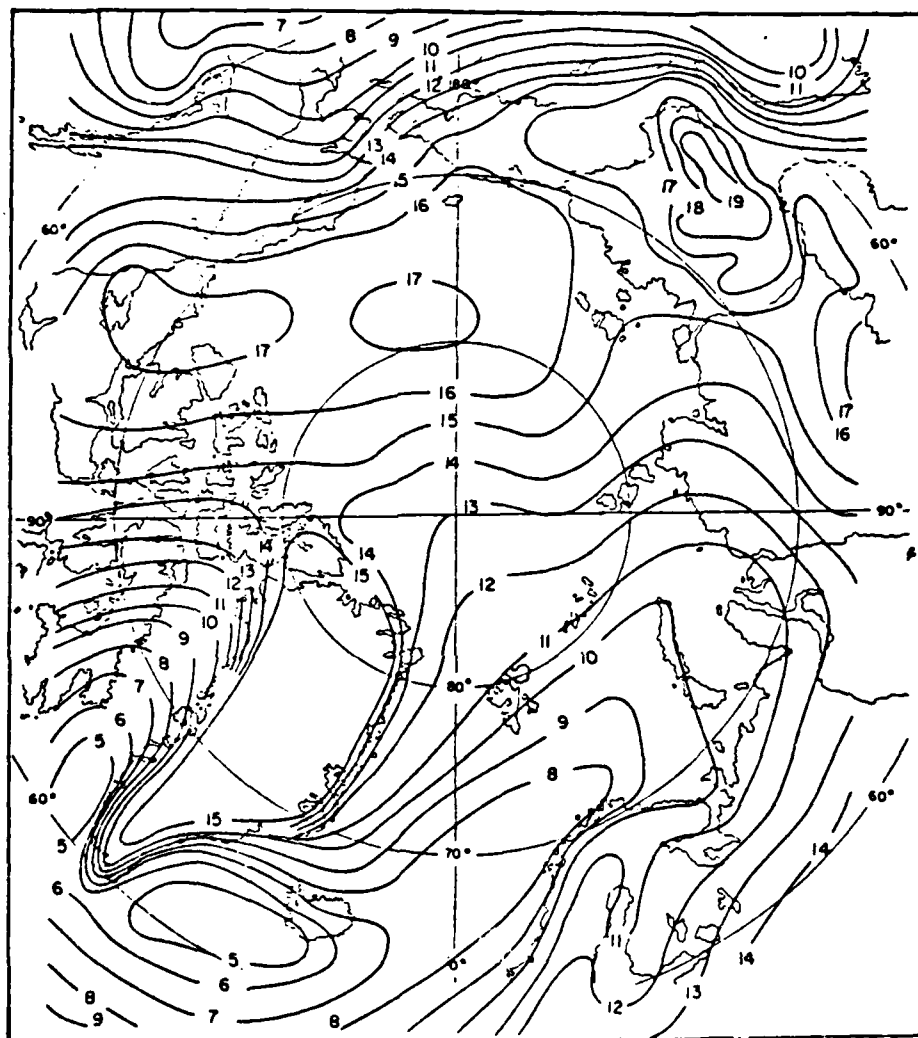
Figure 24.   Annual mean air pressure (mbar) over the north polar region. A value of 10 corrresponds to 1010 mbar, etc. (from Vowinckel and Orvig, 1970).
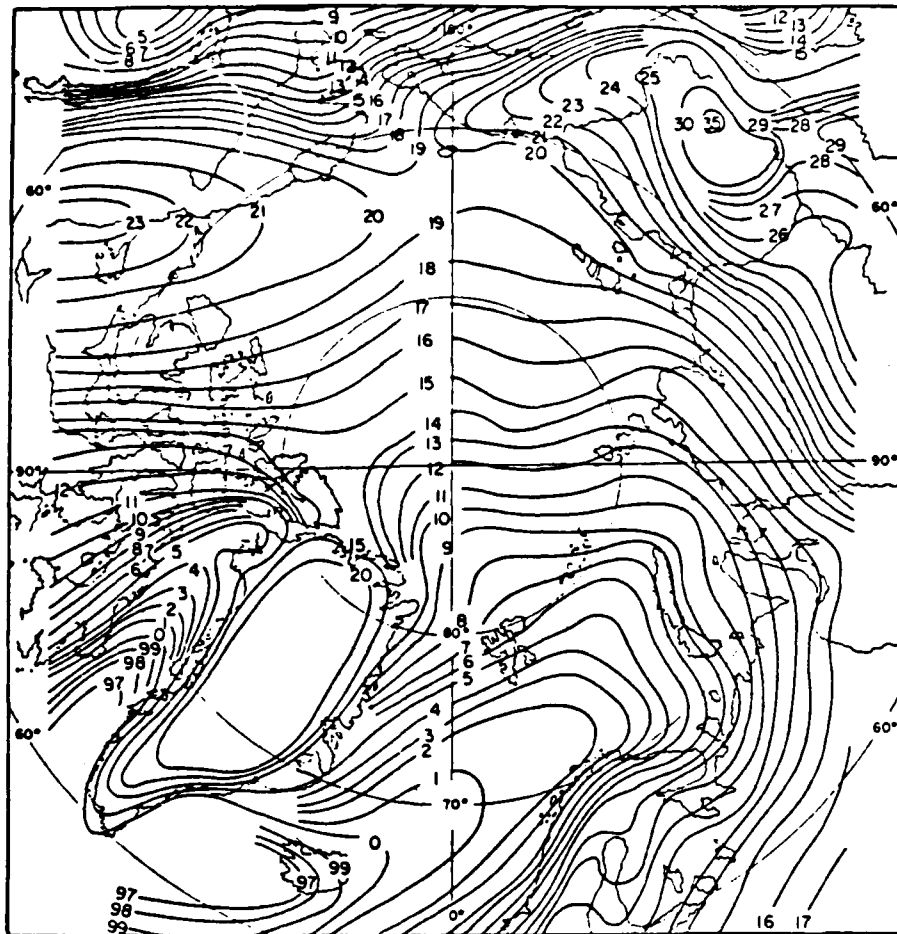
Figure 25.   January mean air pressure (mbar) over the north polar
             region. A value of 10 corresponds to 1010 mbar, a value
             of 99 corresponds to 999 mbar. (from Vowinckel and Orvig,
             1970).
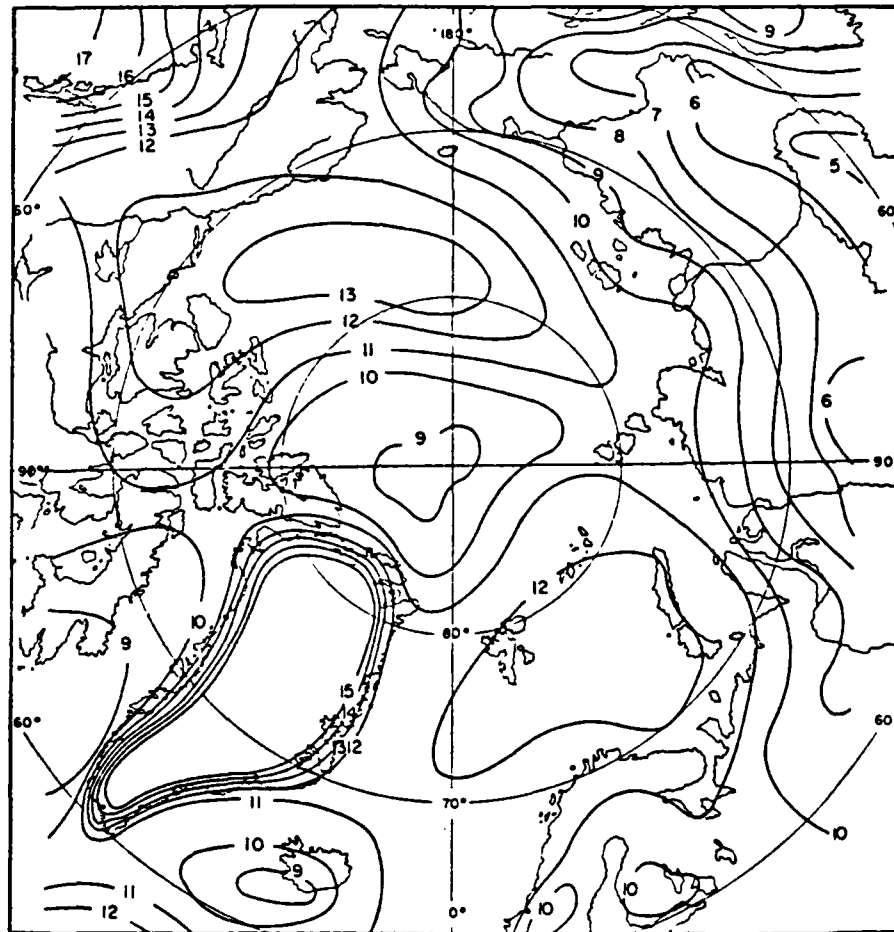
Figure 26.   July mean air pressure (mbar) over the north polar region.
A value of 10 corresponds to 1010 mbar, etc. (from Vowin-
ckel and Orvig, 1970).

curl of the wind stress. The grid provided for the calculation of north-south wind stress at 75°N 7.5°W and 75°N 7.5°E and of east-west wind stress at 77.5°N 0°E and 72.5°N 0°E. The wind stress, τ, was calculated with the square-law:

$$\tau = \rho\, Cu|U|\ ,$$

where ρ is the density of air, 1.27×10^{-3} gm cm^{-3}; C is the drag coefficient, 1.3×10^{-3}; and u is the surface wind speed, assumed equal to the geostrophic wind. This last assumption is not strictly true since surface winds are proportional to geostrophic winds by a factor usually less than unity and are deflected to the left, typically 15-20° (Aagaard, 1969). However, the main goal in comparing atmospheric and water flow data is to investigate statistical relationships and associated time scales, and these relationships are insensitive to the use of geostrophic rather than surface winds.

Table 8 lists the three-year average of daily air pressure at the five grid points from July 1976 to June 1979. This pattern corresponds well with the mean pressure distribution: it reflects the influence of the Icelandic low in the southern and eastern areas, and the higher pressure to the north and west of the central grid point represents the influence of the Greenland high. The mean large-scale geostrophic winds associated with this pattern, and thus the surface stress, are directed toward the southwest. This alone makes the prospect of forcing the mean flow of the WSC by direct wind stress unlikely, simply because the wind stress is in the wrong direction.

The major contributions to the curl of the wind stress arise mainly from the high gradient regions in the north and west of the grid; the mean curl at 75°N 0°E is positive (cyclonic), and this is characteristic over most of the Greenland and Norwegian seas.

Between July 1976 and June 1979, the wind stress curl averaged 1.4×10^{-8} dynes cm^{-2}cm^{-1}. Assuming a zonal section 860 km wide (30° of longitude) at 75°N, the meridional volume transport according to the Sverdrup relation:

$$\int M_y\, dx = (\bar{\nabla} \times \bar{\tau})/\beta\ ,$$

Table 8. Mean surface atmospheric pressure (mbar) derived from daily
          National Weather Service synoptic pressure maps for five
          locations in the Greenland-Norwegian sea region between
          July 1976 and June 1979.

Location		Mean Pressure (mbar)
80°N	00°E	1014
75°N	00°E	1010
70°N	00°E	1009
75°N	15°W	1013
75°N	15°E	1010

was about 20 Sv northward ($\beta = 6 \times 10^{-14}$ cm^{-1}s^{-1} at 79°N). A second transport estimate calculated similarly for the same zonal width but based on a mean value of 0.56×10^{-8} dynes cm^{-2}cm^{-1} derived from wind stress curl data provided by the National Marine Fisheries Service (NMFS) yields about 8 Sv. Either figure can thus account for the total average northward transport of about 5 Sv for the WSC from 1976-79. Further support for the role of wind stress curl in forcing the mean flow is that during 1971-72, the magnitude of the curl was 2.4×10^{-8} dynes cm^{-2}cm^{-1}, nearly twice that during 1976-79. While the mean transport estimate of 7 Sv in 1971-72 is slightly larger than 5 Sv for 1976-79, the mean velocity (unbiased by computational method, in contrast to transport estimates) at approximately the same location was also nearly twice as large in 1971-72.

The difference between the two values for the wind stress curl during 1976-79 stems in part from the grid extent and in part from the conversion of the NMFS wind data from geostrophic to surface values. The western and northern gridpoints used in calculating the larger value lay in the high gradient region near Greenland. A deviation of 1 mbar in the mean pressure at either point would change the estimate of the curl and thus of the volume transport by about 17%. The smaller value for the curl computed from NMFS data was based on a smaller, more local grid around 75°N 0°E. Also, the magnitude of the geostrophic wind vector was multiplied by a factor of 0.7 and rotated 15° left to yield surface winds (cf. Bakun, 1973). Since wind stress is proportional to the square of the speed, this conversion reduced the magnitude of both the wind stress and its curl to 0.49 of their values had geostrophic winds been used. Aagaard (1969) found that for this high latitude area, the conversion factor between geostrophic and surface winds was about 1 rather than 0.7. Transports calculated from NMFS wind stress curl data based on a conversion factor of 1 would thus yield a value comparable to that based on the pressure map data.

The inexactness of the knowledge of the atmospheric pressure field in the region admits uncertainties in calculations of wind stress and its curl, but even so it is probably safe to say that the magnitude of the mean northward volume transports calculated in a previous section can be accounted for by the wind stress curl. Earlier work by Aagaard

(1970) suggested that transports as high as 35 Sv could be maintained by the wind stress curl over the Greenland and Norwegian seas.

5.2 Eastern intensification and vorticity considerations

Greisman and Aagaard (1979) hypothesized that the northward Sverdrup transport might be steered eastward by the steep topography in the Greenland Sea and concentrated into a relatively intensive feature, the WSC, as it followed converging isobaths which curved northward. This is essentially a mechanism for forcing water of the Norwegian Atlantic Current farther northward, which Metcalf (1960) showed to be quite broad at 70°N, extending to nearly 10°W.

Northward transport due to cyclonic wind stress curl has thus been postulated as a driving mechanism for the WSC, but it is important at this point to note that this flow is not a return current in the sense of the Gulf Stream. The Gulf Stream maintains continuity in the North Atlantic by transporting back to the north water which was driven southward in the interior by anti-cyclonic wind stress curl, and vorticity considerations dictate that the return flow be an intensified western boundary current. The WSC is essentially an intensified poleward eastern boundary current. Were it a return flow, then those same vorticity arguments would dictate that it appear as a southward current along the east coast of Greenland. Such a current exists, the East Greenland Current, but it is probably not simply a return flow which closes the flow in the Greenland and Norwegian seas. The East Greenland Current is driven in part by continuity constraints for the Arctic Ocean, but it appears that buoyancy forcing is also important (Griffiths and Linden, 1981). While the vorticity conservation constraint does not prohibit concentrated eastern boundary currents, return transports must be on the westward side of the ocean (Stewart, 1964), and any concentrated eastern transports must be directly driven. The implication is that the mean flow of the WSC is directly driven by the wind (and possibly by thermohaline forcing), in this case by the curl of the wind stress rather than by the stress itself.

It is useful to recall Stommel's (1965) classic heuristic explanation for asymmetric, western intensified flow in the North Atlantic and to comment on the Greenland-Norwegian sea circulation and the WSC in that light. Stommel asserted that the negative wind stress vorticity

tendency could not be balanced in both the western and eastern portions of the ocean if the circulation were symmetrical. Assuming no net meridional flow, the negative and positive planetary vorticity tendencies due to northward and southward moving water columns in the west and east respectively would balance, and unless the velocities were many times as fast as observed in the real ocean, lateral friction could not produce a positive vorticity tendency on the west side of the basin strong enough to balance the negative wind stress vorticity tendency. However, in the case of asymmetric, western intensified flow, the frictional and planetary vorticity tendencies are greatly enhanced on the western side of the basin due to increased shear and velocity in the narrow northward flow. Thus at the western boundary, the primary balance is between the large negative planetary and positive frictional vorticity tendencies, while the balance on the eastern side is between the small negative wind stress and positive planetary vorticity tendencies.

Now consider the Greenland and Norwegian seas where the mean wind stress vorticity tendency is positive. On the eastern side, both the planetary and the frictional vorticity tendencies are negative and will be enhanced by the intense northward flow of the WSC, although the frictional vorticity tendency may dominate over the planetary vorticity tendency because of the small value for beta at high latitudes. Thus they cannot balance each other, and since they are together much greater than the wind stress vorticity tendency, they cannot be balanced by it. The point is that a vorticity argument analogous to that for the North Atlantic/Gulf Stream system does not yield a balance on the eastern side of the Greenland-Norwegian sea region. This in turn implies that eastern intensification cannot result from a constraint that the vorticity tendencies arising from input by wind stress curl, from frictional effects, and from meridional flow all balance. In fact, eastern intensification serves to further destroy the possibility of balancing the negative and positive vorticity tendencies, with the net result that negative vorticity would be transported into the Arctic Ocean by the WSC. Whether or not this is actually true will not be pursued here, although the shallow shelves and extensive ice cover of the Arctic Ocean certainly have the potential to dissipate any vorticity that may be transported in.

More recently, western intensification has been understood in terms of the reflection of westward-propagating planetary waves at a western boundary. Dissipation of the resulting eastward propagating waves near the boundary forms an intense boundary layer (cf. Anderson and Gill, 1979). Thus, vorticity waves generated in the interior give rise to a western boundary current. Over flat topography, dynamical effects constrain these free waves to possess only westward phase velocity, and therefore this mechanism could not produce an intense eastern boundary current. The inclusion of latitudinally-varying topography can allow eastward-propagating free planetary waves if the topographic vorticity effect opposes and dominates the planetary vorticity effect (LeBlond and Mysak, 1978). This condition is met in the Greenland and Norwegian seas, but the orientation of the topography is such that topographic waves would not propagate all the way to the eastern boundary. Thus, reflection of planetary waves and subsequent dissipation of energy at the eastern boundary of Greenland and Norwegian seas is highly unlikely as a mechanism to produce the observed intensification.

The most probable explanation for the eastern intensification is the steering effect exerted on the flow by bottom topography. If the flow is constrained to conserve potential vorticity, it will tend to follow contours of f/H, where f is the Coriolis parameter and H is the depth. This is true regardless of the type of forcing which initiates the motion. In high latitude regions, f is very nearly constant, changing only about 4% between 70°N and 80°N, so that the flow will very nearly coincide with bottom contours. The major topographic feature in the region is the Mohn Rise which trends slightly north of east from Jan Mayen, separating the Greenland and Norwegian sea basins at about 75°N. The typical depth of the top of Mohn Rise is 2 km, and its southern flank ascends northward with a slope of roughly 1/100 from a depth of 3 km in the Norwegian sea. Scale analysis of the barotropic vorticity equation shows that the effects exerted on the circulation by topography and by changes in latitude are comparable when:

$$H_y/H \sim \beta/f \ ,$$

where the subscript denotes differentiation, and y is the meridional

coordinate. The expressions for β and f are:

$$\beta = (2\Omega/R) \cos \theta , \text{ and } f = 2\Omega\sin \theta ,$$

where Ω is the angular rotation of the earth, θ is the latitude, and R is the earth's radius, $\sim 6.4 \times 10^8$ cm. We have at 75°N for the Mohn Rise:

$$H_y/H = (1/100)/((3 \times 10^5 \text{ cm}) = 3 \times 10^{-8} \text{ cm}^{-1} ,$$
$$\beta/f = 1/(6.4 \times 10^8 \text{ cm tan } 75^o) = 4 \times 10^{-10} \text{ cm}^{-1} .$$

The vorticity effect of the Mohn Rise is two orders of magnitude stronger than the planetary effect due to latitudinal changes, so that a general northward drift induced over the relatively flat Norwegian basin would tend to turn and follow depth contours eastward along the southern flank of Mohn Rise. Alternatively, if we define a topographic scale length 1 such that $H_y/H = O(1^{-1})$ then it follows that topographic and planetary effects are equal for $1 \sim f/\rho = 2.4 \times 10^4$ km at 75°N. In practice, the scale length of the topography is much shorter than this, so that topographic effects will in general dominate.

Three numerical studies have shown the potentially strong influence of bottom topography at high latitudes. Galt (1973) ran a barotropic model of the Arctic Ocean, basically wind driven, but using only 5% and 10% topography in order to simulate the possible reduction of topographic control by stratification. Even so, the model topography still dominated the streamfunction pattern. Semtner (1976) included the effects of stratification directly and obtained a streamfunction pattern for the Arctic Ocean similar to Galt's. Creegan (1976) modeled the Greenland and Norwegian seas using a two-layer scheme which was forced by the wind and which included the effects of topography and exchange with adjacent seas. With flat topography, the circulation essentially reflected the wind field. With closed boundaries and topography which she modeled as 30% of actual slopes, the flow pattern clearly showed the influence of the bottom. However, she obtained the most realistic results when she further included inflow through the Faroe-Shetland Channel in the south and allowed exchange through Fram Strait at the northern edge of her model. None of these three models included any thermohaline forcing.

In summary, a plausible mechanism has been presented by which
atmospheric forcing and topographic effects can give rise to the WSC.
Briefly, it is a northward Sverdrup transport in the flat interior
being steered eastward along f/H contours by the Mohn Rise, and concen-
trated by converging isobaths which curve northward. It is essentially
an elaboration of the hypothesis advanced by Greisman and Aagaard
(1979). Available atmospheric and oceanographic data are insufficient
to carry the argument further, but there are also other shortcomings of
this conceptual model. One omission is the role of the Norwegian
Atlantic Current, which flows over the steep slope west of Norway.
This flow constitutes one portion of the WSC, and may be affected
dynamically by processes farther to the south. Another consideration is
the degree to which the response of the ocean to the wind stress curl
is barotropic. For much of the year, low stratification and weak
stability, appropriate to a barotropic response, characterize the
Greenland-Norwegian sea region. However, some baroclinicity exists,
and the resulting tendency toward confining the response to the upper
ocean both diminishes the transport and weakens the effects of bottom
topography. Nonetheless, in light of the earlier discussion on the
relative importance of topographic and planetary effects, and of the
numerical model results, it appears that the baroclinic effects on the
oceanic response are minor. A third concern is the neglect of thermo-
haline forcing, and this merits further discussion.

5.3 Thermohaline forcing of the mean flow

The Mediterranean and Red seas are two examples of semi-enclosed
basins in which density differences due to thermohaline forcing drive
the circulation. In both, water flows in at the surface and denser
water out at depth. Increase of salinity of waters within the basin is
the primary contributor to the density difference between the inflowing
and outflowing waters.

Worthington (1970) discussed the Norwegian Sea as a similar medi-
terranean basin within which inflow of surface water was necessary to
balance the production and subsequent export of dense deep water. A
thermohaline analog for driving the mean flow of the WSC would require
the production in the Arctic Basin of water which would exit as a
density-driven outflow and which would be replaced by a corresponding

inflow in order to maintain continuity. Aagaard, Coachman and Carmack (1981) and Melling and Lewis (1982) have shown that cooling and salinization associated with the freezing of ice can produce density-driven flows over the shelf and slope regions on the perimeter of the Arctic Basin which then inject themselves into the water column at the appropriate density level. Aagaard et al. (1981) suggested this to be a mechanism for maintaining the ubiquitous halocline in the Arctic Ocean, and they estimated the production rate of this water to be about 2.5 Sv. The export of such dense water would represent a thermohaline forcing for the WSC. With respect to the deep circulation, Aagaard (1981) differentiated two primary components of the deep water in the Arctic Ocean; upper deep water less saline than 34.92-34.93, with probable origin in the Greenland or Norwegian Sea, and slightly more saline lower deep water which has had its salinity augmented within the Arctic Ocean. Whether this lower deep water results from brine rejection or from cooling of saline Alantic water upwelled near the margins, it represents the dense product of a (thermohaline) water mass formation process in the Arctic Ocean, capable of driving an exchange with the Greenland Sea. The presence of ice cover complicates the investigation of deep outflows on the Greenland side of Fram Strait, so it is not yet possible to verify a southward flow of lower deep water out of the Arctic Ocean.

The discussion above of thermohaline forcing has been in terms of the transformation of waters within the Arctic Basin and their subsequent export. Stigebrandt (1981) developed an estuarine model for the Arctic Ocean based on buoyancy sources and sinks related to freshwater input and removal through runoff, melting and freezing processes, vertical mixing, and heat exchange with the atmosphere. The significant result was that by using published data and established parameterizations, he was able in the model to balance realistic heat, salt, and volume budgets for the Arctic Ocean. This demonstrated the possibility that estuarine dynamics can account for exchanges comparable to those actually observed. An additional feature of a possible estuarine-like circulation in Fram Strait is that the inflows and outflows are separated horizontally rather than vertically, reflecting the combined influences of rotation and topography.

The question of atmospheric versus thermohaline forcing of the mean flow of the WSC cannot be settled presently. There are simply too few concurrent velocity, hydrographic, and climatic measurements to isolate and compare the effects of both mechanisms. Cases for both can be argued, but from a practical standpoint, some combination of both probably operates, and moreover, the fraction contributed by each is probably far from uniform over time.

5.4 Fluctuations of wind forcing and flow

I turn next to the question of the low-frequency variability of the flow and its relation to variable wind forcing. Stick diagrams for the 1976-77 current records (Fig. 14), and three successive year-long plots of the alongshore velocity at about 100 m depth at mooring C during 1976-79 (Fig. 27) clearly demonstrate that the flow fluctuated markedly even at time scales as short as a week.

5.4.1 Cross-correlations between flow and atmospheric paremeters

To investigate possible connections between observed fluctuations of the flow and changes in the wind field as determined from the large scale daily pressure maps, cross-correlations were calculated. Willebrand (1978) pointed out that one deficiency in wind data derived from hemispheric pressure maps is that variability of length scales 1000 km cannot be defined. This is important because, as shown by Willebrand, et al. (1980), the oceanic response changes qualitatively at length scales of 0(100 km), below which the response may be strongly trapped near the ocean surface. Thus any correlations reflect an oceanic response to forcing on a basin-wide scale, which is about 1000 km for the Greenland-Norwegian sea region. Little if any comment can be made on any smaller scale response based on the pressure data used here.

The bridged current record from about 100 m depth at mooring C was chosen to represent the flow characteristics of the WSC, and cross-correlations were computed between the velocity components and the atmospheric pressure differences across the basin, the wind stress, and the curl of wind stress. This particular current record was selected because it came from the core region of the flow and because it was the longest record available, spanning nearly three years. The current
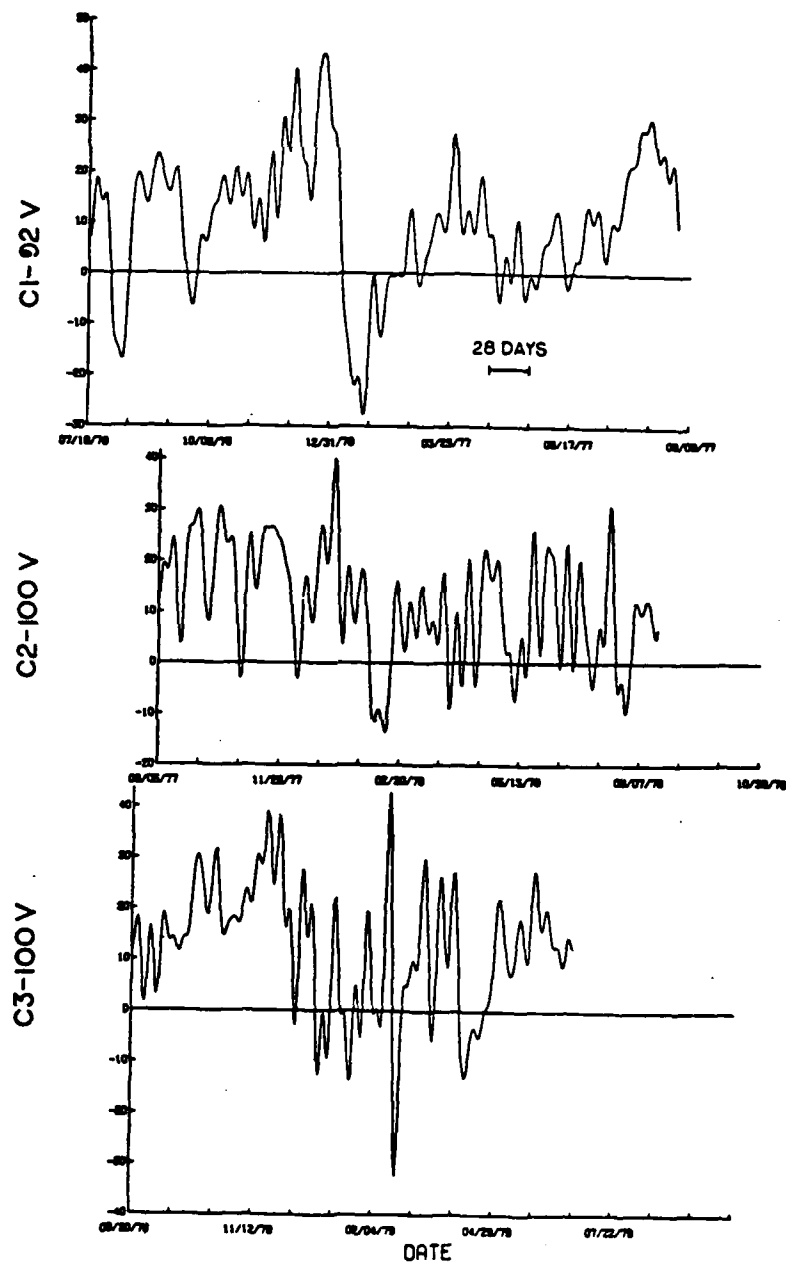
Figure 27. Alongshore velocity (cm s^{-1}) at 100 m at mooring location C during 1976-79. Fluctuations with periods less than 168 hours were removed by filtering.

record from about 400 m depth at mooring C was not included in the calculations because, even though speeds were about 30% smaller, it closely resembled the shallower record and therefore would have yielded similar cross-correlation results. Daily values of current and atmospheric data were used, and the time series were slightly less than 1100 days long. All time series were low-pass filtered at several cutoff frequencies to reduce the noise level in each, thereby smoothing the resulting cross correlation functions and rendering them easier to interpret. Specific details are included in the discussion of the results for each case.

Correlation analysis revealed no significant relation between fluctuations in the cross-isobath velocity component and any of the following atmospheric parameters; 1) curl of wind stress derived from the 5-point grid, 2) meridional component of wind stress at 75°N 7.5°E, and 3) pressure difference between the northern and southern grid points on the prime meridian. Two sets of calculations were made, one in which the time series were filtered with a low-pass cutoff of 84 hours and a second using a cutoff of 360 hours. Oort and Taylor (1969) presented spectra of horizontal wind speed from six northeastern United States locations. The spectra are typical of latitudes poleward of 40°N and show energy primarily in the 2-7 day range with peaks near a period of about 5 days. The cutoff period of 84 hours was chosen to reduce the noise contributed by the high frequency end of the spectrum and still pass periods which contain most of the synoptic atmospheric variability. The cutoff of 360 hours was chosen in order to exclude most of the atmospheric variability and allow examination of longer-term relations between wind and flow. In all cases, the filtered time series were subsampled daily, and the calculations were carried out to 400 lags. Calculations using the higher frequency time series are of little value because the potential forcing mechanisms listed above are essentially remote, and it is quite unlikely that atmospheric fluctuations could be coherent at such short time scales over hundreds of kilometers.

The absence of any strong correlations with the cross-isobath velocity component at longer time scales can be attributed to the rectifying effect of topography at mooring C. The energy spectrum for the cross-isobath flow peaks broadly at a period of about 6 days, and

the energy level at a period of 15 days is nearly an order of magnitude smaller. There is little energy in very-low frequency fluctuations, and thus no reason to expect any strong correlation with the wind at corresponding time scales. An explanation for the cross-isobath variability at time scales on the order of a week is sought subsequently in Section 6.

Correlation analysis revealed no significant connection between the north-south velocity fluctuations and any of the earlier-mentioned atmospheric parameters when the respective time series were filtered passing only signals with periods longer than 84 hours. However, similar calculations using low-passed data with a cutoff period of 15 days did show some correlations (Fig. 28). For example, in the case of the wind stress curl and the meridional flow at mooring C, the maximum magnitude correlation coefficient is -0.35 with 95% confidence limits of ± 0.05, and with the wind stress curl leading the flow velocity by 47 days. The negative (positive) correlation means that positive (negative) fluctuations in the wind stress curl, and therefore positive (negative) fluctuations in the northward Sverdrup transport, are followed by negative (positive) fluctuations in the velocity of the WSC about seven weeks later. If the WSC represents Sverdrup transport, the correlation therefore has the wrong sign. In fact, the wind stress curl and the flow do exhibit a positive correlation, and it reaches a maximum of +0.26 with flow leading by about 85 days. This implies that the response precedes the forcing, which is also inconsistent with the Sverdrup transport hypothesis.

Correlation calculations using very-low-frequency passed data (filter cutoff corresponding to 160 day period) yielded a similarly shaped, but smoother correlation function (Fig. 28) with extremes of +0.69 and -0.59. The cutoff of 160 days was chosen in order to preserve fluctuations with approximately semi-annual and longer period while eliminating the "noise" introduced by shorter period fluctuations. Note that with the wind stress curl leading the current (positive lags), the first extremum of -0.39 compares favorably with the value of -0.35 obtained using 15-day filtered data. However, the lags which are respectively 77 days (160-day filter) and 47 days (15-day filter) differ considerably. The explanation is that the correlation at 47 days is near the beginning of a lag interval of about 80 days
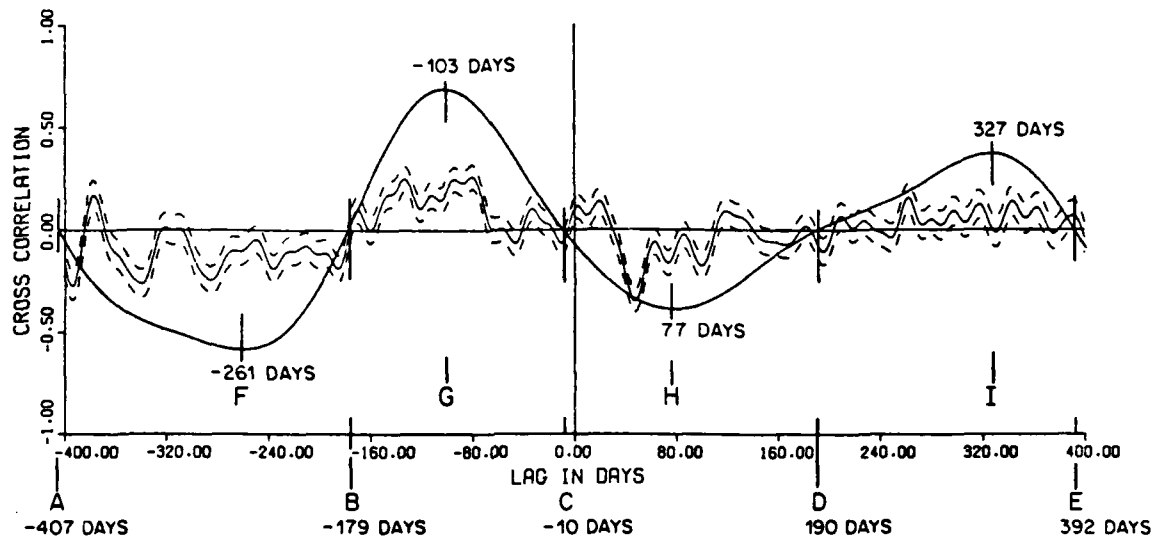
Figure 28.   Cross correlation between the wind stress curl and the alongshore velocity at 100 m at mooring location C during 1976-79.   Wind stress curl was calculated from NWS daily synoptic pressure maps.   Positive (negative) lag means that curl leads (lags) velocity.   The dotted curve is from very-low passed data with a filter cutoff of 160 days. The solid curve is from data filtered with a cutoff of 360 hours.   Dashed curves are 95% confidence intervals.

during which the correlation is nearly always negative and of even smaller magnitude. The occurrence of the first extremum at a 77-day lag using the 160-day filtered data represents the effects of smoothing the negative correlation over the entire 80-day interval and of removing the frequencies which introduce "bumps" in the correlation function. Put another way, for a negative or positive correlation trend bounded by zero crossings, the maximum magnitude is more likely to appear nearer the center of the trend as higher frequencies are removed. In view of the effects of using filters with drastically different cutoff periods, the lack of close agreement between the lag periods of 47 and 77 days is not of great significance.

The main point is that in spite of the great difference in filter cutoff periods, the respective zero crossings which separate intervals of negative and positive correlation trends agree fairly well between the two correlation functions. Thus both correlation functions reflect the same basic pattern, but with the higher frequency data, the short term correlations on the order of 2-4 weeks tend to obscure the pattern. Similar results are obtained when similarly filtered wind stress data rather than curl of wind stress data are used. The conclusion is that the correlation pattern which appears between the wind stress curl and the meridional flow at mooring C using 160-day filtered data is not just an artifact of the filter.

The fundamental pattern evident from Fig. 28 is that over an 800-day interval corresponding to lags from -400 days (velocity leads curl) to +400 days (curl leads velocity), the correlation function calculated from the 160-day filtered data displays two cycles so that there are two negative extremes, two positive extremes, and five zero crossings. The three possible sets of three successive zero crossings, A-B-C, B-C-D, and C-D-E, define three complete oscillations, and the average period of these three oscillations is 389 days. The intervals between the successive negative extremes, F-H, and positive extremes, G-I are respectively 338 and 430 days. These intervals of 389, 338, and 430 days point to a correlation at the annual time scale between atmospheric variability and the flow of the WSC. Similarly, the flow at mooring C and the meridional wind stress at 75°N 7.5°E (not shown) are correlated at an annual time scale. Moreover, the first maximum correlation of +0.60 between these two series occurs with the wind stress

leading by 86 days, corresponding to a situation where an increase (decrease) in the northward wind stress preceded an increase (decrease) in the northward flow of the WSC. Neither the wind stress nor the wind stress curl were correlated with the flow at zero lag. An independent verification of these results is that calculations using monthly NMFS wind stress and wind stress curl data yielded correlation functions similar in pattern and phase to those obtained above, albeit with poorer time resolution and less significant extrema. The main point is that fluctuations in the northward flow of the WSC are correlated with fluctuations in both the wind stress curl and the meridional wind stress at the annual time scale.

However, the data are not sufficient to isolate the wind stress curl as the sole forcing mechanism for fluctuations of the WSC at the annual time scale. Both the wind stress and the simple meridional pressure gradient were correlated with the meridional flow, similarly to the wind stress curl. Clearly, these three atmospheric parameters are not independent and share the same annual cycle. Even so, investigations of large-scale ocean response to atmospheric forcing are generally made in the context of vorticity input by the wind stress curl. This theory is examined later in this section and applied to the Greenland and Norwegian sea region.

To examine the stationarity of the relation between forcing and response, cross-correlations between seven successive overlapping segments of wind stress curl and meridional velocity at mooring C were also calculated. The chosen segment length of 268 days was long enough to grant confidence in results at lags comparable to those of 50-80 days at which correlations were found using the entire data series lengths of about 1100 points. Calculations were carried out to lags of ± 100 days. The segment length of 268 days was intentionally chosen shorter than annual to lessen the chance of biasing by the connection between wind stress curl and water velocity at the annual time scale. Also, the segments overlapped by 50% such that the start and end dates progressed by 134 days segment-to-segment. Thus, no particular season interval could bias the results.

The cross-correlation functions for the 268-day segments of the current and wind stress curl data differ greatly among the respective segments, indicating a high degree of non-stationarity in the relation

END
FILMED
3-84
DTIC

MICROCOPY RESOLUTION TEST CHART
NATIONAL BUREAU OF STANDARDS-1963-A
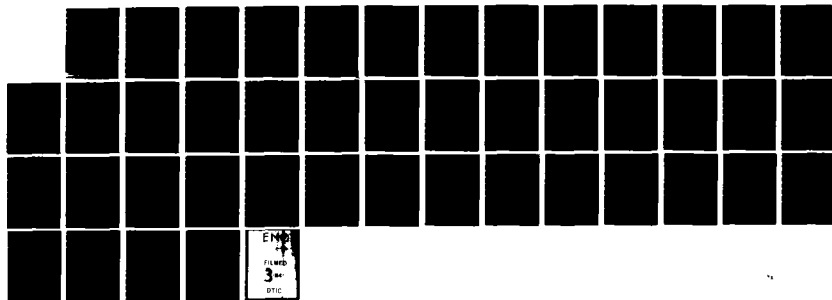
between the two. Together, they show correlations ranging from -0.71 to +0.56 variously at lags in the interval of 0 to ± 100 days. The only major correlation, after averaging over all segments, is -0.30 with the fluctuations of the wind stress curl leading fluctuations of the current by about 50 days, corresponding with the results when the entire data series lengths of about 1100 points were used. The main point is that with time, the relation between the wind stress curl and the meridional flow at mooring C varies greatly at time scales of 100 days or less. The important implication is that fluctuations in the flow of the WSC are in general not consistently related to fluctuations in atmospheric forcing in the 0-100 day time range, and probably even longer. The fluctuations of both in this time range are not jointly deterministic, but rather the short term relation between them appears more stochastic, so that there may be only episodes where the two are related. It is apparent that short term fluctuations in the wind stress curl are not solely responsible for short term fluctuations in the flow of the WSC.

5.4.2 Theory

The theory of oceanic response to large-scale atmospheric forcing can provide a basis for understanding the results of the various correlation analyses between atmospheric and oceanic fluctuations in the Greenland and Norwegian seas. The response at sub-inertial frequencies is generally considered in terms of the generation and propagation of planetary (Rossby) waves (cf. Anderson and Gill, 1975). The vertically-averaged equations of motion describe the barotropic response of the ocean, and from these can be derived the barotropic vorticity equation on a beta-plane:

$$(\nabla^2 - f^2/c^2)\psi_t + \psi_x \nabla^2 \psi_y + \psi_y \nabla^2 \psi_x + H\left[\psi_x(f/H)_y - \psi_y(f/H)_x\right] = F \ . \quad (5.1)$$

The derivation appears in many texts and is not repeated here. The assumptions are that the flow is frictionless and quasi-geostrophic. The symbol   is the transport streamfunction, H is the depth, g is the acceleration of gravity, c is the shallow-water wave speed equal to $(gH)^{\frac{1}{2}}$, and F represents a general forcing term. The zonal and meridional velocity components are respectively:

$$u = -(1/H)\Psi_y , \quad \text{and} \quad v = (1/H)\Psi_x ,$$

and assuming spatially uniform atmospheric pressure, the surface elevation is:

$$\eta = (f/c^2)\Psi .$$

Equation (5.1) may be simplified further by ignoring the influence of topography and by ignoring the non-linear terms under the assumption of small Rossby number. For the present, ignoring topographic effects is done as a convenience to simplify the initial discussion. It was shown earlier in this section that the topographic influence in the vicinity of the Mohn Rise exceeds the beta-effect; possible effects of topography are discussed subsequently. The assumption of small Rossby number is valid: assuming a length scale comparable to the basin width of 1000 km and a velocity of 10 cm s^{-1}, it is of $O(10^{-3})$, and even assuming a local length scale of 10 km for the WSC, it is of $O(10^{-1})$. Equation (5.1) then reduces to:

$$(\nabla^2 - f^2/c^2)\psi_t + \beta\psi_x = F . \tag{5.2}$$

To provide a basis for general discussion, the left-hand side of (5.2) may be scaled to yield a response time scale:

$$T = L/\beta(L^{-2} + \lambda^{-2}) , \tag{5.3}$$

where $\lambda^2 = c^2/f^2$ is the square of the radius of deformation, and L is the horizontal scale of the motion. Taking L = 1000 km and H = 3 km ($c^2 = gH$), (5.3) yields a value T ~ 4 days which corresponds to a period P = 2πT on the order of a month. According to Philander (1979), three frequency ranges characterize the response of the system described by (5.2) for forcing at time scale t:

1) If t << P, the term $\beta\Psi_x$ is negligible, and so in this frequency range the result is forced waves. The fluctuations are too rapid for the beta-effect to be important.

2) If t ~ P, both terms on the left-hand side of (5.2) are comparable, and winds which vary on this time scale can excite Rossby waves.

3) If t >> P, the first term on the left-hand side of (5.2) is

negligible, and the response is always in Sverdrup balance with the slowly-varying wind stress.

Thus, forcing at annual time scales will tend to produce a slowly varying Sverdrup response in the ocean which will manifest itself in annual variations in the WSC. Shorter term fluctuations can be attributed to local, higher frequency disturbances and appear superimposed on the slow Sverdrup response. The response at periods shorter than about a month will reflect the temporal nature of the forcing, which is largely aperiodic in this frequency range. This can account for the absence of any strong correlation in the calculations using the higher frequency time series of the wind stress curl and observed velocity of the WSC. Willebrand, et al. (1980) pointed out a second factor: the scale of the topography introduces other response scales which can obscure or destroy any clear correspondence between the wind stress curl and the flow velocity. Use of a sufficiently long filter cutoff period for oceanic data should remove the noise introduced by the effects of topography and nonstationary inhomogeneous forcing, leading to stronger correlations between oceanic and atmospheric data series. The results of the correlation analyses reflect this conclusion, which in turn implies that these two factors (and possibly others) introduce stochastic variability in the WSC time scales much shorter than annual, perhaps on the order of tens of days.

Solution of (5.2) combined with physical parameters for the Greenland and Norwegian sea region allows a rough estimation of the response to large-scale atmospheric forcing at the annual time scale. Assuming a wavelike form for the streamfunction:

$$\Psi = \Psi_0 \cos(kx + ly - \omega t) \ ,$$

substitution into (5.2) with F = 0 yields the familiar planetary wave dispersion relation:

$$\omega = -\beta k(k^2 + l^2 + f^2/c^2) \ , \tag{5.4}$$

where ω is the angular frequency and k and l are the zonal and meridional wave numbers, respectively. Since k and l are inversely proportional to wavelength, the phase velocity, defined as ω/k, is

directly proportional to the square of the wavelength. The maximum wavelength possible in the Greenland and Norwegian sea region is the basin length scale of about 1000 km and thus the corresponding maximum phase speed of a free barotropic planetary wave at 75^ON would be about 4 cm s^{-1} to the west. The phase speed of the first baroclinic mode would be much slower still. Lighthill (1969) showed that the length of time required to establish a Sverdrup balance after a sudden change in wind forcing is equal to the time it takes a long Rossby wave to propagate from the eastern boundary to the location of interest. For the ideal case mentioned above, a planetary wave with a phase speed of 4 cm s^{-1} would take about five months to propagate to the center of the Greenland-Norwegian sea region. Accordingly, the most rapid free oceanic response would be confined to time scales of this order.

However, as shown previously, the topographic influence of the Mohn Rise cannot be neglected. On both its northern and southern flanks, the restoring force due to the bottom slope is two orders of magnitude greater than that due to the beta-effect, and therefore the topographic wave phase speeds would be close to 4 m s^{-1}, leading to much faster adjustment on the order of 1.5 days. In this case, though, the topography would support eastward phase velocities on the northern flank and westward phase velocities on the southern flank, and the integrated effect across the basin would be small. Furthermore, the lateral expanse of each of the slope regions of the Mohn Rise is only about a tenth of the basin scale, and so any response supported by topography would be spatially limited.

The arguments above imply that the Greenland and Norwegian seas can establish a Sverdrup balance type of response only if the forcing by wind stress curl is at semi-annual or greater time scales. This conclusion, coupled with the inconsistency of an initial negative correlation with wind stress curl leading current by about 50-80 days, suggests that fluctuations in the wind stress curl do not account for fluctuations in the current at time scales of less than several months. However, it is important to reiterate that annual fluctuations of the wind stress curl can account for the variability of the WSC at the annual time scale.

6. Variability with time scales of a few weeks or less

The previous section dealt with the seasonal and annual varia-
bility of the flow of the WSC. The velocity records also show a high
degree of variability with time scales of a few weeks or less. This
variability is consistent in that it repeats over record lengths of
several multiples of the period of the variability. In addition, the
velocity records exhibit variability which is not periodic, that is, it
appears more as isolated events. This section addresses mainly the
former variability and discusses the dynamics which may explain it.
Greisman (1976) treated the topic of tidal variability in the WSC, and
since the focus in the present work is on sub-tidal variability, tides
are not discussed.

6.1 Spectral features of velocity and temperature records

Spectra were computed for the cross-isobath (U) and alongshore (V)
velocity components and for the temperature for each data record (see
Table 2 for mooring and data record details) for each of the three
years 1976-79 and for 1980-81. In general, spectra computed for data
obtained in successive years from the same location and depth had
approximately similar shapes, although there were differences in their
finer scale features. However, spectra computed for each of eight
successive segments (about 50 days long) of selected data records
differed markedly within each given record. Under the assumption that
spectra computed from longer records are representative of dynamical
features of the flow which tend to be more permanent, it was decided to
use the three-year bridged current and temperature records from CB-100
and CB-400 to establish the general spectral characteristics. This
decision is also a practical one which reflects, among other things,
the limitations imposed by the lack of sufficient spatial and temporal
resolution of wind and hydrographic data to determine the dynamical
characteristics of the flow.

I begin with a brief description of the spectral features of the
velocity and temperature measured at mooring location C.

6.1.1 U-component spectra

Figure 29 shows the U-component spectra for the three-year bridged

Figure 29. Energy-conserving spectra for the cross-isobath (U) compo-
nent of velocity at 100 m and 400 m at mooring location C.
Spectra were computed from three-year long direct measure-
ments. Smoothing is done by averaging over equal log
frequency intervals.

current records CB-100 and CB-400. The spectra are very similar in shape and reflect the close correspondence of the temporal variability of cross-isobath flow at 100 m and 400 m. For periods shorter than about 1000 hours, the energy at 400 m is roughly half that at 100 m. The general shape of the spectra shows a broad maximum at a period of about 6 days. The decrease of energy with decreasing frequency is a result of the constraint imposed by the sloping bottom topography, which in steering the flow, damps cross-isobath motions. Spectra for the U-component of velocity at locations A, B, C, and D during the 1976-77 deployment show an increase in low-frequency energy with distance offshore. However, the general peaked shape of the spectra is maintained, and in no case does the energy at the low-frequency end of the spectra approach the maximum energy level. Although two small peaks appear at periods of 6 days and 4 days in both CB-100 and CB-400 spectra, they are not significant within 95% confidence limits. The significance of any of the lower frequency peaks is questionable.

6.1.2 V-component spectra

Figure 30 shows the V-component spectra for the three-year bridged current records CB-100 and CB-400. As with the corresponding U-component spectra, the shapes of the V-component spectra are very similar to each other. In general, the spectrum for the deeper current contains less energy, especially at periods shorter than about 6 days, for which the V-component spectra have slopes and energy levels similar to their respective U-component counterparts. However, in contrast to the U-component spectra which show a decrease in energy with decreasing frequency, the V-component spectra tend to remain fairly level with decreasing frequency. Since the spectra are energy conserving, this means that the energy is distributed fairly uniformly over frequencies less than that which corresponds to a period of about 6 days. While close inspection of the V-component spectra does show a small tendency to peak, centered broadly at about 6 days, it is not statistically significant.

6.1.3 Temperature spectra

The corresponding temperature spectra both show marked peaks at the annual period. While they are not statistically significant, the

V-COMPONENT SPECTRUM
100 M

FREQ*(CM/S)**2 PER CPH

6 days

CPH

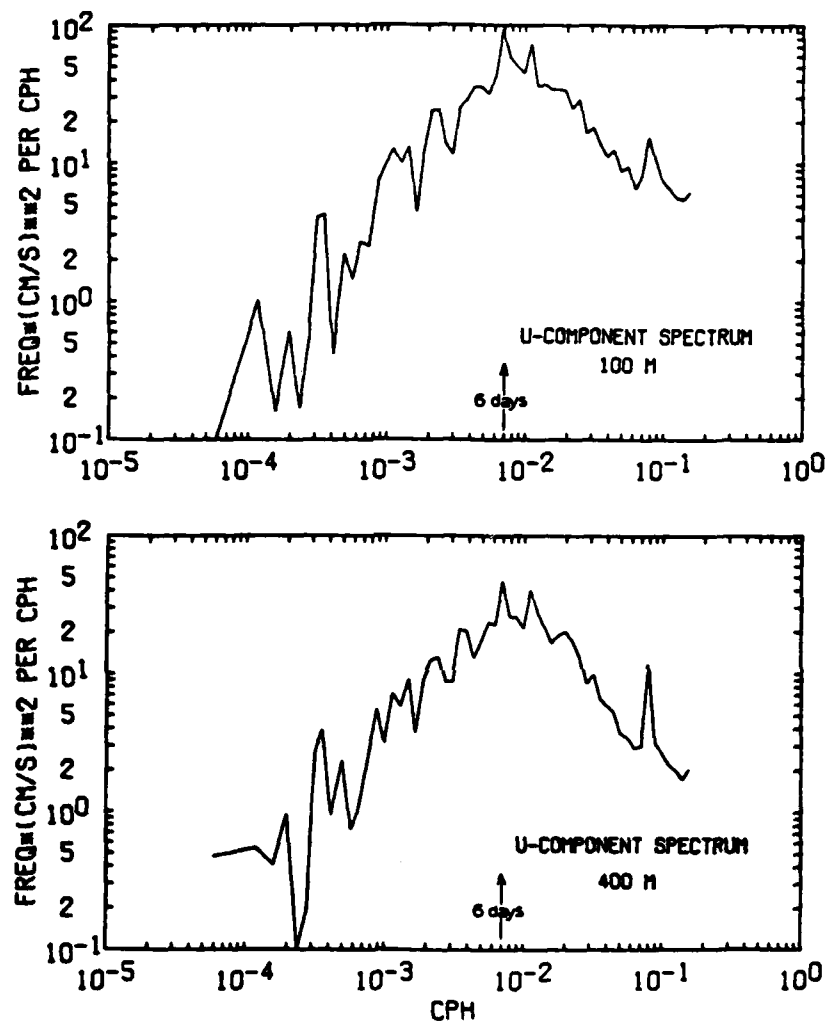V-COMPONENT SPECTRUM
400 M

FREQ*(CM/S)**2 PER CPH

6 days

CPH
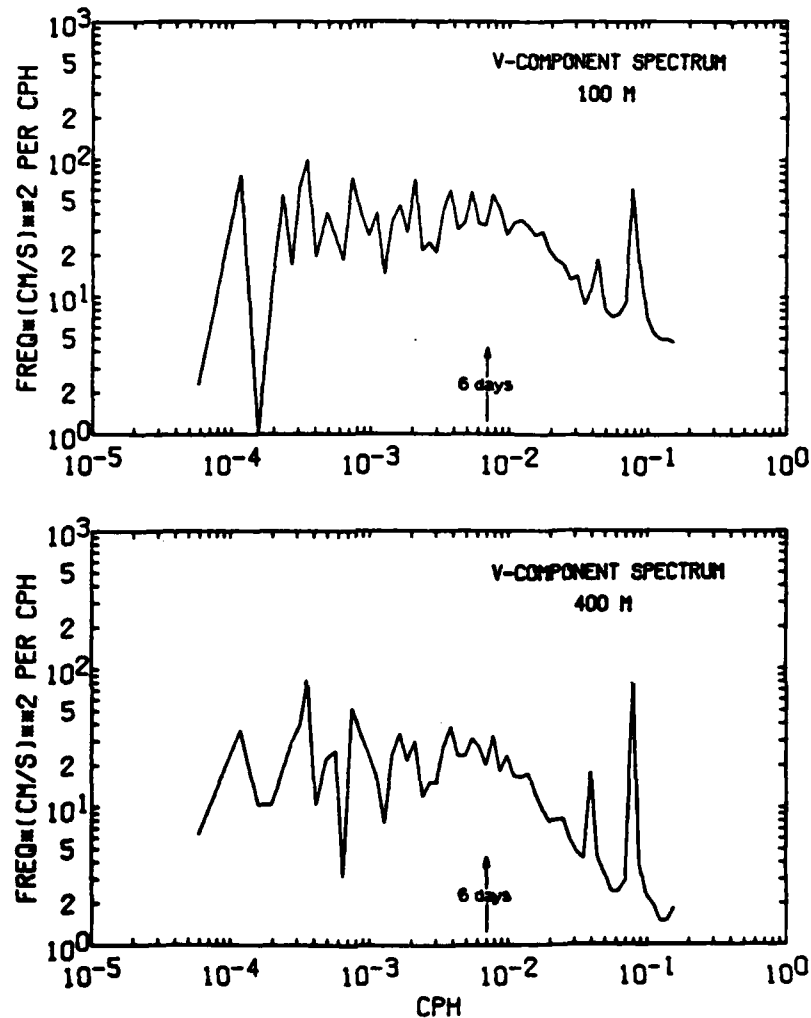
Figure 30.   Energy-conserving spectra for the alongshore (V) component of velocity at 100 m and 400 m at mooring location C. Spectra were computed from three-year long direct measurements. Smoothing is done by averaging over equal log frequency intervals.

distinct seasonal temperature cycle clearly apparent in Fig. 20 (and similarly in the two succeeding years, not shown) strongly implies that the peaks are not fictitious. The temperature spectrum from 100 m tends to stay fairly level with frequency until the annual period frequency is approached. There appear to be no other distinct features in the temperature spectrum. At 400 m, the spectrum contains about an order of magnitude less variability than that at 100 m. However, the 400 m spectrum does have a weak maximum centered at about 10 days and extending over a frequency range corresponding to periods from 1 to 70 days.

6.1.4 Spectra of vertical differences of velocity and temperature

Spectra were also computed for three-year bridged time series of the velocity and temperature differences between 100 m and 400 m depth at mooring location C. The only notable feature of the temperature difference spectrum is a strong peak at the annual period. Both the U-component and V-component shear spectra are nearly level and coincident for periods shorter than about 10 days. At lower frequencies, to about the annual period, the U-component shear spectrum decreases linearly by almost two orders of magnitude. The V-component shear spectrum reaches a minimum at a period of about 80 days then increases with decreasing frequency, with a peak at the annual period.

6.1.5 Nonstationarity

Spectra computed for successive 67-day segments of the bridged velocity records display marked differences. For each segment, the mean and standard deviation of the smoothed spectral estimates were also computed for each respective frequency band. Generally, the standard deviation is about the same as the mean. A plot of these means reproduces the shape of the spectra which were computed for the record-length data series. The basic conclusion is that the statistics of the velocity time series are not stationary, which in turn implies that the dynamics of the flow change with time. This is another reason for investigating the dynamics by using the statistics of the maximum record lengths available.

The U-component spectra offer the primary evidence of variability at time scales of a few weeks and less. The absence of significant

spikes (except tidal) indicates that such variability is not confined to a narrow range of frequencies but rather is distributed in a broad peak reaching a maximum at a period of about 6 days. Small sharp peaks jut above this general spectral shape at periods of 6 days and 4 days. These two sharp peaks coincide in period with small peaks in the temperature spectrum, which implies some correlation between cross-isobath flow and temperature, if the peaks are real. Neither the temperature spectra nor the V-component spectra reflect the broad U-component peak at 6 days. Although the V-component spectra contain energy levels similar to those of the U-component spectra at 6 days, the V-component spectra remain nearly level with decreasing frequency.

6.2 Instability mechanisms

I next consider dynamical explanations for variability of the flow at a time scale of about 6 days. The first of these are instabilities.

6.2.1 Barotropic instability

A characteristic of the current records is that both velocity components are strongly correlated in the vertical. It is sensible, then, to examine first whether or not a barotropic instability mechanism can account for the variability at time scales of about a week. Tareyev (1971) investigated the stability of a laterally sheared barotropic flow over sloping topography. He found that for instability, the total gradient of the vorticity (G);

$$G = (f - v_x)(H_x/H) - v_{xx} , \qquad (6.2.1)$$

must change sign within the lateral bounds of the flow, i.e. within the flow, G =0 at some point. Here, f is the Coriolis parameter, v the velocity, H the depth, and the subscripts denote differentiation (x is cross-isobath). Scaling by a characteristic velocity V and length L yields:

$$(f - V/L)(H/LH) - V/L^2 = 0 . \qquad (6.2.2)$$

Simplifyi · (6 ∠) yields the condition that the Rossby number V/Lf should be greater than 0.5. For the WSC, V ~ 0.1 m s^{-1} and L ~ 100 km, so with f ~10^{-4} s^{-1} the Rossby number is 0.01, and barotropic insta-

bility is unlikely. Even assuming a length scale of 20 km, comparable to the width of one of the velocity cores, and a velocity of 0.6 m s^{-1} corresponding to the largest observed lateral velocity difference, the Rossby number is 0.3, so that instability is still only a marginal possibility.

The scaling argument is only a guideline, so the question of whether the basic conditions for instability obtain is explored further by using a simple model. Niiler and Mysak (1971) used a model to investigate the barotropic stability of a laterally sheared flow, and they applied it to the Gulf Stream. Mysak and Schott (1977) used the same model (model b of Niiler and Mysak, 1971) in connection with an investigation of variability of the Norwegian Current with time scales of 2-3 days. Basically, the physical model is of a barotropic triangular current profile (maximum velocity at the middle) centered over the discontinuity of a single step bottom topography configuration with lateral boundaries at infinity. The depth of the lower step is H_2 and the upper H_1. The stability of the triangular profile with maximum velocity V is considered with respect to small perturbations of the form:

$$\Psi = \Psi(x) \exp(ily + i\omega t) ,$$

where Ψ is the transport stream function, l is the wavenumber, and ω is the wave frequency. Niiler and Mysak (1971) derived the dispersion relation $\sigma = \sigma(k)$ according to linear hydrodynamic theory, and the details are not be repeated here. The dispersion relation (their equation 8) is:

$$(\sigma + R \exp(-k)\sinh k) (a\sigma^2 + b\sigma + c) = 0 , \qquad (6.2.3)$$

where $a = 1 + (H_2/H_1$,

$b = aR(k - 1 + \exp(-k)\cosh k) + 2 - a$,

$c = R \exp(-k) (aR(k \cosh k - \sinh k) + (2 - a)\sinh k)$,

the non-dimensional frequency σ is the dimensional frequency ω divided by f, the non-dimensional wavenumber k is the dimensional wavenumber l multiplied by the current half-width L, and R is the Rossby number V/Lf. As Niiler and Mysak (1971) pointed out, the first factor of

(6.2.3) describes a stable wave which propagates over the depth discontinuity. For a given k, the second factor yields two roots which may be either real or complex conjugates. Complex conjugate roots denote instability where the wave frequency is σ_r, the real part of the complex frequency, and where one of the waves grows at a rate proportional to $\exp(\sigma_i t)$ ($\sigma_i t$ is the imaginary part of the complex frequency). Figure 31 shows the dispersion curves calculated for two cases for the WSC using (6.2.3). The parameters used for case A correspond to treating the current as a single broad flow; L (the current half width) = 75 km; H_1 (depth of the shelf) = 250 m, H_2 (depth at about 5°E) = 2500 m, V = 15 cm s^{-1}, and f = 0.000142 s^{-1}. The small Rossby number, 0.014, would imply stable flow, and the results in Fig. 31a support this. The upper curve, with frequency which increases slowly with wavenumber from an initial value of σ = 0.82, corresponds to a double-Kelvin wave modified by the flow. The two lower curves coincide, both of them having a non-dimensional frequency σ = 0.007 for k > 1.3. All three waves are stable, and their periods of about 1 day and 72 days do not correspond with major spectral features of the WSC. Similar calculations using V = 50 cm s^{-1} also failed to identify any unstable waves or any stable waves with periods prominent in the fluctuations of the current. This is notable because 50 cm s^{-1} represents an extreme velocity estimate for the WSC, and therefore a maximum likelihood for instability.

The second case, B, is representative of the stability at local scales characteristic of the lateral structure of the flow. The parameters were L = 20 km, H_1 = 250 m, H_2 = 1250 m, and V = 15 cm s^{-1}; the computed Rossby number was 0.053. Figure 31b shows the dispersion curves for this case. Again, no instability is indicated. Two roots coincide at σ = 0.026 for k > 2, while the root corresponding to the third wave grows only slightly from an initial value of σ = 0.67. In addition, neither of the periods of about 1 and 19 days associated with these calculated stable waves corresponds with prominent fluctuations in the flow, and the periods differ markedly from the 6 days observed in the broad peak in the U-component spectra. Using a value of 50 cm s^{-1} for V (Rossby number = 0.176) also suggested no instability. However, one of the stable waves did have a period of about 6 days for a wavelength less than about 100 km. As evidenced by the current records
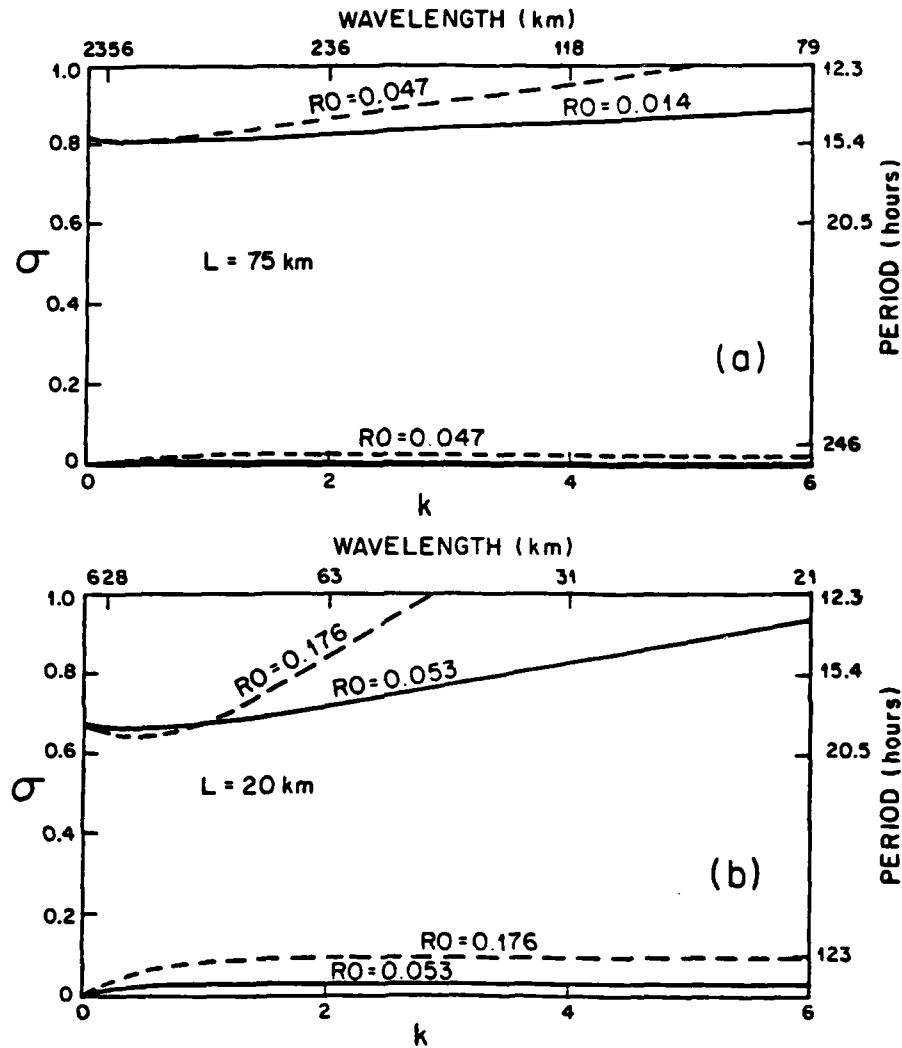
Figure 31.   Dispersion diagram for the Niiler and Mysak (1977) baro-
tropic instability model for two different current widths
(L) and two different velocities (V). a) Case A: L = 75
km, V = 15 cm s^{-1} (Rossby number 0.014), V = 50 cm s^{-1}
(Rossby number 0.047). b) Case B: L = 20 km, V = 15 cm
s^{-1} (Rossby number 0.053), V = 50 cm s^{-1} (Rossby number
0.176). Non-dimensional frequency σ is the dimensional
frequency ω divided by f. Non-dimensional wavenumber k is
the dimensional wavenumber 1 multiplied by L.

. at A and C, a lateral velocity difference of 50 cm s^{-1} was very infrequent, and so it is unlikely that this result has any significance in accounting for any major features of the variability of the WSC.

In summary, barotropic instability is not a major contributor to the variability of the WSC, as determined from results of scaling considerations and of a model. The mean velocities and horizontal shears are too small to produce this kind of instability given the length scales characteristic of the current.

6.2.2 Baroclinic instability

Perturbations due to this type of instability draw energy from the available potential energy stored in the water column, expressed by tilted isopycnals. Buoyancy fluxes effect the transfer of this potential energy into kinetic energy of the perturbations. A simple way of expressing the situation is that a flow may be baroclinically unstable when the vertical velocity shear is greater than the geostrophic velocity based on the sloping isopycnals. The buoyancy flux acts to level the isopycnals. One indication of a buoyancy flux in the proper direction to feed energy into perturbations is that the mean lateral turbulent heat flux, $\overline{u'T'}$, is down-gradient. For the WSC, $\overline{u'T'}$, as determined from the current and temperature records, is negative (down-gradient), and so is at least in the proper direction to transfer energy from the mean flow into perturbations.

Details of the derivations of necessary conditions for the occurrence of baroclinic instability may be found in LeBlond and Mysak (1978) and Gill (1982) among others, and only the result is summarized and discussed here. The conditional equation is:

$$\int_{-H_T}^{0} Q_y \left(|Z| / |U - c| \right)^2 dz + (f/N)^2 \left(|Z|/|U - c| \right)^2 U_z \bigg|_{-H_T}^{0} = 0 \quad (6.2.4)$$

where Z is a complex amplitude of the perturbation streamfunction, c is the complex phase speed, f is the local value of the Coriolis parameter, N is the buoyancy frequency, U_z is the vertical gradient of the velocity of the mean field, $Q_y = \beta_T - ((f/N)^2 U_z)_z$ is the cross-isobath gradient of mean potential vorticity, and β_T is the topographic beta-

effect. Thus it is necessary that either the first or the second term of (6.2.4) be negative for instability to be possible. As enumerated by Wright (1981) there are four possibilities: 1) Q_y changes sign within the fluid; 2) somewhere in the fluid, the sign of Q_y is opposite to that of U_z at the surface; 3) somewhere in the fluid, Q_y has the same sign as that of U_z at the bottom; and 4) the sign of U_z is the same at the surface and the bottom. Errors in the observed vertical profiles of Q_y and U_z may lead to incorrect conclusions as to whether or not any of the above possibilities is actually fulfilled. In order to argue with any confidence the question of whether or not baroclinic instability is possible in terms of necessary conditions, it is thus very important that the vertical profiles of Q_y and U_z be accurate. The data set for the WSC is insufficient to establish the required profiles of Q_y and U_z, and so no attempt can be made here to _a priori_ predict whether or not the flow is unstable in the baroclinic sense.

Schott and Bock (1980) examined low-frequency fluctuations of the Norwegian Current from the standpoint of energy interaction terms. They calculated vertical profiles of barotropic and baroclinic instability terms, and they used them in conjunction with a kinetic energy budget equation for fluctuating motions to determine the magnitude and direction of transfer of energy between the mean and fluctuating fields. In order to do so, they required extensive hydrographic measurements as well as current measurements from a diamond array of moorings. A similarly comprehensive data set is not available for the WSC, so that it is not possible to address the baroclinic (and barotropic) instability problem from energy transfer considerations, either.

Another approach is to consider a simple baroclinic model of the WSC and to investigate the stability of traveling wave perturbations in the model. The model used is of a two-layer geostrophic flow in a channel with a sloping bottom. Smith (1976) used this configuration to show that baroclinic instability could explain fluctuations in the Denmark Strait overflow with a period of about 2 days. Mysak and Schott (1977) applied this configuration to explain the presence of a spectral peak at 2-3 days in the flow of the Norwegian Current. In view of the positive results obtained in these two investigations and of the similarity between the physical settings for the WSC and the Norwegian Current, this model likewise is applied to the WSC.

Mysak, Johnson, and Hsieh (1981) subsequently examined the validity of using a channel model to investigate instabilities of coastal currents in cases where there is actually an open boundary on the seaward side and a shelf leading to a coastal wall. They found that either an outer boundary consisting of a quiescent ocean, or an inner boundary of a shallow sloping region rather than a rigid wall, gave rise to a new class of baroclinic instabilites due to interaction between waves of differing cross-stream structure. Even so, the dominant baroclinic instability was that associated with the gravest mode. In the WSC case, only the gravest mode instability is investigated.

I describe the model briefly below and refer the reader to Mysak and Schott (1977) for details of the derivation of the dispersion relation for waves in the flow. Basically, the derivation seeks traveling wave solutions of the linearized, quasi-geostrophic potential vorticity equations for each of the two layers, subject to the condition of no normal flow at the channel walls. The resulting dispersion relation is:

$$a\sigma^2 + b\sigma + c = 0 , \tag{6.2.5}$$

where $a = K^2(K^2 + F_1 + F_2)$,

$$b = -k((V_1 + V_2)a + K^2(V_1 - V_2)(F_2 - F_1) + T(K^2 + F_1)),$$

$$c = k^2(aV_1V_2 + K^2(V_1 - V_2)(V_1F_2 - V_2F_1) + (K^2 + F_1)).$$

For the model, the width of the channel is L, the upper and lower layer thicknesses are h_1 and h_2 respectively, and the bottom slope is s, positive upward toward the shoreward wall. The horizontal velocity scale is U, and reduced gravity is denoted by g_r. The other parameters are F_1, $F_2 = f^2L^2/g_rh_1$, f^2L^2/g_rh_2, the internal Froude numbers for each layer; $T = sfL^2/Uh_2$, a topographic parameter; V_1, V_2 are non-dimensional velocities equal to v_1/U, v_2/U where v_1 and v_2 are actual velocities in the respective layers; k is the dimensional wavenumber l multiplied by L; and $K^2 = k^2 + n\pi^2$, a wavenumber parameter where n is the mode number. The non-dimensional frequency is $\sigma = \omega/(U/L)$, the frequency divided by an inverse time scale. Solving the dispersion relation (6.2.5) yields two values for σ which may be real or complex

conjugates. The latter case corresponds to a baroclinic instability, and one of the waves will grow at a rate proportional to $\exp(\sigma_i t)$. On a dispersion diagram, the line along which the two roots coalesce indicates the frequency-wavenumber range over which instability is possible.

Calculations were made for two channel widths, 75 km (Case A) and 20 km (Case B), corresponding to current-width and core-width length scales, respectively. In each case, the upper layer depth h_1 was taken as 250 m, based on vertical density profiles which showed the strong pycnocline above 100 m to have decayed away for the most part by 250 m. For case A, the lower layer depth h_2 was 2000 m, typical of the depth of the outer slope region, and for case B, h_2 was 1000 m, typical of the depth in the region of moorings A and C. In each case, calculations were made using two velocity sets: one set was $(U, v_1, v_2) = (25, 15, 4)$ cm s^{-1}, and the second was $(25, 25, 4)$ cm s^{-1}. Results depend only on the values of v_1 and v_2, and using a common scaling velocity U allows results to be plotted on the same σ-k diagram. The value of 4 cm s^{-1} for v_2 was determined from the direct current data from C5-984 (1980-81). The value of 15 cm s^{-1} for v_1 is typical of the mean current in the upper 250 m. The value of 25 cm s^{-1} for v_1 was chosen in order to investigate the effect of larger vertical shear. A velocity histogram from C5-84 indicates that about 80% of the speed measurements were 25 cm s^{-1} or less (14% in the range 20-25 cm s^{-1}), so that 25 cm s^{-1} seems a good choice for an upper limit which might still be expected to occur a significant part of the time. Reduced gravity was 0.003 m s^{-1}, determined from density profiles, and the bottom slopes were 0.031 and 0.010 respectively, for cases A and B.

Figure 32a shows the dispersion curves for case A with $(v_1, v_2) = (15, 4)$ cm s^{-1} and with larger shear $(25, 4)$ cm s^{-1}. Baroclinic instability is possible for both sets of values. For the smaller shear, the wave with the maximum growth rate (indicated by the dot) has a wavelength of 34 km and a period of 3.8 days. The range of periods for instability is about 3.4-4 days. For the larger shear the maximum growth rate is at wavelength 41 km and period 3.4 days. The instability range is about 2.9-3.9 days. Thus, while doubling the value of the shear increases the range over which instability may occur, it does not greatly affect the wavelength and period of the maximally unstable
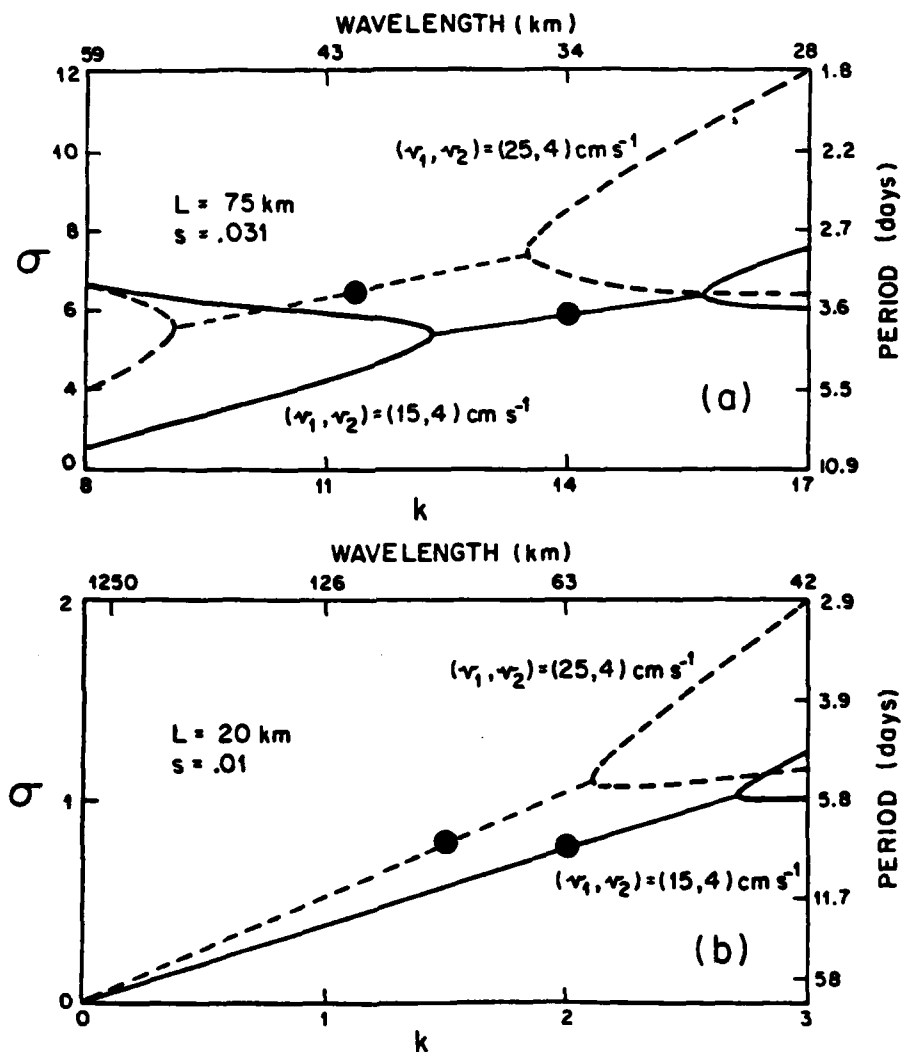
Figure 32. Dispersion diagram for the Mysak and Schott (1977) baroclinic instability model for two different current widths (L) and two different velocity pairs (v_1,v_2). The pair (v_1,v_2) are the upper and lower layer velocities, respectively. Dot denotes maximum growth-rate wave. The scale velocity, U, is 25 cm s^{-1}. a) Case A: L = 75 km; bottom slope, s = 0.031; (v_1,v_2) as shown. b) Case B: L = 20 km, s = 0.01. Non-dimensional frequency σ is the dimensional frequency ω divided by U/L. Non-dimensional wavenumber k is the dimensional wavenumber l multiplied by L.

wave. However, the maximum growth rate associated with the larger shear is about twice that associated with the smaller shear.

The periods mentioned above are shorter than the period of about 6 days corresponding to the broad peak in the U-component spectra. The wavelengths are one and one-half to two times the horizontal scale of approximately 20 km estimated from direct current measurements and from hydrographic data. Thus, baroclinic instability of the current-width mean flow does not appear to account for the spectral peak at 6 days. However, it is quite possible that this type of instability does make a contribution at slightly shorter periods, but insufficient to cause a distinct spectral peak. While this may simply be a result of smearing of the energy about a period of 6 days due to nonstationarity, it is more likely that the broad spectral peak represents contributions from more than one source. This is discussed in Section 6.3.

Calculations for case B, corresponding to a core-width length scale of 20 km and shallower bottom slope of 0.01 yielded instability over a much wider range of wavelengths and periods than did case A. This is a result of the lesser slope. Recall that the term Q_y in the stability condition equation (6.2.4) contains a positive term β_T which corresponds to the restoring effect due to topography. Reducing the bottom slope reduces the value of β_T, and therefore lessens the constraints on this type of instability. This effect is reflected in the dispersion curves for case B (Fig. 32b). For the same smaller and larger shear values as used in case A, the maximum growth rate waves respectively have wavelength-period pairs of (63 km, 7.5 days) and (84 km, 7.3 days), and again the difference is due to the smaller restoring force exerted by the shallower slope. The wavelengths greatly exceed the observed horizontal length scales, but the periods are only slightly greater than 6 days. The comments at the end of the discussion of case A as to whether or not there is a discernible contribution to the spectra generally apply here also.

Case B is essentially a hypothetical case based on an underlying assumption that a velocity core scales the instability problem correctly. For the WSC, this is not necessarily so, especially with respect to the vertical shear. In general, the vertical shear has the same sign across the entire current width. Thus it is probably more

appropriate to consider baroclinic instability in terms of the entire width of the general northward flow rather than of a single core width.

To conclude, baroclinic instability of the mean flow of the WSC is a possible mechanism for producing variability in the flow at time scales of 3-4 days and wavelengths of 35-40 km. However, there is no distinct spectral indication of the contribution, although any such indication may be masked by unsteadiness or other unexplored sources.

In order to proceed further in assessing the contribution by baroclinic instability to the variability of the WSC, it is necessary to complement model studies with an energy budget approach. This approach requires extensive current data coupled with hydrographic data, so that the magnitude and the direction of the various energy transfer terms can be determined. Such data are not available for the WSC, and therefore the model results can only be considered suggestive.

6.3 Coastal trapped waves

Coastal trapped waves have been advanced as an explanation for low-frequency variability of currents and sea level in various coastal regions of the world. (Mysak, 1980a,b). These waves, trapped over the continental shelf and slope, are another possible source of velocity fluctuations with time scales on the order of a week. Two broad categories of trapped waves are possible. In a stratified, constant-depth ocean, one type of free wave, internal Kelvin waves, can propagate along a coastal boundary. In a homogeneous ocean with shelf topography, a second type of free wave, continental shelf waves, can also exist and propagate along the boundary. Generally, both stratification and topography are present and give rise to hybrid waves with characteristics of both Kelvin and shelf waves. These hybrid waves are called coastal trapped waves (Gill, 1982). Details of the properties of these waves have been studied by (among others) Allen (1975), Wang and Mooers (1976), Clarke (1977), Huthnance (1978), and more recently, Brink (1982a,b) and Kawabe (1982).

Kelvin waves owe their existence to the presence of a coastal wall. They stem from a balance between the Coriolis force and the pressure field with the constraint of no normal flow at the lateral boundary. Thus in the northern hemisphere, this balance requires that

Kelvin waves propagate with the coast on the right, and they decay exponentially away from the coastal wall.

Continental shelf waves are a form of topographic Rossby wave, and owe their existence to both rotation and offshore variations in depth. Shelf waves conserve potential vorticity and thus are confined to traveling along contours of f/H, so that trapping occurs over the steeply sloping topography of shelf and slope regions. Their motion consists essentially of a series of horizontal eddies of alternating sign propagating along the shelf/slope margin. They are also right-bounded in the northern hemisphere (Huthnance, 1978).

Mysak (1980a,b) provides both an extensive reference list and a comprehensive review of observations of coastal trapped waves and of the theories accociated with various topography/stratification models.

6.3.1 Generation of shelf waves

The generation of continental shelf waves requires an input of vorticity over the shelf region, and this is usually accomplished by the wind. However, other mechanisms not related to atmospheric forcing such as scattering by topographic irregularities, nonlinear interactions, longshore variations in topography, incident Rossby waves, and variable discharge at the coast may also excite shelf waves (Mysak, 1980a).

Adams and Buchwald (1969) and Gill and Schumann (1974) investigated the generation of shelf waves by the wind. Gill and Schumann (1974) solved the forced vorticity equation for long, non-divergent shelf waves. They found that an oscillating alongshore wind stress in conjunction with the coastal boundary provided the most efficient means of adding vorticity over the shelf. Alongshore wind stress in the proper direction produces an onshore Ekman transport in the surface layers. Mass is conserved by an offshore transport in the deeper water, and it is this deep flow over the changing shelf topography which adds vorticity through vortex stretching. If the direction of the wind stress reverses, the directions of the shallow and deep flows reverse, and vorticity of the opposite sign is produced. Thus an alternating wind stress field could produce vortices of alternating sign which would propagate with the coast on the right. Gill and Schumann (1974) also showed that vortex stretching or shrinking due to

either the curl of the wind stress (Ekman pumping) or to changes in atmospheric pressure (inverse barometer effect) was at least an order of magnitude less important than that due to variations in the long-shore wind stress.

The discussion so far has concerned the generation of free waves, that is, waves which are generated and then propagate away from the generating region. Gill and Schumann (1974) showed that if the generating disturbance moves along the coast, then forced shelf waves with time and length scales comparable to the disturbance may also result, in addition to the free waves. If the disturbance moves in the direction opposite to free wave propagation, the forced and free waves may travel in opposite directions along the shelf.

For all but very special cases, the governing equations defy analytical solution, and so numerical methods have been applied to the problem of calculating the properties of trapped waves. Brink (1982b) used a numerical model to compute free coastal trapped wave frequencies and cross-isobath modal structure for several locations along the Peru coast, and he compared his results with direct observations. Off Spitsbergen, the bottom topography (Fig. 3), with steep slope and shallow shelf, appears quite suitable for supporting coastal trapped waves. I therefore examine the possibility of these waves appearing in the WSC by applying Brink's (1982b) model.

6.3.2 Description of the model

The following presentation of the model is summarized from Brink (1982b). The model system is linear and inviscid with constant rotation, stratification is horizontally uniform, and the bottom topography does not vary in the longshore direction. The system of equations for momentum, continuity, and conservation of density reduce to an equation for the conservation of potential vorticity:

$$p_{xxt} + p_{yyt} + (f^2 + \partial_{tt})(p_z/N^2)_{zt} = 0, \qquad (6.3.1)$$

subject to boundary conditions:

$$p_{zt} + (N^2/g)p_t = 0 \quad \text{at } z=0, \qquad (6.3.1a)$$

$$(f^2 + \partial_{tt})p_{zt} + N^2 h_x (p_{xt} + fp_y) = 0$$
$$\text{at } z = -h(x),$$

$$(6.3.1b)$$

$$p_{xt} + fp_y = 0 \quad \text{at } x=0,$$

$$(6.3.1c)$$

$$p \to 0 \quad \text{as } x \to \infty ,$$

$$(6.3.1d)$$

where x, y, and z are the onshore, alongshore, and vertical coordinates, p is the perturbation pressure, f is the Coriolis parameter, g is gravity, N is the Brunt-Vaisala frequency, h(x) is the local depth, and subscripts denote differentiation. The boundary conditions express: a) a free surface, b) no normal flow at the bottom, c) no normal flow at the coastal wall, and d) coastal trapping. Searching for free coastal waves, a propagating pressure perturbation with wavenumber l and frequency ω:

$$p = p(x,z) \exp(i\omega t + ily)$$

is assumed, so that the system (6.3) becomes a two-dimensional eigenvalue problem, and numerical techniques can be employed to solve it. The problem is solved on a grid of 25 horizontal points by 17 vertical points proportionally spaced across the breadth and local depth limits. Parameterizations of stratification and bottom topography are profiles of Brunt-Vaisala frequency squared and depth with distance offshore. For a given wavenumber, l, the model seeks a corresponding frequency, ω, by the technique of resonance iteration. That is, the model assumes forcing at wavenumber l and iterates to find ω for which the response is a maximum. This (ω,l) pair specifies one point on the dispersion curve for a free wave of particular mode which would be supported by the stratification/topography combination. The model also produces a matrix of the pressure distribution p(x,z) from which the alongshore velocity distribution v(x,z) is derived, and thus the pressure and velocity structures over the shelf and slope may be mapped.

The bottom profile used here is essentially that in Fig. 3, but with a flat shelf. Two Brunt-Vaisala profiles, derived from CTD data obtained in September and November, 1977, and differing mainly in the

upper 200 m, were used. Subsequent computations showed that the pressure structures obtained for both stratification profiles were quite similar, but that phase speeds were about 25% smaller using the more weakly stratified November profile. This is consistent with earlier findings that phase speeds of shelf waves tend to increase with increasing stratification (Mysak, 1967; Wang, 1975). Weak stratification characterizes the region much of the year, so only the results computed using the November profile are presented here.

6.3.3 Results of the model

Figure 33 shows dispersion curves for the first two trapped wave modes. The third mode was also computed, but typical phase speeds were only a few centimeters per second, and periods ranged from about 50-200 days, so that this mode is unlikely to contribute to variability with a time scale of a week or so. The curve for the first mode wave shows that for a period of about 3 days, the corresponding wavelength is nearly 2100 km, and the phase speed is about 8.2 m s^{-1}. Longer periods correspond with longer wavelengths. The first mode velocity structure is essentially barotropic. From a practical standpoint, two factors rule out the applicability of the first mode: 1) shelf waves are usually generated by synoptic scale weather systems and therefore reflect the typical length and time scales of about 1000 km and 1 week, respectively, and 2) the longest wavelengths which might be expected are basin-scale wavelengths (~1000 km), but these have periods slightly less than 1.5 days.

For the second mode, a period of 14 days corresponds to a wavelength of about 1000 km, and a period of 4 days to about 260 km. In this range, the second mode is nearly non-dispersive with northward phase and group velocities both of about 75 cm s^{-1}. This period range corresponds well with the broad spectral peak in the U-component spectra, and the wavelength range is compatible with the physical setting. In addition, the decay time and decay length scales inferred from the model are about 10 days and 1000 km, so that waves generated on the east side of the basin are able to persist long enough to affect the flow off Spitsbergen.

In order to make comparisons with observations, longshore wavenumber information is necessary to define a trapped wave of given period from
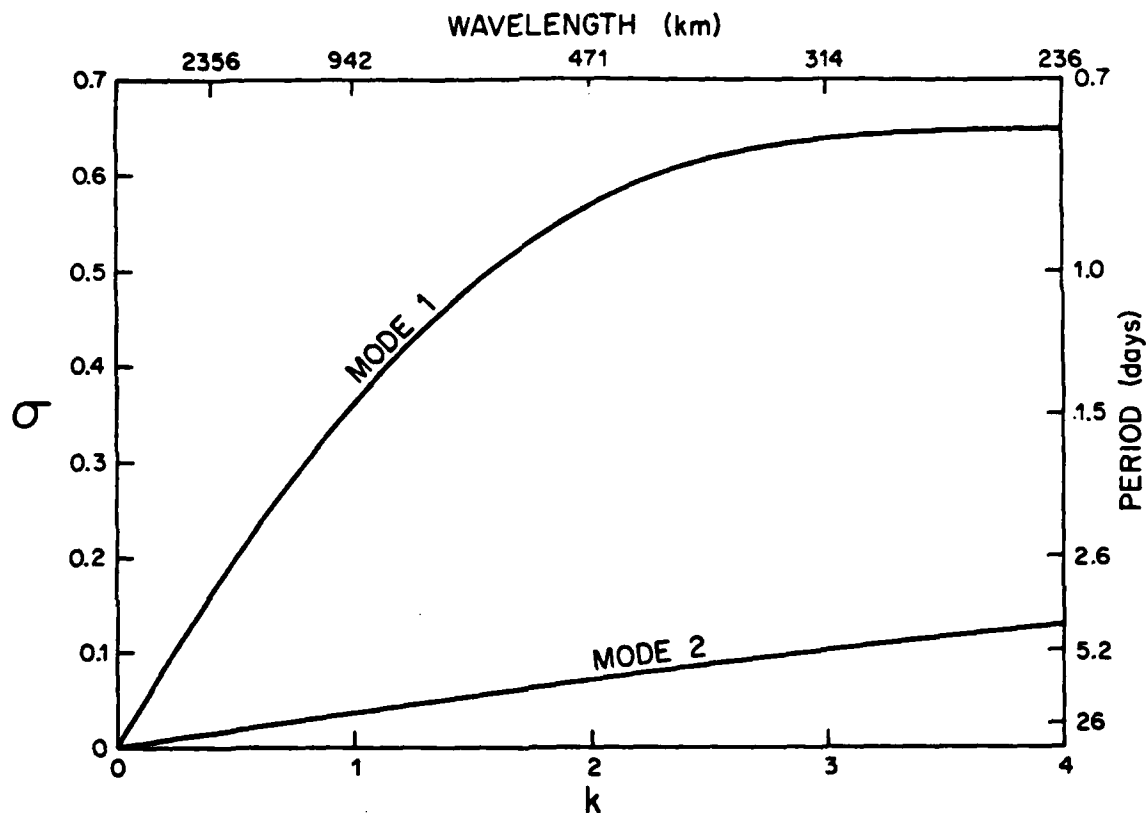
Figure 33.   Mode 1 and 2 dispersion curves for the Brink (1982b) coastal trapped wave model using stratification and topography applicable to the West Spitsbergen Current west of Spitsbergen at 79°N. The non-dimensional frequency σ is the dimensional frequency ω divided by f. The non-dimensional wavenumber k is the dimensional wavenumber l multiplied by the shelf/slope width L = 150 km.

the dispersion curve. Usually, records of sea level height at the coast or current records from moorings separated in the longshore direction are used to determine the longshore wavenumber (e.g., Smith, 1978). In the absence of such data, it is only possible to guess at the wavelength in an effort to arrive at an associated wave period. One approach is to consider the most efficient forcing mechanism, which is the forcing of a cross isobath flow in the deep layers by Ekman convergence or divergence at the coast. Approximately 850 km of open water separate Norway from Spitsbergen, while Spitsbergen has a western coastline about 350 km long. Thus, any trapped waves generated locally near Spitsbergen would have length scales comparable to the length of the coastline. From the dispersion curve, a second mode trapped wave with a wavelength of 363 km has a period of 5.8 days, which is consist-ent with the center of the broad spectra peak in the cross-isobath velocity spectra. This is not sufficient grounds to conclude that coastal trapped waves of the above characteristics account for the variability around a period of about 6 days, but the results certainly suggest the possibility that they are a feature of the WSC.

Figure 34 shows the velocity structure over the upper slope and shelf computed by the model for a second mode trapped wave with wave-length 500 km and period 7.7 days. This structure is representative of the frequency-wavenumber range of Fig. 33. The velocity structure is nearly barotropic, consistent with model studies conducted by Brink (1982b) and with findings by Allen and Romea (1980) which indicated that with increasing latitude, the characteristics of trapped waves approach those of barotropic shelf waves. In comparison, while there is some degree of shear in the mean flow of the WSC (see Table 5), the current measurements show that the fluctuations tend to be mostly barotropic in nature. The velocity structure indicates a high speed region close to the coast, a node over the shelf, a region of high velocity over the shelf break which decays offshore, and another node over the slope. This modal structure implies that the variability due to the second mode should be largest near the shelf break, decrease offshore, and then increase again seaward of the node over the slope.

Spectra of alongshore velocity show comparable energy content between A1-98V and C1-93V in the 3-10 day range. In addition, the velocity fluctuations of A1-98V and C1-93V are negatively correlated,
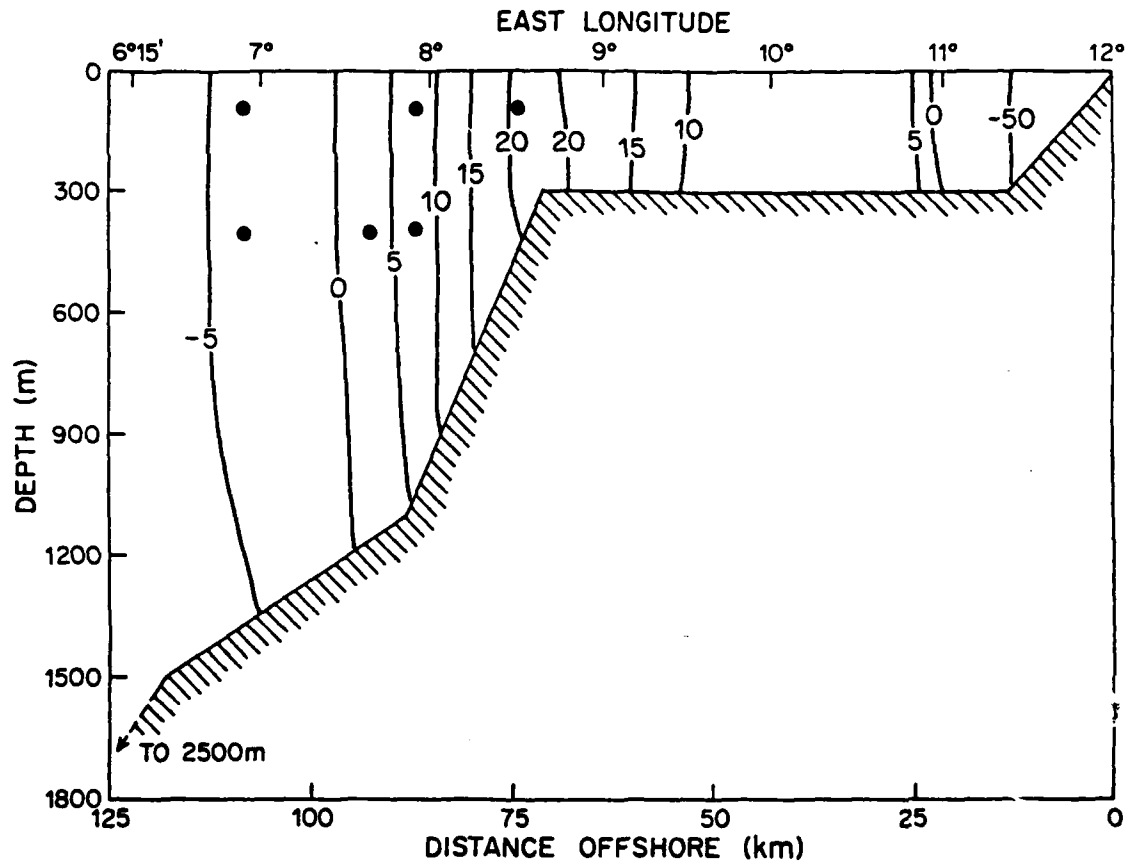
Figure 34. Mode 2 perturbation velocity structure for the Brink (1982b) coastal trapped wave model west of Spitsbergen along 79°N. Wavelength and period are 500 km and 7.7 days. Contours are in arbitrary units.

and coherence calculations between them yield phase differences between 90° and 180° for periods longer than about 3 days. A node between A and C would in fact yield such a negative correlation and comparable energy levels. However, while the mean alongshore velocity at D is highest of all the mooring locations, the energy content of its spectrum shows levels comparable to those at A and C over similar time scales. In the 3-10 day range, the energy is comparable between A1-98U and C1-93U, but both are a decade greater than D1-98U. Observations thus do not bear out strong trapping of fluctuating energy at the shelf break, even though the alongshore mean velocity is highest there.

The model results show that the physical setting west of Spitsbergen can support free coastal trapped waves with a period which, assuming a reasonable wavelength, corresponds with a broad peak in the cross-isobath velocity spectra. The model predicts a nearly barotropic velocity structure, which is slightly different than shown by direct velocity measurements. The model also shows a node in the velocity structure over the slope region, consonant with the observed and calculated correlation between A and C. In spite of the highest mean velocity occurring at D, direct observations do not bear out the strong concentration of energetic fluctuations over the shelf break (compared with farther offshore as indicated by the model).

6.4 Lateral movement of banded flow

Historical evidence for banded flow in the WSC was presented earlier in Section 1, and observational evidence for banded flow from the 1976-77 deployments was presented in Section 3. Lateral movement of such a flow back and forth across the line of moorings is one way of producing the negative correlation between currents at A and C. Overlayed plots of longshore velocities A1-98V and C1-93V show the negative correlation. With few exceptions, major fluctuations in the records are coincident but opposite in sign. Moveover, they are out-of-phase even when the velocity fluctuations are irregular in time. This last observation suggests the lateral structure may be relatively invariant, in agreement with the evidence from hydrographic data. In addition, the average phase difference between the cross-isobath velocity fluctuations of A1-98U and C1-93U is approximately zero for periods longer than about 3 days. These results support the concept of a definite,

invariant flow structure meandering back and forth over the slope. The propagation of trapped waves is one way to account for the lateral movement, but not necessarily the sole explanation, since the fluctuations do not appear to be strictly periodic or of consistent time scales. Observations have shown that the Kuroshio may occupy different paths (cf. Stommel and Yoshida, 1972) which appear related to topography, and the flow of the WSC over the slope may represent another example.

6.5 Atmospheric forcing and short term variability of the West Spitsbergen Current

In Section 5, it was shown that annual variation in the wind field could account for annual fluctuations of the WSC if the response were in the form of Rossby waves. Higher frequency wind forcing can be expected to generate higher frequency fluctuations (bounded by the inertial frequency). However, at these shorter time scales, the nature of the oceanic response will also be different, as was pointed out in Section 5. I now discuss the possible role of atmospheric forcing in relation to fluctuations of the WSC with time scales of a few days to a few weeks. But note that the data needed to realistically assess the degree of wind forcing on time scales this short (at least daily values of local winds and atmospheric pressure) are not available for the area under study.

Willebrand (1978) found, in a study of the North Atlantic wind field, that most of the wind variance is associated with eastward traveling cyclones with time scales of 2-10 days. This is consistent with Vowinckel and Orvig's (1970) observation that 4-6 cyclones per month traverse the Greenland and Norwegian seas in winter. Philander (1978) showed that eastward traveling disturbances could not directly excite free Rossby waves. Instead the oceanic response is trapped in the vicinity of the disturbances, and therefore should show similar space and time scales. Philander (1978) also pointed out that the forcing by these cyclones, which are characteristic of mid- and high latitudes, penetrates to the ocean bottom. Thus, bottom topography can assume an important role in the oceanic response to the passage of the disturbances by introducing topographic waves with spatial or temporal

characteristics which differ from those of the forcing; the oceanic response will reflect the characteristics of both these contributions.

The generation of shelf waves by Ekman convergence or divergence at a coastline has already been discussed. A second possible source of waves is atmospherically forced cross-isobath water movement over the section of steep continental slope between Spitsbergen and Norway, leading to the generation of bottom trapped topographic Rossby waves confined to the slope. The phase relation between temperature and cross-isobath velocity fluctuations as calculated from C5-984, where temperature leads by about 90°, is in the proper sense to indicate bottom trapping (Thompson and Luyten, 1976). However, the fluctuating energy is greater at C5-384 than at C5-984, in disagreement with bottom trapping, which speaks against this explanation unless the C5-384 record primarily represents variance originating in the upper ocean. Deeper measurements, e.g., at 600-700 m, are required to shed further light on the possibility of bottom trapping.

The separation of forced from free response poses a problem. The periods and wavelengths of free second mode coastal trapped waves are similar to those of the wind field, and the cross-isobath velocity spectra peak broadly at about the same time scale as the winds. Figure 35 shows a spectrum for the meridional wind stress at $75^\circ N$ $7.5^\circ E$ which was calculated from the daily NWS pressure maps. The shape is not identical to the U-component spectra, but it is apparent that there is also a broad concentration of energy in the wind field at time scales which correspond with fluctuations of the current.

The lack of appropriate data hamper reaching any definite conclusion about the true relationship between wind and flow of the WSC at time scales of a few days to a few weeks. However, it seems likely that the mid-frequency fluctuations of the WSC reflect the complicated response of the ocean to the eastward passage of cyclones across the slope and shelf on the eastern side of the Greenland Sea.
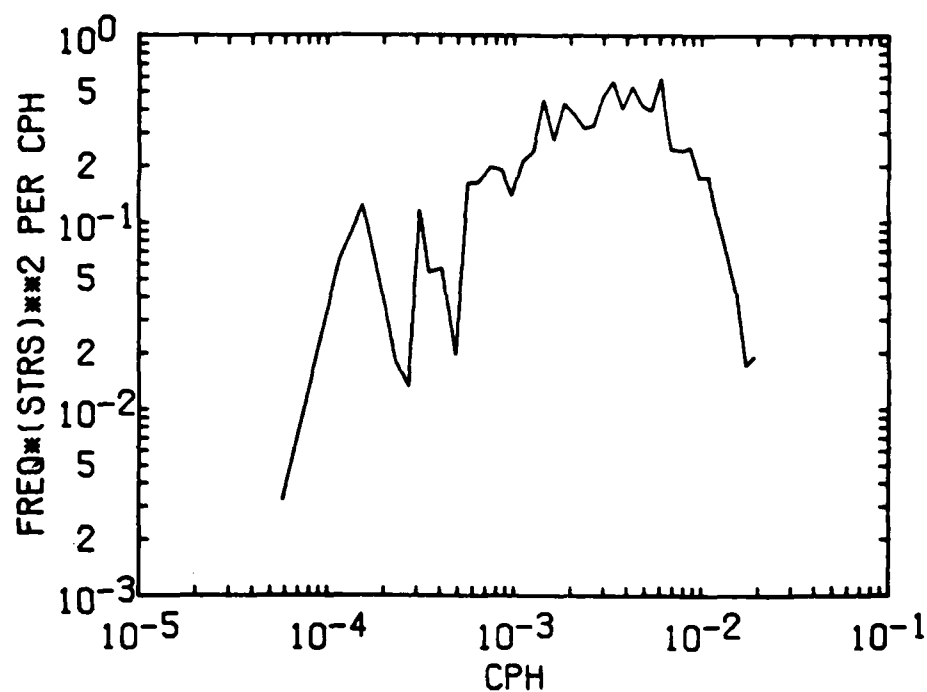
Figure 35.   Energy conserving spectrum of meridional wind stress at
75°N 7.5°E calculated from NWS daily pressure maps, 1976-
79.

7. Summary

Current and temperature records have been used to calculate the volume and heat transports of the West Spitsbergen Current, and to investigate the temporal and spatial variability of the flow. In 1976-77, four moorings were spaced laterally in the flow, and from 1977 to 79 and during 1980-81, moorings were maintained at the same location as one of the 1976-77 moorings in the main core of the flow.

Over the upper continental slope region, lateral spatial scales of 10-20 km characterized the flow, and while the current was in general strongly correlated vertically, there were episodes of days to weeks during which the vertical shear of alongshore velocity was large or even reversed. Current meters separated by only about 15 km across the flow were strongly, but negatively correlated. Mean cross-isobath velocities were offshore and generally about 10-20% of the alongshore mean. A broad range of time scales of variability, from tidal to annual, appears in the current records.

During 1976-77, volume transports ranged from 1.4 Sv southward to 11.9 Sv northward, and the year-long mean was 5.6 Sv. Of this, the baroclinic and barotropic components were 1.0 and 4.6 Sv, respectively. The seasonal pattern indicated is for maximum transport in late fall and winter, miniumum in February-March, and reduced transport (less than maximum) during spring.

The mean heat transport during 1976-77 was 46 TW northward with extrema of 8 TW southward and 122 TW northward. The seasonal pattern was similar to that of the volume transport. The mean alongshore turbulent heat transport was 3.2 TW. In terms of heat flux, the alongshore mean advective flux was almost one order of magnitude greater than the alongshore turbulent flux, and at least two orders of magnitude greater than the cross-isobath flux. The cross-isobath turbulent heat flux was down-gradient (offshore), in the proper direction to feed energy from the mean flow into fluctuations.

Bridged current records three years long clearly showed the strong seasonal fluctuations of speed and temperature which occurred during the period 1976-79. There appeared to be decreasing trend in the transport temperature, but no significant interannual differences in the volume transport over this three-year interval.

The mean wind stress curl over the Greenland-Norwegian sea region appears to be important in driving the northward transport of the West Spitsbergen Current. During 1976-79, the wind stress curl was about one-half that in 1971-72, and the mean velocities of the West Spitsbergen Current over those respective periods were similarly related. Topography likely plays an important role in steering and causing convergence in the flow. In addition, dynamic considerations imply that fluctuations of the wind stress curl can only cause fluctuations in the mean flow at time scales longer than about one-half year. Thus, the general condition in the Greenland-Norwegian sea region seems to be a slowly varying Sverdrup balance, responding to low-frequency fluctuations of the wind stress curl.

The West Spitsbergen Current exhibits much high-frequency (but subtidal) variability, and many possible causes were investigated. Spectra of alongshore current records showed fairly uniform energy levels at periods longer than about about four days. At shorter periods, energy fell off sharply except for a strong peak at the semidiurnal tidal frequency. Spectra of cross-isobath current records peaked broadly about a period of six days and decreased by three orders of magnitude to the annual period. Shorter than six days, cross-isobath and alongshore spectra were quite similar.

Model results indicated that barotropic instability in the West Spitsbergen Current was highly unlikely because of generally low Rossby numbers for the flow, and thus, barotropic instability is probably not a source of variability which appears in the cross-isobath current spectra at a period of about a week.

Baroclinic instability is one possible contributor to variability at periods somewhat less than a week. For parameters corresponding to the width and speed of the West Spitsbergen Current, model results indicated that the flow may exhibit baroclinic instability over a range of wavelengths and periods of 30-50 km and 3-4.5 days, respectively. For vertical shear characteristic of the West Spitsbergen Current, the fastest growing wave had a wavelength of 34 km and a period of 3.8 days. Doubling the shear nearly doubled the growth rate, but changed the corresponding wavelength and period by only about 20%.

The topography and stratification west of Spitsbergen along 79°N may support a variety of coastal trapped waves. However, only the

second mode wave is a likely candidate for accounting for variability at periods of about one week. For periods longer than 1.5 days, first mode wavelengths are longer than the basin scale length of about 1000 km, while third mode waves are clearly unimportant. Corresponding wavelength and period ranges for the second mode trapped waves are 260-1000 km and 4-14 days. This wavelength range is physically reasonable for the region, and the period range corresponds with the range in the cross-isobath spectra in which energy is concentrated. The second mode trapped wave velocity structure is essentially barotropic over the shelf/slope region, and contains a node over the slope. Both of these features are consistent with the current measurements. Alongshore wavelength information is necessary to confidently assess the role of the second mode trapped wave concerning variability of the West Spitsbergen Current.

In winter, 4-6 cyclones per month traverse northeastward across the region, and at high latitudes, forcing extends to the bottom. It is highly likely that these traveling disturbances contribute to the variability of the West Spitsbergen Current at periods corresponding with the frequency of passage. It is also likely that the oceanic response is modified by the influence of strong topographic features.

8. Future Investigations

There are two different directions in which to progress, and the data requirements are somewhat different for each. One is the investigation of the short-term variability and associated dynamics of the WSC, and the other is the maintenance of a long-term monitoring program to measure the transports into the Polar Basin in order to assess the implications for the heat budget.

Needed for further investigation of the short-term variability are alongshore wavelength information, local wind stress data, and sea surface height records at some point on the west coast of West Spitsbergen in conjunction with current measurements. Ideally, periodic hydrographic sections of closely spaced stations would complement the measurements. These types of data are necessary for differentiating between possible dynamic sources of variability in the flow and for determining the importance of local winds in generating that variability. All are obtainable with the existing technology in oceanographic instrumentation. There are many existing studies of boundary currents, and further detailed study of the dynamics of the short-term variability of the WSC presents still another unique addition to that branch of physical oceanography.

One of the key factors in the success of a long-term monitoring program in the WSC is refining the transport estimates of the flow and linking the transport to some index such as the flow at a single location. Refining the estimates requires an accurate characterization of the lateral and vertical structure of the flow, and based on the present work, this would require an array of moorings about 10 km apart spanning from the coast of Spitsbergen westward to about 3^OE, with at least some deep current meters to guage the bottom flow. Linking the transport to a single index is simply a matter of correlation calculations. The present work represents a step in this direction, and is probably sufficient for making coarse estimates of long-term transport fluctuations. However, it is important that future experimental work take into account the lateral structure.

Such an extensive program of measurements is an expensive and formidable undertaking, and the use of remote sensing techniques is one way of reducing the amount of ground-based data required. The strong

temperature signature of the WSC and the variation of dynamic height across the flow suggest that remote sensing of surface temperature and sea surface height is a possible way of defining the lateral and along-shore structure of the flow, particularly if it is possible to obtain ground truth information by simultaneous earth-based and space-based monitoring.

The work reported in this investigation made limited use of models. As better data become available for inserting into model equations, models will become better descriptors of the flow. As such, models have valuable potential which should not be neglected in opti-mizing the design of field experiments.

The WSC is rich in both spatial and temporal variability, and it has some consequence for the budgets of the Polar Basin. Future inves-tigations thus have the great potential to be fruitful, interesting, and important.

REFERENCES

Aagaard, K., 1969: Relationship between geostrophic and surface winds at weather ship M. J. Geophys. Res., 74, 3440-3442.

Aagaard, K., 1970: Wind-driven transports in the Greenland and Norwegian seas. Deep-Sea Res., 17, 281-291.

Aagaard, K., 1981: On the deep circulation of the Arctic Ocean. Deep-Sea Res., 28A, 251-268.

Aagaard, K. and P. Greisman, 1975: Toward new mass and heat budgets for the Arctic Ocean. J. Geophys. Res., 80, 3821-3827.

Aagaard, K., L.K. Coachman, and E. Carmack, 1981: On the halocline of the Arctic Ocean. Deep-Sea Res., 28A, 529-545.

Adams, J.K. and V.T. Buchwald, 1969: The generation of continental shelf waves. J. Fluid Mech., 35, 815-826.

Alekseev, A.P. and B.V. Istoshin, 1956: Chart of constant currents in the Norwegian and Greenland seas. PINRO, Trudy, 9: 62-68. (Translation: U.S. Fish and Wildlife Service Special Scientific Report-Fisheries No. 327, pp 69-76, 1959.)

Alekseev, A.P. and B.V. Istoshin, 1960: Some results of oceanographic investigations in the Norwegian and Greenland seas. Soviet Fisheries Investigations in North European Seas, (VNIRO-PINRO), 23-37, Moscow. (in Russian).

Allen, J.S., 1975: Coastal trapped waves in a stratified ocean. J. Phys. Oceanogr., 5, 300-325.

Allen, J.S., and R.D. Romea, 1980: On coastal trapped waves at low latitudes in a stratified ocean. J. Fluid Mech., 98, 555-585.

Anderson, D.L.T. and A.E. Gill, 1975: Spin-up of a stratified ocean, with applications to upwelling. Deep-Sea Res., 22, 583-596.

Anderson, D.L.T. and A.E. Gill, 1979: Beta-dispersion of inertial waves. J. Geophys. Res., 84, 1836-1842.

Bakun, A., 1973: Coastal upwelling indices, west coast of North America, 1946-71. NOAA Tech. Rep. NMFS SSRF-761, 103 pp.

Brink, K.H., 1982a: The effect of bottom friction on low-frequency coastal trapped waves. J. Phys. Oceanogr., 12, 127-133.

122

Brink, K.H., 1982b: A comparison of long coastal trapped wave theory with observations off Peru. J. Phys. Oceanogr., 12, 897-913.

Bryden, H.L. and R.D. Pillsbury, 1977: Variability of deep flow in the Drake Passage from year-long current measurements. J. Phys. Oceanogr., 7, 803-810.

Carmack, E., 1972: On the hydrography of the Greenland Sea. Unpublished thesis, University of Washington, 186 pp.

Carmack, E. and K. Aagaard, 1973: On the deep water of the Greenland Sea. Deep-Sea Res., 20, 687-715.

Coachman, L.K. and K. Aagaard, 1974: Physical oceanography of Arctic and Subarctic seas. In: Arctic Geology and Oceanography, H. Nelson and Y. Herman, Eds, Springer-Verlag, 1-72.

Clarke, A.J., 1977: Observational and numerical evidence for wind-forced coastal trapped long waves. J. Phys. Oceanogr., 7, 231-247.

Creegan, A., 1976: A numerical investigation of the circulation in the Norwegian Sea. Tellus, 28, 451-459.

Davis, R.E., 1976: Predictability of sea surface temperature and sea level pressure anomalies over the North Pacific Ocean. J. Phys. Oceanogr., 6, 249-266.

Dickson, R.R., 1972: Variability and continuity within the Atlantic Current of the Norwegian Sea. Rapp. Cons. Explor. Mer, 162, 167-183.

Dickson, R.R. and T.C. Doddington, 1968: Hydrographic conditions off Spitsbergen in the summers of 1966 and 1967. Ann. Biol., 24, 24-29.

Dickson, R.R. and T.C. Doddington, 1970: Hydrographic conditions off Spitsbergen in the summers of 1968 and 1969. Ann. Biol., 26, 26-32.

Dietrich, G., 1969: Atlas of the hydrography of the northern North Atlantic. International Council for the Exploration of the Sea, Copenhagen, 140 pp.

Eggvin, J., 1961: Some results of the Norwegian hydrographic investigation in the Norwegian Sea during the IGY. Rapp. Cons. Explor. Mer., 149, 212-218.

Fandry, C. and R.D. Pillsbury, 1979: On the estimation of absolute geostrophic volume transport applied to the Antarctic Circumpolar Current. J. Phys. Oceanogr., 9, 449-455.

Fuglister, F.C., 1954: Average temperature and salinity at a depth of 200 m in the North Atlantic. Tellus, 6, 46-58.

Galt, J.A., 1973: A numerical investigation of Arctic Ocean dynamics. J. Phys. Oceanogr., 3, 379-396.

Gill, A.E., 1982: Atmosphere-Ocean Dynamics Academic Press, New York, 662 pp.

Gill, A.E. and E.H. Schumann, 1974: The generation of long shelf waves by the wind. J. Phys. Oceanogr., 4, 83-90.

Greisman, P., 1976: Current measurements in the eastern Greenland Sea. Unpublished thesis, University of Washington, 145 pp.

Greisman, P. and K. Aagaard, 1979: Seasonal variability of the West Spitsbergen Current. Ocean Modelling, 19, 3-5, 6 fig.

Griffiths, R.W. and P. F. Linden, 1981: The stability of buoyancy-driven coastal currents. Dyn. Atmos. Oceans, 5, 281-306.

Helland-Hansen, B., 1934: The Sognefjord section. Oceanographic observations in the northernmost part of the North Sea and the southern part of the Norwegian Sea. James Johnstone Memorial Volume, 257-274, Liverpool. University Press.

Helland-Hansen, B. and F. Nansen, 1909: The Norwegian Sea. Report on Norwegian Fishery and Marine Investigations, vol. 2, part 1, no. 2, Bergen, Norway.

Hill, H.W. and A.J. Lee, 1957: The effect of wind on water transport in the region of the Bear Island fishery. Proc. Roy. Soc., B, 148, 104-116.

Huthnance, J.M., 1978: On coastal trapped waves: analysis and numerical calculation by inverse iteration. J. Phys. Oceanogr., 8, 74-92.

Johnson, G.L. and P.R. Vogt, 1973: Marine geology of the Arctic ocean north of the arctic circle. Arctic Geology Memoir 19, Amer. Assoc. of Petrol. Geol., 161-170.

Kawabe, M., 1982: Coastal trapped waves in a two-layer ocean: wave properties when the density interface intersects a sloping bottom. J. Oceanogr. Soc. Japan, 38, 115-124.

Kiilerich, A., 1945: On the hydrography of the Greenland Sea. Meddelelser om Grolund, 144(2), 63 pp.

Kislyakov, A.G., 1960: Fluctuations in the regime of the Spitsbergen Current. Translation: Soviet Fisheries Investigations in North European Seas (VNIRO-PINRO), 39-49, Moscow.

Krauss, W., 1955: Zum system der meeresstromungen in den hoheren beiten. Dt. Hydrogr. Z., 8, 102-111.

Laktionov, A.F., 1959: Oceanographic researches in central Arctic. Some problems and results of oceanology researches. Articles. X-Section of the IGY Program (Oceanology), No. 1 (in Russian).

LeBlond, P.H. and L.A. Mysak, 1978: Waves in the Ocean. Elsevier Scientific Publ. Co., Amsterdam, 602 pp.

Lee, A., 1959: Some observations on the structure of the West Spitsbergen Current. First Int. Ocean. Cong., preprints of abstracts, ed. by M. Sears, pp. 408-409.

Lee, A., 1961a: The effect of wind on water movements in the Norwegian and Greenland seas. Proc. Symp. Math.-Hydrodyn. Methods in Phys. Oceanogr., 353-373. Inst. f. meereskunde Univ. Hamburg, Sept. 1961.

Lee, A., 1961b: Hydrographic conditions in the Barents Sea and Greenland Sea during the IGY compared with those in previous years. Rapp. Cons. Explor. Mer., 149, 40-43.

Lee, A., 1963: The hydrography of the European Arctic and Subarctic Seas. Oceanogr. Mar. Biol. Ann. Rev., 1, 47-76. Harold Barnes, Ed., Publ. George Allen and Urwin Ltd., London.

Lighthill, M.J., 1969: Unsteady wind-driven ocean currents. Quart. J. R. Met. Soc., 95, 675-688.

Mandel, S.Z., 1976: The water level in Barentsburg as an index of the inflow of Atlantic waters into the Arctic basin. Ark. i Antark. Nauchno-Issled. Inst., Trudy (transl.), 319, 129-136.

Mandel, S.Z., 1978: Concerning the seasonal and year-to-year variations of the heat flow of Atlantic waters into the Arctic basin. Ark. i Antark. Nauchno-Issled. Inst., Trudy (transl.), 349, 50-54.

Mandel, S.Z., 1979: Basic features of seasonal and year-to-year variations of the inflow of Atlantic water and heat into the Arctic basin through Fram Strait. Ark. i Antark. Nauchno-Issled. Inst., Trudy (transl.), 361, 24-29.

Melling, H. and E.L. Lewis, 1982: Shelf drainage flows in the Beaufort Sea and their effect on the Arctic Ocean pycnocline. Deep-Sea Res., 29, 967-985.

Metcalf, W.G., 1960: A note on water movement in the Greenland-Norwegian Sea. Deep-Sea Res., 7, 190-200.

Mosby, H., 1938: Svalbard Waters. Geofys. Publ., 12 (4), 85 pp.

Mosby, H., 1962: Water, salt, and heat balance of the North Polar Sea and of the Norwegian Sea. Geofys. Publ., 24, 289-313.

Mosby, H., 1970: Atlantic water in the Norwegian Sea. Geofys. Publ., 28(1), 60 pp.

Mysak, L.A., 1967: On the theory of continental shelf waves. J. Mar. Res., 25, 205-227.

Mysak, L.A., 1980a: Recent advances in shelf wave dynamics. Rev. Geophys. Space Phys., 18, 211-241.

Mysak, L.A., 1980b: Topographically trapped waves. Ann. Rev. Fluid Mech., 12, 45-76.

Mysak, L.A. and F. Schott, 1977: Evidence of baroclinic instability of the Norwegian Current. J. Geophys. Res., 82, 2087-2095.

Mysak, L.A., E. R. Johnson and W.W. Hsieh, 1981: Baroclinic and barotropic instabilities of coastal currents. J. Phys. Oceanogr., 11, 209-230.

Niiler, P.P. and L.A. Mysak, 1971: Barotropic waves along an eastern continental shelf. Geophys. Fluid Dyn., 2, 273-288.

Oort, A.H. and A. Taylor, 1969: On the kinetic energy spectrum near the ground. Mon. Weather Rev., 97, 623-636.

Palfrey, K.M., 1967: Physical oceanography of the northern part of the Greenland Sea in summer 1964. Unpublished thesis, University of Washington, 52 pp.

Pattullo, J., W. Munk, R. Revelle, and E. Strong, 1955: The seasonal oscillation in sea level. J. Mar. Res., 14, 88-156.

Philander, S.G.H., 1978: Forced oceanic waves. Rev. Geophys. Space Phys., 16, 15-46.

Philander, S.G.H., 1979: Variability of the tropical oceans. Dyn. Atmos. Oceans, 3, 191-208.

Reid, J.L., 1979: On the contribution of the Mediterranean Sea outflow to the Norwegian Greenland Sea. Deep-Sea Res., 26, 1199-1224.

Rudels, B. and L. Andersson, 1982: Observations of the mass, heat, and salt exchange through Fram Strait. Report no. 42, Oceanografiska Institutionen, Goteborgs universitet, 47 pp.

Saelen, O.H., 1963: Studies in the Norwegian Atlantic Current. Part II: Investigations during the years 1954-59 in an area west of Stad. Geofys. Publ., 23(6), 82 pp.

Schott, F. and M. Bock, 1980: Determination of energy interaction terms and horizontal wavelengths for low-frequency fluctuations in the Norwegian Current. J. Geophys. Res., 85, 4007-4014.

Semtner, A.J. Jr., 1976: Numerical simulation of the Arctic Ocean circulation. J. Phys. Oceanogr., 6, 409-425.

Smith, P.C., 1976: Baroclinic instability in the Denmark Strait overflow. J. Phys. Oceanogr., 6, 355-371.

Smith, R.L., 1978: Poleward propagating perturbations in currents and sea levels along the Peru coast. J. Geophys. Res., 83, 6083-6092.

Solonitsina, L.R., 1976: Hydrographic conditions in the Norwegian Sea in 1976. Ann. Biol., 33, 25-27.

Solonitsina, L.R., 1978: Hydrographic conditions in Norwegian Sea waters in 1978. Ann. Biol., 35, 64-67.

Stefansson, U., 1962: North Icelandic Waters. Rit Fiskideildar, 3, 269 pp.

Stewart, R. W., 1964: The influence of friction on inertial models of oceanic circulation. Studies on Oceanography, 3-9.

Stigebrandt, A., 1981: A model for the thickness and salinity of the upper layer in the Arctic Ocean and the relationship between the ice thickness and some external parameters. J. Phys. Oceanogr., 11, 1407-1422.

Stommel, H., 1965: The Gulf Stream: A Physical and Dynamical Description. University of California Press, 248 pp.

Stommel, H. and K. Yoshida, eds., 1972: Kuroshio, Physical Aspects of the Japan Current. Univ. of Washington Press.

Swift, J.H., 1980: Seasonal processes in the Iceland Sea. Unpublished thesis, University of Washington, 296 pp.

Tareyev, B.A., 1971: Gradient-vorticity waves on the continental shelf. Izv., Atmos Oceanic Phys., 7, 283-285. (translation)

Thompson, R.O.R.Y. and J.R. Luyten, 1976: Evidence for bottom-trapped topographic Rossby waves from single moorings. Deep-Sea Res., 23, 629-635.

Timofeyev, V.T., 1962: The movement of Atlantic water and heat into the Arctic Basin. Deep-Sea Res., 9, 358-361.

Timofeyev, V.T., 1963: Interaction of the Arctic ocean waters with Atlantic and Pacific waters. Okeanologiya, 3, (transl.), 569-578.

Trangeled, S., 1974: Oceanography of the Norwegian and Greenland Seas and adjacent areas. NATO SACLANTCEN memorandum SM-47, 2 vols.

Treshnikov, A.F., 1960: New data on the bottom topography and the waters of the Arctic basin. Priroda, 2, 25-32. Defence Research Board, Canada, translation T 357 R.

Vowinckel, E. and S. Orvig, 1970: The climate of the North Polar basin, in Climates of the Polar Regions, 129-252, Elsevier, New York.

Wang, D-P., 1975: Coastal trapped waves in a baroclinic ocean. J. Phys. Oceanogr., 5, 326-333.

Wang, D-P. and C.N.K. Mooers, 1976: Coastal-trapped waves in a continuously stratified ocean. J. Phys. Oceanogr., 6, 853-863.

Willebrand, J., 1978: Temporal and spatial scales of the wind field over the North Pacific and North Atlantic. J. Phys. Oceanogr., 8, 1080-1094.

Willebrand, J., S.G.H. Philander, and R.C. Pacanowski, 1980: The oceanic response to large-scale atmospheric disturbances. J. Phys. Oceanogr., 10, 411-429.

Worthington, L.V., 1970: The Norwegian Sea as a mediterranean basin. Deep-Sea Res., 17, 77-84.

Wright, D.G., 1981: Baroclinic instability in Drake Passage. J. Phys. Oceanogr., 11, 231-246.

Zaitsev, G.N., 1960: The heat balance of the Norwegian and Greenland seas and factors governing its formation. Soviet Fisheries Investigations in North European Seas, (VNIRO-PINRO), 67-80, Moscow, (in Russian).

Zaitsev, G.N., M.V. Fedosov, N.L. Iljina, and I.A. Ermachenko, 1961: Components of the water, thermic and chemical budget of the Greenland and Norwegian seas. Rapp. Cons. Explor. Mer, 149, 46-52.

VITA

Dennis Joe Hanzlick

Born: January 23, 1946   Russell, Kansas

Parents: George and Margaret Hanzlick

High School: Hoisington Rural High School
              Hoisington, Kansas

B.S. University of Kansas
      Lawrence, Kansas   June, 1968

M.S. University of Washington
      Seattle, Washington   December, 1976

END

FILMED

3-84

DTIC